

Alternative Conductive Coatings Based on Multi-Walled Carbon Nanotubes

Dissertation

zur Erlangung des Grades
des Doktors der Ingenieurwissenschaften
der Naturwissenschaftlich-Technischen Fakultät III
Chemie, Pharmazie, Bio- und Werkstoffwissenschaften
der Universität des Saarlandes

Vorgelegt von

Mayra Rúbia Silva Castro

Saarbrücken

2007

ACKNOWLEDGMENTS

I am very thankful to Prof. Dr. Helmut Schmidt for the opportunity to work under his supervision in a very interesting research field. I am thankful to his ideas and advices which contributed a lot for the completion of this Ph.D. work.

This work was carried out at the Leibniz Institute for New Materials GmbH (INM) in Saarbrücken, where I had all the facilities necessary to develop the research. The support by the library team and the characterization methods specialists is gratefully appreciated.

I would like to thank Dr. Peter W. Oliveira for his encouragement and his support since the beginning of this Ph.D. work, as well as for his ideas, discussions and for the opportunity to work in his group in a very friendly atmosphere.

I acknowledge the fruitful discussions and collaboration work with my colleagues at INM and the constructive suggestions and support of Dr. Gerd Schäfer and Dr. Naji Al-Dahoudi.

I am grateful to Dr. Edward "Ted" McRae (Université Henri Poincaré, Nancy) for the reading proof and important discussions about the scientific aspect of this thesis. I also thank Prof. Sanjay Mathur (Universität Würzburg) for his time to read through the preliminary version of this thesis and Prof. Young Hee Lee (SKKU, South Korea) for his valuable comments.

I am deeply thankful to Dr. Siegmur Roth (Max Planck Institute, Stuttgart) for the chance to visit his group and for his suggestions. I appreciate interesting discussions with Mônica Jung de Andrade, Eduardo Lee and Dr. Ursula Dettlaff-Weglikowska. I also thank Armin Schultz for the Raman spectroscopy characterization of my samples at the MPI facilities.

I am very much indebted to my parents Ana and Eurico and my brother Marcelo for always being there, loving, supporting and guiding me. I dearly thank Thomas for his patience and encouragement in all these years by my side as well as for the constant support in editing this thesis.

Finally, I express my gratitude to the Leibniz Association and the German Academic Exchange Program (DAAD) for the funds granted to me. I appreciate the assistance of Prof. Dr. Michel Aegerter and Martina Bonnard before I come to Germany, as well as the support and advices of Prof. Dr. Reginaldo Muccillo (USP, Brazil). I am thankful to Nicole Müller, Irmgard Kasperek and Susanne Scherzer for their help in all these years.

ABSTRACT

The aim of this work was to develop coatings as possible replacements for tin-doped indium oxide (ITO) systems. The alternative material of choice was carbon nanotubes, due to their flexibility, the abundance of carbon element in nature, their high aspect ratio and high electrical conductivity. Focusing on cost benefits, very thin multi-walled carbon nanotubes (MWNTs) were investigated rather than single-walled nanotubes (SWNTs) normally presented in the literature. Moreover, spin coating sol-gel technique was performed as a less expensive alternative to sputtering techniques used in the production of ITO films. MWNTs were studied both as pure networks as well as embedded in conductive and insulating matrixes. As networks, MWNTs presented sheet resistances as low as $20\text{ k}\Omega/\text{sq}$ with transparency in the visible range of 87%, values comparable to some of SWNT networks presented in the literature. MWNTs were investigated as additional conductive elements in antimony-doped tin oxide (ATO) matrix. The results showed that the addition of concentrations as low as 0.1 wt.-% MWNTs is sufficient to decrease the resistivity of conducting ATO films by a factor of 16, with preserved transparency (90%) in the visible range. Less ATO nanoparticles and lower temperatures of sintering are required in order to obtain films with comparable resistivities and even higher transparency than that presented by ATO films reported in the literature. MWNTs have also provided resistivities in the order of $10\ \Omega.\text{cm}^{-1}$ to an initially insulating TiO_2 matrix. The transparency of these films was, however, affected by the concentration of MWNTs necessary in order to reach the percolation threshold. Although the studied coatings did not meet the requirements necessary for a proper substitution of ITO in opto-electronic devices, their optical and electrical response as well as their low cost and simplicity of preparation allow them to be used in other applications where the high conductivity of ITO is not a requirement. The structural, optical, mechanical and electrical properties of all coatings were studied using different techniques and are demonstrated in this work.

ZUSAMMENFASSUNG

Das Ziel dieser Arbeit bestand in der Entwicklung von Schichten als Ersatz für Zinn-dotiertes Indiumoxid (ITO). Das Material der Wahl waren Kohlenstoff-Nanoröhren aufgrund ihrer Flexibilität, des häufigen Vorkommens von Kohlenstoff in der Natur, ihres hohen Aspektverhältnisses und vor allem ihrer hohen elektrischen Leitfähigkeit. Während normalerweise in der Literatur einwandige Nanoröhren (SWNTs) beschrieben werden, standen in dieser Arbeit aus Kostengründen die mehrwandigen Kohlenstoff-Nanoröhren (MWNTs) im Vordergrund. Außerdem wurde in dieser Arbeit die Rotationsbeschichtungstechnik in Verbindung mit Sol-Gel-Verfahren eingesetzt. Diese ist eine günstigere Alternative zur Sputtertechnik, welche zum Herzustellen von ITO-Schichten verwendet wird. MWNTs wurden sowohl als Netzwerke, als auch eingebunden in leitfähige und isolierende Matrices untersucht. In Netzwerken zeigten MWNTs Schichtwiderstände von $20 \text{ k}\Omega/\text{sq}$ und eine Transparenz von 87% im sichtbaren Bereich des Lichtes, was durchaus vergleichbar mit den Werten von SWNT-Netzwerken in der Literatur ist. Ferner wurden MWNTs als leitfähige Additive in Antimon-dotierten Zinnoxid (ATO) Matrices untersucht. Die Ergebnisse zeigten, dass bereits die Zugabe von 0.1 Gew. – % MWNTs ausreichend ist, um den Widerstand einer leitfähigen ATO-Schicht unter Beibehaltung von 90% Transparenz im Sichtbaren, um den Faktor 16 zu senken. Dadurch werden weniger ATO-Nanopartikel und niedrigere Sintertemperaturen benötigt, um Schichten mit vergleichbarem Widerstand und sogar höherer Transparenz als in der Literatur zu erhalten. Mit MWNTs ließen sich auch in einer zuvor isolierenden TiO_2 -Matrix Widerstände in der Größenordnung von $10 \text{ }\Omega.\text{cm}^{-1}$ erreichen. Die Transparenz dieser Schichten wurde jedoch durch die Konzentration der MWNTs, die für ein Erreichen der Perkolationsschwelle nötig waren, negativ beeinflusst. Obwohl die in dieser Arbeit untersuchten Schichten die Spezifikationen, die für einen Ersatz von ITO in opto-elektronischen Elementen nötig wären, noch nicht erreicht haben, erlauben ihre optischen und elektrischen Eigenschaften, wie auch ihre niedrigen Herstellungskosten und die Einfachheit ihrer Herstellung, sie in anderen Anwendungen einzusetzen, in denen die hohe Leitfähigkeit von ITO nicht erforderlich ist. Die strukturellen, op-

tischen, mechanischen und elektrischen Eigenschaften aller Schichten wurden mit verschiedenen Techniken untersucht.

CONTENTS

1. Introduction	1
2. Theoretical Background	3
2.1 Transparent conducting oxides	3
2.1.1 Tin oxide	4
2.1.2 Indium oxide	5
2.1.3 Zinc oxide	7
2.2 Carbon Nanotubes	8
2.2.1 Multi-Walled Carbon Nanotubes	11
2.2.2 Dispersion of Nanotubes	12
2.2.2.1 The effect of surfactants	13
2.2.2.2 Dispersion techniques	15
2.2.3 Applications of Carbon Nanotubes	16
2.2.4 Percolation of conductive additives	17
3. State of the Art	19
3.1 TCOs	19
3.1.1 TCO semiconductors for thin-film transparent electrodes	19
3.1.2 TCO films made by the sol-gel technique	21
3.1.2.1 In_2O_3 based coatings	21
3.1.2.2 SnO_2 based films	22
3.1.2.3 ZnO based films	23
3.1.2.4 Ternary compounds coatings	24
3.2 CNT composites and networks	25
3.3 Sum up of the literature review:	
Identification of the problematic	27
4. Objective	29

5. Experimental	31
5.1 MWNT networks	31
5.1.1 Characterization of the MWNT powder	31
5.1.2 Surfactant-assisted dispersion of MWNTs	32
5.1.3 Characterization of the dispersion	34
5.1.4 Preparation of the networks	35
5.1.5 Characterization of the networks	35
5.2 ATO/MWNT nanocomposites	37
5.2.1 Preparation of the $SnO_2 : Sb$ (ATO) powder	37
5.2.2 Characterization of the ATO powder	37
5.2.3 Preparation of the ATO suspension	38
5.2.4 Characterization of the ATO solution	38
5.2.5 Preparation of the ATO/MWNT nanocomposite solutions	39
5.2.6 Preparation of the coatings	39
5.2.7 Characterization of the ATO and ATO/MWNT coatings	41
5.3 TiO_2 /MWNT nanocomposites	41
5.3.1 Dispersion of MWNTs in the TiO_2 -based sol	42
5.3.2 Preparation of the coatings	42
5.3.3 Characterization of the TiO_2 /MWNT coatings	42
6. Results and Discussion	43
6.1 MWNT Networks	43
6.1.1 Characterization of the MWNT powder	43
6.1.2 Characterization of the MWNT dispersion in HDTAC	47
6.1.3 Characterization of the MWNT networks deposited on borosilicate substrates	48
6.1.4 Conclusion of the MWNT network studies	57
6.2 ATO/MWNT nanocomposites	59
6.2.1 Characterization of the ATO powder	59
6.2.2 Characterization of the sols used in the ATO/MWNT studies	61
6.2.3 ATO and ATO/MWNT coatings	61
6.2.3.1 Structural characterization	63
6.2.3.2 Electrical properties	66
6.2.3.3 Transmittance in the visible range	70
6.2.3.4 Mechanical Properties	70

6.2.4	Conclusion of the ATO/MWNT nanocomposites studies	72
6.3	<i>TiO₂</i> /MWNT nanocomposites	73
6.3.1	<i>TiO₂</i> sol and <i>TiO₂</i> /MWNT dispersions	73
6.3.2	<i>TiO₂</i> /MWNT coatings	73
6.3.2.1	Structural properties	73
6.3.2.2	Electrical properties	77
6.3.2.3	Transmittance in the visible range	79
6.3.2.4	Mechanical properties	79
6.3.3	Conclusion of the <i>TiO₂</i> /MWNT nanocomposite studies	81
7.	Summary and conclusions	82
8.	Outlook	85
9.	Appendix	86
9.1	List of abbreviations	86
9.2	List of used chemicals	87
9.3	List of instruments and equipment used	88
9.4	Metallic behavior of MWNTs	89
9.5	ATO/MWNT coatings prepared with MWNTs dispersed in anionic and non-ionic surfactants	90
9.6	Preparation of <i>TiO₂</i> -based sol used as a matrix for the dispersion of MWNTs.	91
9.7	Prices of commercially available carbon nanotubes.	92
9.8	Coatings deposited on polycarbonate (PC) substrate	93
9.9	Direct laser interference patterning of the coatings	94
9.10	Thermogravimetric analysis of MWNTs under forming gas atmosphere	97

LIST OF FIGURES

2.1	Structure of tin (IV) oxide.	4
2.2	Structure of indium oxide.	5
2.3	Structure of zinc oxide.	7
2.4	Transmission electron microscopy images of multi-walled coaxial nanotubes with various inner and outer diameters and numbers of cylindrical shells [After Iijima, 1991]. (a) Five graphitic sheets, diameter 6.7 nm; (b) Two-sheet tube, diameter 5.5 nm; and (c) Seven-sheet tube, diameter 6.5 nm.	8
2.5	Publications related to carbon nanotubes since 1991 (Source: search on the “Web of Science” for publications containing the keyword “carbon nanotube”).	9
2.6	Models of different kinds of carbon nanotubes: (a) a single-walled nanotube; (b) a rope of single-walled nanotubes; and (c) a multi-walled nanotube.	10
2.7	Schematic representations of different mechanisms by which surfactants help disperse SWNTs [After Yurekli, 2004]. (a) SWNT encapsulated in a cylindrical surfactant micelle (right: cross section view); (b) hemimicellar adsorption of surfactant molecules on a SWNT; and (c) random adsorption of surfactant molecules on a SWNT.	15
2.8	Typical curve demonstrating the behaviour of the resistivity measured as a function of the loading of nanotubes [After Colbert, 2003].	17
2.9	Representation of percolation networks showing the concentration necessary to form a conducting pathway.	18
2.10	A schematic representation of the surface of a CNT-polymer composite where CNTs percolate.	18
5.1	High shear processor. (a) M110-Y Microfluidizer processor and (b) its schematic view.	33
5.2	Flow chart of the dispersion of MWNTs in HDTAC.	34
5.3	Flow chart of the preparation of antimony-doped tin oxide powder [After Goebbert <i>et al.</i> , 1999].	38

5.4	Flow chart of the preparation of ATO suspension [After Goebbert, 1999].	39
5.5	Flow chart of the preparation of ATO/MWNT nanocomposite sols.	40
5.6	Flow chart of the preparation of ATO and ATO/MWNT coatings.	40
6.1	(a) SEM images of as-received $-NH_2$ functionalized MWNTs and (b) TEM images of the same MWNTs, revealing an outer diameter of 10 nm.	44
6.2	Raman spectra of $-NH_2$ and $-COOH$ functionalized MWNTs.	44
6.3	TG curves showing the behavior of $-COOH$ and $-NH_2$ functionalized MWNTs with the increase of the temperature under synthetic air.	46
6.4	Investigation of the metal catalyst particles present in the $-NH_2$ MWNT powder by (a) TEM and (b) EDX methods.	46
6.5	X-ray spectra of functionalized MWNT powders. The inserted lines correspond to graphite structure.	47
6.6	Zeta potential distribution of MWNTs dispersed in HDTAC (5 wt.-% in water) with concentration of 3 mg/ml.	48
6.7	TEM micrographs of (a) MWNT-NET and (b) MWNT-NET-Si deposited on borosilicate substrates and sintered at 300 °C for 20 min.	50
6.8	EDX spectrum of MWNT-NET-Si deposited on borosilicate and sintered at 300 °C for 20 min	50
6.9	FESEM images of (a) MWNT-NET and (b) MWNT-NET-Si deposited on borosilicate substrates and sintered at 300 °C for 20 min.	51
6.10	AFM image of MWNT-NET deposited on borosilicate and sintered at 300 °C for 20 min.	51
6.11	Average roughness of MWNT-NET as a function of the heating temperature.	52
6.12	WLI image of (a) MWNT-NET; and (b) MWNT-NET-Si, both sintered at 350°C for 20 min.	52
6.13	Variation of the sheet resistance of MWNT-NET prepared at 300 °C for 20 min with the concentration of nanotubes.	53
6.14	Transmittance of MWNT-NET containing different concentrations of MWNTs heated at 300 °C for 20 min.	53
6.15	Variation of the sheet resistance of MWNT-NET (10 mg/ml) with the heating temperature.	54
6.16	Variation of the sheet resistance of MWNT-NET (10 mg/ml in HDTAC) with the increase of the concentration of adhesion promoters during the preparation of MWNT-NET-Si.	56

6.17	Photograph comparing the optical transparency of MWNT-NET (left) and MWNT-NET-Si (right) deposited on borosilicate glass at 350 °C.	56
6.18	SEM image of MWNT-NET after the performance of the tape test.	57
6.19	Comparison of the sheet resistance of MWNT networks obtained in this work with others reported in the literature as a function of their transparency measured at $\lambda = 550 \text{ nm}$	59
6.20	X-ray diffraction of nanoscaled, crystalline $\text{SnO}_2 : \text{Sb}$ powder prepared under hydrothermal conditions (150 °C for 3 h) [After Goebbert <i>et al.</i> , 1999]. The inserted lines correspond to the cassiterite form of SnO_2	60
6.21	Investigations of ATO nanopowder obtained by hydrothermal crystallization at 150 °C for 3 h [After Goebbert <i>et al.</i> , 1999]. (a) HRTEM evidencing overall particle diameter of 3 nm; (b) EDX analysis of the powder.	60
6.22	TEM micrograph of ATO sol (25 wt. – % in TMAH) after Goebbert <i>et al.</i> 1999. A picture of the sol is depicted in the inset.	62
6.23	Ultrafine particle size analysis of ATO sol (25 wt. – % in TMAH 0.78 M) after Goebbert <i>et al.</i> 1999.	62
6.24	HRTEM investigations of 3-layers ATO coating on borosilicate sintered at 400 °C for 30 min. (a) Cross-section view of the 3 layers; and (b) magnified micrograph highlighting the ATO particle size.	64
6.25	EDX spectrum of 3-layers ATO coating deposited on borosilicate at 400 °C for 30 min.	64
6.26	TEM micrographs of S_NH2_20 (ATO/MWNT coatings).	65
6.27	SEM micrographs of (a) S_ATO and (b) S_NH2_20, sintered at 400 °C in air for 15 minutes.	66
6.28	Sheet resistance of ATO and ATO/MWNT coatings as a function of the sintering temperature.	67
6.29	Thickness of ATO/MWNT nanocomposites with different compositions.	69
6.30	Resistivity of ATO/MWNT coatings as a function of the concentration of MWNT dispersion in the matrix precursor.	69
6.31	Photograph illustrating the transparency of S_ATO (left) and S_NH2_20 (right).	70
6.32	Transparency of ATO and ATO/MWNT coatings.	71
6.33	TiO_2 -based sol developed at INM facilities [After Mennig <i>et al.</i> , 2003].	73

6.34 HRTEM images of TiO_2 /MWNT (5 mg/ml) with different magnifications. (a) Defects on the structure of the MWNTs; (b) curved end-caps of MWNTs; (c) a MWNT containing 6 inner nanotubes; and d) the EDX spectrum of the coating.	74
6.35 Investigations of TiO_2 coatings deposited on borosilicate and sintered at $400\text{ }^\circ\text{C}$. (a) HRTEM image shows that no crystalline phase is present; (b) X-Ray investigations confirms the observation.	75
6.36 Raman spectrum of TiO_2 /MWNT coatings containing 5 mg/ml MWNTs	76
6.37 FESEM micrographs of (a) TiO_2 and TiO_2 /MWNT coatings containing (b) 1, (c) 3, and (d) 5 mg/ml MWNTs.	77
6.38 WLI image of TiO_2 /MWNT coating (5 mg/ml MWNTs) deposited on borosilicate glass.	78
6.39 Variation of the sheet resistance of TiO_2 /MWNT composites as a function of the concentration of MWNTs in the coatings.	78
6.40 Transmittance of TiO_2 and TiO_2 /MWNT coatings prepared with different concentrations of MWNTs.	80
6.41 Photograph comparing the transparency of TiO_2 (left) and TiO_2 /MWNT nanocomposites containing 3 mg/ml MWNTs (right).	80
9.1 Typical behavior of MWNTs: (a) source drain current through the MWNTs measured as a function of the bias voltage; and (b) derived resistance as a function of the gate voltage. MWNT networks show no gate action.	89
9.2 Scanning electron microscopy micrographs of ATO/MWNT coatings prepared with $-NH_2$ MWNTs dispersed in (a) sodium dodecyl sulphate and (b) Triton X-100; and $-COOH$ MWNTs also dispersed in (c) sodium dodecyl sulphate and (d) Triton X-100. The poor appearance denotes aggregation of nanotubes in the cited surfactants.	90
9.3 Preliminary studies of the deposition of ATO/MWNT and MWNT networks on polycarbonate (PC) substrates. (a) Sheet resistance as a function of the concentration of MWNTs; and (b) transparency of the coatings. Both ATO/MWNT and MWNT networks were deposited by spin coating and sintered in air at $130\text{ }^\circ\text{C}$ for 3 h	93

-
- 9.4 Scanning electron microscope micrographs of irradiated ATO/MWNT coatings with (a, b) two and (c, d) three laser beams interference patterns: (a) Laser fluence = 207 mJ/cm^2 ; (b) Laser fluence = 483 mJ/cm^2 ; (c, d) Laser fluence = 644 mJ/cm^2 . The insert in (d) shows the surface morphology at the interference maximum (Max.) and minimum (min.). The scale bar in the insert of (d) is 200 nm . Well defined arrays of conductive nanostructures can be fabricated in one single laser pulse. 94
- 9.5 Scanning electron microscope micrographs of irradiated MWNT-NET-Si with (a, b) two and (c, d) three laser beams interference patterns. The laser fluences were (a) 272, (b) 251, (c) 163, and (d) 211 mJ/cm^2 . The insert in (b) shows the surface morphology at the interference maximum (Max.) and minimum (min.). The scale bar in the insert of (b) is 200 nm 95
- 9.6 Scanning electron microscope micrographs of low-adherent MWNT-NET irradiated with two laser beam configuration. The laser fluence was 309 mJ/cm^2 . In (a), three laser interference minima are observed. (b) Detail at interference minimum and maximum. The insert in (b) shows the surface morphology at the maxima (Max.) and minima (min.). The scale bar in the insert of (b) is 200 nm 96
- 9.7 Thermal behaviour of MWNTs under forming gas atmosphere ($10 \text{ }^\circ\text{C/min}$). 97

LIST OF TABLES

3.1	TCO semiconductors used as thin-film transparent electrodes.	21
6.1	Classification of MWNT-NET and MWNT-NET-Si deposited on borosilicate after standard mechanical tests.	55
6.2	Nomenclature adopted for the different coatings studied in Section 6.2.3 . .	63
6.3	Thickness, resistance and resistivity values obtained for ATO and ATO/MWNT coatings.	66
6.4	Classification of ATO and ATO/MWNT coatings deposited on borosilicate after standard mechanical tests.	71
6.5	Classification of TiO_2 and TiO_2 /MWNT coatings deposited on borosilicate after standard mechanical tests.	81
9.1	List of abbreviations	86
9.2	Chemicals used in the preparation of ATO powder	87
9.3	Surfactants used for the dispersion of MWNTs	87
9.4	Prices of different commercially available CNTs.	92

1. INTRODUCTION

This work was motivated by the necessity to find replacements for tin-doped indium oxide, which is constantly used as a thin film transparent electrode in most opto-electronic devices. Although high-conductive tin-doped indium oxide (commonly called ITO) thin films deposited by magnetron sputtering (MSP) have been in practical use for such applications, there are several reports in the literature on different transparent conductive oxide semiconductors as well as alternative deposition methods, as presented in the Chapter 3, Section 3.1 of this thesis. The necessity to replace ITO lies on the fact that a stable supply of this material may become difficult to achieve for the recently expanding market of opto-electronic devices, mainly because of the cost and scarcity of indium, the main element of ITO. Another point of consideration is the high cost of MSP as a deposition method for ITO coatings. In this case, sol-gel techniques would represent a more attractive alternative, since they enable coating on a desired shape and area and provide easy control of the doping level, solution concentration and homogeneity without the need of expensive and complicated equipments [1].

A significant discovery was that of carbon nanotubes (CNTs) [2], which are essentially single graphene layers wrapped into tubes, either single-walled (SWNT) or multi-walled (MWNT) formed into several concentric layers. More information about this material is provided in Chapter 2, Section 2.2. Nanotubes possess unique mechanical and electronic properties which make them promising building blocks for molecular electronics, such as high electrical conductivity ($3 \times 10^4 S/cm$) and intrinsic high aspect ratio ($> 10^3$). This combination of properties together with their small diameter and light weight allows the formation of conductive networks through a host material with tunable electrical resistivity. For the fabrication of composite materials, carbon nanotubes have an advantage in comparison with other conducting particles. Since conduction is by electrical charge percolation from particle to particle through the coating, typically the matrix material must be filled with high loading levels of the conductive media (higher than 50 wt.-%) to reach significant electrical conductivity. This high loading levels normally result in poor mechanical

and optical properties. In the carbon nanotube case, the composites reach the electrical percolation threshold at much lower loading levels (sometimes as low as 0.04 *wt. %* in the case of SWNTs), what, consequently, does not affect other properties of the matrix material, such as its optical transparency.

Compared to existing transparent conductor technologies, CNT-based films could have a number of potential advantages. These include the use of an abundant material (carbon) with high aspect ratio, flexibility and easy solution processability. A review on CNT-based materials with this purpose is given in Chapter 3, Section 3.2. Taking advantage on the potential of nanotubes and considering the problematic regarding the use of ITO, it was the aim of this work to study carbon nanotube-based coatings as alternative materials for transparent conductive systems (Chapter 4). Since the cost benefits were one of the priorities in this study, low-cost, commercial multi-walled carbon nanotubes (MWNTs) produced by the chemical vapor deposition process (CVD) were investigated. Moreover, the sol-gel spin coating process was chosen as deposition method for the films on borosilicate substrates, since it is a fast, relatively simple method which requires small amount of precursor materials and has a high reproducibility. The experiments performed in this work are listed in Chapter 5, followed by the discussion of the obtained results in Chapter 6. Finally, the results of this thesis are summarized in Chapter 7. The thesis contains also an Appendix (Section 9), where technical and extra information are provided.

2. THEORETICAL BACKGROUND

This chapter will introduce the reader to the materials most used nowadays as transparent conductive coatings (2.1) and to carbon nanotubes (2.2). Since multi-walled carbon nanotubes were the material of choice in this investigation, special attention is given to this type of nanotubes in Section 2.2.1. Aspects such as fabrication and purification methods, dispersion in different media (2.2.2) and applications of CNTs (2.2.3) are presented. Also the percolation theory in which the concentration of carbon nanotubes plays an important role for the conductivity of CNT-based composites is reported in the last Section of this Chapter (2.2.4).

2.1 Transparent conducting oxides

Transparent conducting oxides (TCOs) are the most commonly used materials to produce transparent conducting films. They are essentially based on oxides such as In_2O_3 , SnO , ZnO and CdO . These materials are usually insulators and have a wide band gap ($> 3 eV$) and excellent transparency in the visible region. To provide them conductivity, non-stoichiometry and/or appropriate dopants, like Sn for In_2O_3 , Sb or F for SnO_2 , and Al or Ga for ZnO , should be introduced in order to create an electron degeneracy in the wide band gap [3]. The large free-carrier concentrations attainable in these high conductivity oxides shift the plasma-reflection edge to near-infrared wavelengths and induce high reflectivities beyond the plasma edge. This property, in combination with high transparency to solar radiation, can be exploited for applications such as heat-reflective coatings in solar thermal collectors [4]. Taking advantage of additional properties of these materials, such as mechanical hardness and good environmental stability, numerous other applications have been reported, including flat panel displays, thin film transistors, electroluminescent devices, gas sensors, organic light emitting diodes, solar cells and in demisting and deicing glasses for automotive, train and aircraft industries [5–8].

The dominant transparent conducting oxides vastly studied in the last thirty to forty years are listed below.

2.1.1 Tin oxide

Tin oxide (SnO_2) was the first transparent conductor to have received significant attention and commercialization. It is an *n*-type, chemically stable, wide band gap semiconductor ($E_g = 3.97 \text{ eV}$) with a transmittance cut off at 330 nm and a refractive index in the visible spectral range of about 2.0 [9, 10]. It is largely used as a transparent conductive layer for ovens and electrodes [11], in the fabrication of gas sensor devices [12], white pigmented conductive paint coatings [13], and as active catalyst for the partial oxidation and the amino oxidation of olefins [14]. Tin oxide has a tetragonal (rutile) structure [15]. Each tin atom is at the center of six oxygen atoms placed approximately at the corners of a regular octahedron and every oxygen atom is surrounded by three tin atoms located approximately at the centers of an equilateral triangle, as shown in Fig. 2.1.

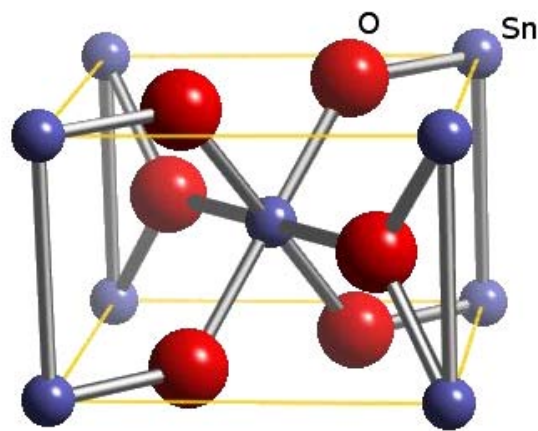


Fig. 2.1: Structure of tin (IV) oxide.

SnO_2 is an insulator or at most an ionic conductor when it is stoichiometric. The formation of oxygen vacancies in the lattice (for example, by heating the material in a reducing atmosphere) leads to a non-stoichiometry state and gives rise to free electrons which make the material conductive. This non-stoichiometry is, however, metastable. Stable conductivity of SnO_2 thin films is normally obtained by doping the coating with ions such as fluorine [16, 17], antimony [18, 19], or boron [20]. The doping is done by controlling the valence mechanism: the dopant should be either a higher valency cation (e.g. Sb^{5+}) or a

lower valency anion (e.g. F^-) than tin, providing additional electrons to the semiconducting material.

Doping of SnO_2 with antimony results in a larger grain size (about 600 Å) with no change in the lattice parameters [21]. Clearly, the dopant is incorporated substitutionally. Doping also affects the preferred orientation of crystallites [22, 23]. The doping of SnO_2 with antimony gives rise to a donor level at 35 meV [24]. Antimony doping in SnO_2 films results also in a large shift in the fundamental absorption edge [21, 25], which is attributed to the Moss-Burstein effect [26].

Different deposition techniques can be used in the production of tin oxide films, for instance, spray pyrolysis [27, 28], chemical vapour deposition (CVD) [29], sputtering [30], evaporation [31, 32] and also sol-gel deposition methods [33, 34].

2.1.2 Indium oxide

Indium oxide (In_2O_3) is the most widely used material for transparent conductive materials in technical applications due to its superior electrical properties, combined with high transparency and high infrared reflectivity [35]. In_2O_3 exists in a modified cubic crystallographic phase called the bixbyite structure (also called *c*-type rare earth oxide structure) with two non-equivalent *In* sites, 16 molecules (80 atoms) per unit cell and a lattice constant of 1.012 nm [36–38], as demonstrated in Fig. 2.2.

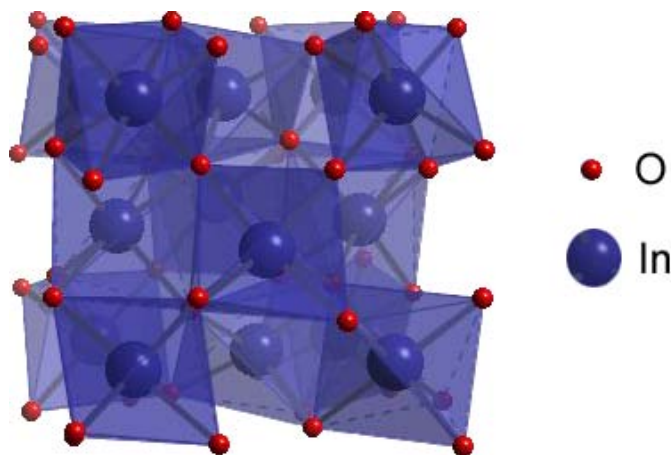


Fig. 2.2: Structure of indium oxide.

The band structure of In_2O_3 is not well understood. Well accepted is the explanation of the conductivity mechanism by Hamberg and Granqvist [39], who assumed a simple

parabolic band structure characterized by an effective mass m_c^\bullet , for the conduction band and m_v^\bullet , for the valence band, with a direct band gap of 3.75 eV .

In_2O_3 is a poor conductive material when it is stoichiometric. The conductivity is strongly enhanced by a reducing treatment or by doping the lattice with an appropriate dopant such as Sn . The reducing process of indium oxide material creates oxygen vacancies, each one leaving two extra electrons in the lattice. The donor state lies just below the conduction band. High electron concentrations ($10^{17} - 10^{20} \text{ cm}^{-3}$) can be achieved with an oxygen deficiency (e.g. In_2O_{3-x}) or an excess of metal atoms (e.g. $In_{2+y}O_3$).

The doping process leads to controlled valence semiconductors. The replacement of indium by higher valence cations as aluminium, titanium, zinc, germanium and tin, increases the n -type conductivity, the last element being the most popular for this purpose [40, 41]. In tin doped indium oxide (ITO), Sn replaces the In^{3+} atom in the cubic bixbyite structure by substitutional doping. An Sn atom forms an interstitial bond with oxygen and exists either as SnO or SnO_2 . The valence state has a decisive effect on the ultimate conductivity of ITO. The low valence state, Sn^{2+} , acts as a trap for the charge carriers and therefore reduces the electrical conductivity, as there is a lower concentration of free electrons. On the other hand, Sn^{4+} acts as a n -type donor releasing one free electron to the conduction band. In fact, both substitutional Sn^{4+} and oxygen vacancies contribute to the high conductivity, and the chemical formula of the material can be represented as $In_{2-x}Sn_xO_{3-2x}$. ITO films have a lattice parameter close to that of indium oxide and lies in the range of 1.012 to 1.031 nm , which has been found to depend on the deposition parameters [42].

The high conductivity of ITO films is due to the high carrier concentration rather than to the high Hall mobility [35]. The observed low mobility of ITO, compared to that of bulk In_2O_3 , and its dependence on carrier concentration and deposition temperature has been explained in terms of scattering mechanisms due to ionized impurities or grain boundaries. The high degree of crystallinity obtained by depositing the film at high temperature enhances the mobility of the films [43].

The high optical transmittance of ITO films is a direct consequence of the wide band gap of the semiconductor. The direct band gap ranges from 3.5 to 4.1 eV , so that the fundamental absorption edge lies in the ultraviolet region. It shifts to shorter wavelength with increasing the carrier concentrations, n , due to the Moss-Burstein shift [26, 44]. The transmittance of ITO films is also influenced by the surface roughness and optical inhomogeneity in the direction normal to the film surface.

ITO thin films have been obtained by many deposition techniques such as spray pyro-

ysis [45], ion beam pulsed laser deposition [46, 47], sol-gel deposition techniques [48–51] and sputtering [52–54], the last technique being the most extensively used.

ITO coatings are used as transparent heating elements for aircraft and car windows, antistatic coatings over electronic instrument display panels, heat reflecting mirrors, antireflection coatings and even in high temperature gas sensors. Many electro-optic devices such as display devices, solar cells, light emitting and photo diodes, photo transistors and lasers use ITO coating as electrodes [55]. However, if the increase in usage of ITO films for flat panel displays and solar cells continues, not only will the price of ITO keep rising, but also the availability of In may be jeopardized in the near future due to limited capacities in the few deposits worldwide [56].

2.1.3 Zinc oxide

Zinc oxide (ZnO) is also an important material used in many fields of applications [57]. It is an n -type semiconductor with poor electrical conductivity in its pure state and has a direct band gap of about 3.2 eV . Zinc oxide is a tetrahedrally coordinated solid that crystallizes in the wurtzite structure demonstrated in Fig. 2.3.

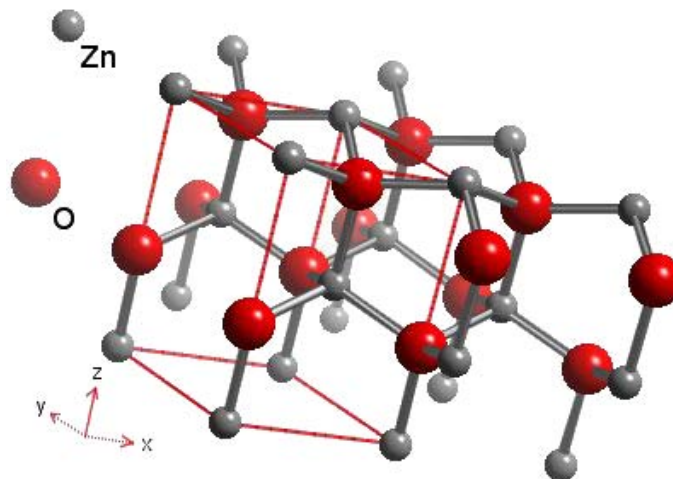


Fig. 2.3: Structure of zinc oxide.

The electrical conductivity of intrinsic ZnO materials is mainly due to an excess of zinc in interstitial positions. The electrical properties of zinc oxide materials can be improved by thermal treatment in hydrogen, or by an appropriate doping process, by cationic substitution, using ion dopants like Al , Ga , Si , Ge , Ti , Zr or Hf [58, 59], the first two elements

being the most studied. This is attributed to the fact that the ionic radius of Al^{3+} and Ga^{3+} are slightly smaller than that of Zn^{2+} , in comparison with the other ions.

Doped zinc oxide films are extensively studied due to their high optical transmission and electrical conduction. They have great potential for application in solar cells [60], displays and as low emissivity coatings in windows [61]. ZnO films have been prepared by many techniques such as reactive evaporation [62], sputtering [63,64], spray pyrolysis [65] and by sol-gel deposition methods [66,67].

2.2 Carbon Nanotubes

Iijima's report in 1991 [2] has brought carbon nanotubes (CNTs) into the awareness of the scientific community as a whole (Fig. 2.4). Since then, a lot of research has been performed in order to elucidate their properties [68–70] and the prospect of developing novel nanomaterials based on these structures is constantly increasing [71,72]. The worldwide interest among researchers in the study of carbon nanotubes is reflected by the elevated number of publications in the field in the last years, as shown in Fig. 2.5.

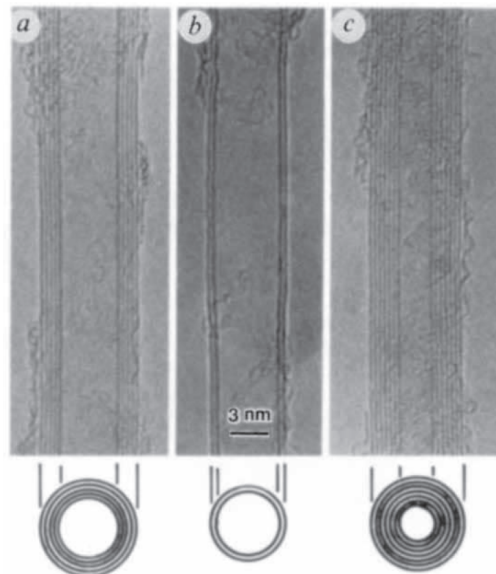


Fig. 2.4: Transmission electron microscopy images of multi-walled coaxial nanotubes with various inner and outer diameters and numbers of cylindrical shells [After Iijima, 1991]. (a) Five graphitic sheets, diameter 6.7 nm; (b) Two-sheet tube, diameter 5.5 nm; and (c) Seven-sheet tube, diameter 6.5 nm.

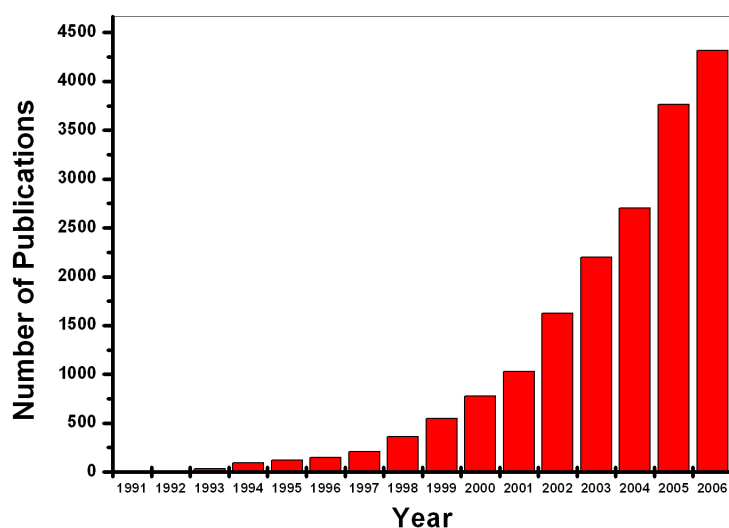


Fig. 2.5: Publications related to carbon nanotubes since 1991 (Source: search on the “Web of Science” for publications containing the keyword “carbon nanotube”).

There are two main types of CNTs with high structural perfection: single-walled nanotubes (SWNTs) (Fig. 2.6a), which consist of a single graphene sheet seamlessly wrapped into a cylindrical tube, and multi-walled nanotubes (MWNTs) (Fig. 2.6c), which comprise an array of concentric cylinders. Most frequently, the diameter of CNTs varies roughly between 0.4 and 3 *nm* for SWNTs and from 1.4 to 100 *nm* for MWNTs [73]. SWNTs often aggregate into bundles (ropes) of weakly interacting tubes that can easily slide on each other, as depicted in Fig. 2.6b. These bundles can contain up to several hundred SWNTs arranged in a hexagonal lattice [74].

SWNTs and MWNTs are usually produced by arc-discharge [75,76], laser ablation [77], chemical vapour deposition (CVD) [78], or gas-phase catalytic process (HiPco) methods [79]. Up to now, all currently known production methods generate CNTs with impurities, normally consisting of carbon-coated metal catalysts and amorphous carbon. Also, structural defects such as dangling bonds are often found in most types of CNTs [80]. The main techniques applied for purification of CNTs are oxidation of contaminants [81, 82], flocculation and selective sedimentation [83], filtration [84], size-exclusion chromatography [85], selective interaction with organic polymers [86], or microwave irradiation [87–89]. However, considerable problems remain for most of the present purification techniques. Some of these methods rely on the difference in resistance to oxidation, either thermal or

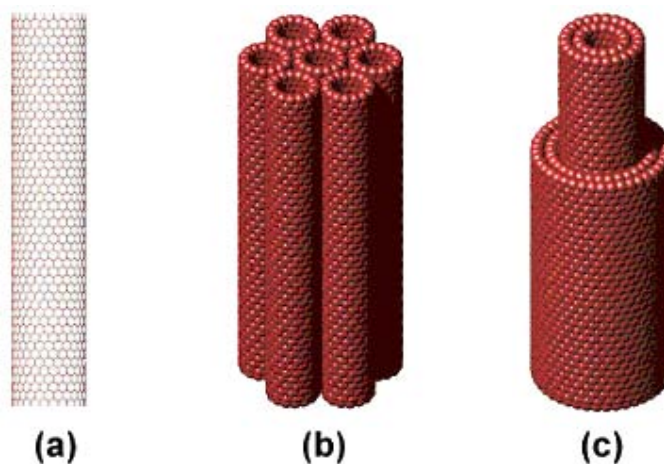


Fig. 2.6: Models of different kinds of carbon nanotubes: (a) a single-walled nanotube; (b) a rope of single-walled nanotubes; and (c) a multi-walled nanotube.

chemical, between CNTs and impurities. Since this difference is often marginal, significant quantities of CNTs are destroyed or altered before all impurities are removed. Alternatively, non-destructive methods such as microfiltration or size-exclusion chromatography can be employed, but tend to be slow and are considered as inefficient processes.

The most important general properties of carbon nanotubes are briefly stated below.

Electrical conductivity: Carbon nanotubes with a small diameter are either semiconducting or metallic, depending on their chiral vector. The differences in conducting properties are caused by the molecular structure that results in a different band structure and thus a different band gap. The differences in conductivity can easily be derived from the graphene sheet properties. A (n, m) nanotube is metallic when the following rule is satisfied: $n = m$ or $(n - m) = 3i$, where i is an integer and n and m define the nanotube. The conductivity is determined by quantum mechanical aspects and was proved to be independent of the nanotube length [90].

Chemical reactivity: The chemical reactivity of a CNT is, compared with a graphene sheet, enhanced as a direct result of the curvature of the CNT surface. Therefore, a distinction must be made between the sidewall and the end caps of a nanotube. For the same reason, a smaller nanotube diameter results in increased reactivity. Covalent chemical modification of either sidewalls or end caps has shown to be possible. Though, direct investigation of chemical modifications on nanotube behaviour is difficult as the crude nanotube samples are still not pure enough [91].

Optical activity: Theoretical studies have revealed that the optical activity of chiral nanotubes disappears if the nanotubes become larger [92]. Therefore, it is expected that other physical properties are also influenced in this case. Use of the optical activity might result in optical devices in which CNTs play an important role.

Mechanical strength: Carbon nanotubes have a very large Young modulus in their axial direction. The nanotube as a whole is very flexible because of its great length. Therefore, these compounds are potentially suitable for application in composite materials that need anisotropic properties [93].

2.2.1 Multi-Walled Carbon Nanotubes

A multi-walled carbon nanotube (MWNT) consists of several single-walled carbon nanotubes (SWNTs) that are concentrically nested. They show a predominant metallic behaviour since they have several shells and larger diameters than SWNTs. Due to their larger diameter, they show less distinct one-dimensional features.

MWNTs take an intermediate position between the world of identical molecules and disordered solids. On one hand, they can be considered as a set of seamlessly rolled up graphene sheets which are put one into another. In this respect, they have to be classified as perfect molecules. On the other hand, their typical length of several micrometers and diameters up to 100 *nm* exceed by far the dimensions of most other molecular systems. Their large size allows the occurrence of imperfections of the atomic structure, without turning the molecule into a completely different one, what would be the case for smaller systems. Such imperfections are introduced, for instance, by atomic displacements and adsorbates on the outermost nanotube shell. In this sense, MWNTs represent a disordered molecular system, in which electronic transport is influenced both by the molecular wavefunctions and the imperfections of the atomic structure [94].

In the last years, large effort has been made in order to clarify and characterize the transport properties of MWNTs [95]. One main reason for that is the fundamental interest in electronic transport on a molecular scale, which is most easily accessed with MWNTs. Furthermore, a variety of microelectronic devices bear the perspective of being assembled by nanotubes [96, 97].

Despite the extensive efforts, the electronic properties of MWNTs have not been clarified to a satisfying extent. For example, the interaction of adjacent nanotube shells is not clear, since in the measurement only the outermost shell is contacted. If only the outer-

most shell of a structural perfect MWNT is contacted, then only this shell will contribute to the current transport. The current transport through the inner shells is hindered and requires intertube tunnelling [98]. Intertube tunnelling will be additionally hindered if an adjacent shell is semiconducting.

Generally, the electronic properties of a MWNT will largely depend on the fabrication method (arc discharge, evaporation, catalytic chemical vapour deposition) and the treatment after growth (cleaning, oxidation, ultrasound, lithography). MWNTs with very high structural perfection have been produced by arc-discharge evaporation using a pure carbon arc. Ballistic transport has been reported for unprocessed nanotube material obtained by this method [99, 100].

To properly exploit the potential of MWNTs, it is very important to achieve conduction through all of their (metallic) layers. This might be possible by alloying formation or contacting open-ended MWNTs. Relatively low contact resistances ($< 5 \text{ k}\Omega/\text{sq}$) have been reported for instance by TiC formation after annealing of Ti/Au contacts between 600 and 800 °C [101]. In particular, alloy formation will be crucial if the outermost shell is semiconducting. This avoids the possibility that the MWNT is only contacted via a Schottky barrier. A Schottky barrier would considerably increase the contact resistance and make the transport gate dependent. This effect has been experimentally observed during thinning of a MWNT by electric breakdown [102].

2.2.2 Dispersion of Nanotubes

Nano-scale dimensions of CNTs turn dispersion into a challenge, since as the surface area of a particle increases, so does the attractive forces between aggregates [103]. High aspect ratios, combined with high flexibilities [104], increase the possibility of nanotube entanglement and close packing. The low dispersibility stems from the tendency of pristine nanotubes to assemble into bundles or ropes, which contain hundreds of close-packed CNT tightly bound by van der Waals attraction energy of $500 \text{ eV}/\mu\text{m}$ of tube-tube contact [105].

CNTs have been dispersed in polymers, surfactants and different organic solvents. Bonard *et al.* [83] noted that stable dispersion of nanotubes could not be formed in organic solvents such as ethanol, methanol and acetone. Nanotubes in these solvents have a tendency to form large aggregates of about $100 \mu\text{m}$, which sediment rapidly. Nanotubes also exhibit poor sensitivity to inorganic solvents due to the poor reactivity of the closed graphene structure. The method of synthesis of the nanotubes also highly influ-

ences on their dispersion. Highly polar solvents such as *N,N*-dimethylformamide (DMF), *N*-methylpyrrolidinone (NMP), and hexamethylphosphoramide (HMPA) were found to properly disperse SWNTs prepared by laser-oven [106]. In addition, stable suspensions of SWNTs were prepared by sonicating purified material in DMF [107]. Purified SWNTs obtained by oxidation were found to dissolve in aromatic amines [108], what was explained by the formation of charge-transfer complexes between amine solvent molecules and SWNTs. The dispersibility of SWNTs prepared by the HiPco method was studied in several organic solvents and investigations by UV/VIS absorption spectroscopy have shown that 1,2-dichlorobenzene is the most appropriate medium [109].

2.2.2.1 The effect of surfactants

Dispersing agents, such as surface-active agents, have been used to disperse fine particles of hydrophobic materials in aqueous solution [110, 111]. In general, there are three principles for dispersing fine particles in water [112]: (i) the repulsion between the particles with their zeta potentials, (ii) the steric hindrance of the adsorption layer, and (iii) the reduction of hydrophobic linkages among dispersed particles.

One can understand the effect of adding a charged surfactant by considering Stokes' Law [113] for the rate of sedimentation of a dispersed system:

$$\frac{dx}{dt} = \frac{d^2(p_1 - p_2)g}{18\eta} \quad (2.1)$$

where d is the size of the particle, p_1 and p_2 are the densities of the solid and liquid, g is the acceleration due to gravity and η is the viscosity of the liquid.

The charged surfactant produces a potential between the particles called the Zeta Potential (ζ), derived by Smoluchowski [114] as

$$\mu = \frac{\zeta\epsilon}{\eta} \quad (2.2)$$

where μ is the electrophoretic mobility and ϵ is the permittivity of the liquid.

As ζ rises, the repulsion between the particles becomes stronger and the stability of the dispersion system gets higher. As $\zeta \rightarrow 0$, the electrostatic build up is relaxed, allowing easier aggregation. When the absolute value of ζ is higher than 25 mV colloids are very stable, but at $\zeta = 0$ coagulation occurs.

In the case of nanotubes in a water solution, if the nanotubes are close enough to each

other they will fall into the secondary minimum and flocculate. They can be temporarily separated again by sonication, but this is followed by a slower process of re-flocculation making the colloid unstable [115]. By adding a surfactant, the particles are kept apart through increased electrostatic repulsion.

Surfactants provide one of the most efficient and non-intrusive ways of preparing stable CNT dispersions. This non-covalent method is straightforward and classically employed to disperse both organic and inorganic particles in aqueous solutions. The nature of surfactant, its concentration and type of interaction are known to play a crucial role in the phase behaviour of classical colloids [116] as well as carbon nanotubes [117]. Surfactants are classified in three types according to the charge types of their hydrophilic “heads”: non-ionic, cationic or anionic. They may have non-polar and lipophilic “tails” with hydrocarbons. The hydrophile-lipophilic balance (HLB) between head and tail can be used as a measure to determine the effect of surfactant on the stability of the dispersion of nanotubes in water. In principle, a more stable dispersion of nanotubes is achieved with surfactants that have lipophilic alkyl chain lengths equal to that of a decyl group or longer. Recently, however, it has been shown that the dispersion state of the nanotubes does not depend on the total solubility parameter of solvents or the HLB value of the surfactant, but on the dispersive component of the solubility parameter. Stable nanotube dispersions were obtained when the dispersing media had dispersive component values higher than $16.5 \text{ MPa}^{1/2}$ and molar volumes larger than $179.5 \text{ cm}^3/\text{mol}$ [118]. Also to be considered is the concentration of surfactants in water, which should not exceed in much the critical micellar concentration (CMC) of the surfactant. Above this concentration, surfaces are saturated by the surfactant and the remaining surfactant molecules begin to aggregate into micelles. In a surfactant micelle both the head and tail groups adopt a position that maximizes their interactions with like groups only.

Water-nanotube suspensions containing the ionic surfactant sodium dodecylsulphate (SDS) are often seen in the literature as stable for several weeks with only a few nanotubes aggregates [119, 120]. However, some groups have demonstrated insufficient debundling power of the this surfactant due to charge-repulsions [121]. Moore *et al.* [122] studied a series of anionic, cationic and non-ionic surfactants for their ability to suspend individual single-walled nanotubes. A non-ionic surfactant’s ability to suspend nanotubes appears to be due mostly to the size of the hydrophilic group, with higher molecular weights suspending more nanotube material because of enhanced steric stabilization with longer polymeric groups. Whitsitt and Barron [123] explained the high efficiency in dispersing SWNTs of the surfactant dodecyl-trimethylammonium bromide as a consequence of the pH stability of

the surfactant-SWNT interaction.

Some controversy exists as to the form taken by a nanotube dispersed in a surfactant solution. It has been postulated that SWNTs form the core of cylindrical micelles of surfactants (Fig. 2.7a) or are coated by adsorbed hemimicellar surfactants (Fig. 2.7b) [124, 125]. Yurekli *et al.* [117], however, refute the formation of cylindrical micelles in aqueous dispersions of SDS and suggest that structureless random adsorption with no preferential arrangement of the head and tail of the surfactants is responsible for the stabilization of the dispersion (Fig. 2.7c).

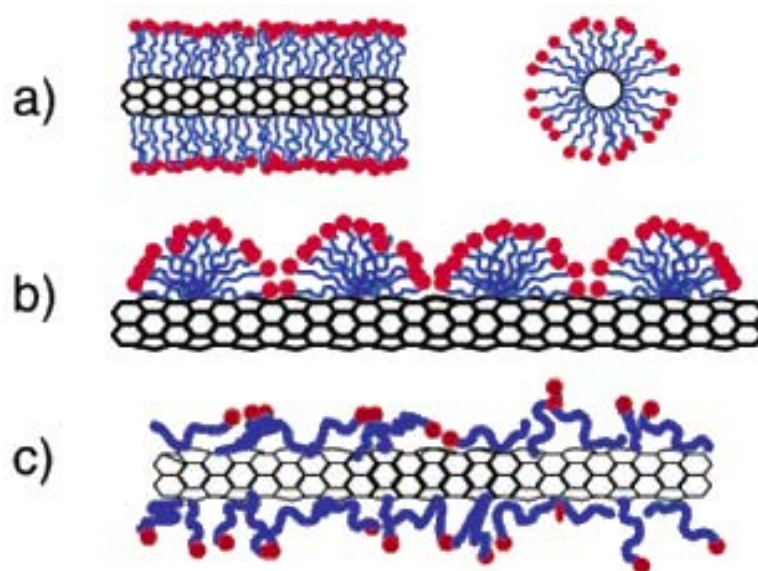


Fig. 2.7: Schematic representations of different mechanisms by which surfactants help disperse SWNTs [After Yurekli, 2004]. (a) SWNT encapsulated in a cylindrical surfactant micelle (right: cross section view); (b) hemimicellar adsorption of surfactant molecules on a SWNT; and (c) random adsorption of surfactant molecules on a SWNT.

2.2.2.2 Dispersion techniques

Mechanical methods and methods that are designed to alter the surface energy of the solids (physically or chemically) have been employed in order to obtain stable and reproducible dispersions of individual CNTs. Ultrasonic dispersion, for example, uses sound waves above the limits of human audibility to separate particles in a liquid. Frequencies greater than 18 kHz are considered to be ultrasonic, and dispersion occurs with the collapse and implosion of myriad cavitation bubbles throughout an ultrasonically activated

liquid. Czerw *et al.* [126] noted that extremely strong sonication with a sonic probe was required to disperse the nanotubes. O'Connell *et al.* found that sonication does not substantially damage nanotube sidewalls [127]. With high shear, these ropes can be untangled, but it is extremely difficult to further disperse them at the single-tube level. However, this limitation can be overcome by introducing various functional groups on the CNT surface that can help dispersion in a composite material. The surface functionalization of CNTs aid to improve their chemical compatibility with the target medium, reducing their tendency to agglomerate [128].

2.2.3 Applications of Carbon Nanotubes

Among the many applications that have been envisioned for CNTs, polymer composites [129], anti-static coatings [130], field-effect transistors [131], gas sensors [132], pH sensors [133], field-emission displays [134], and solar cell electrodes [135] appear to be the most promising areas. CNTs have been considered to be novel components for molecular electronics and for integration into conventional circuits [136–138].

The unique structural and mechanical properties of CNTs make them ideal candidates for incorporation into new families of composite materials. Interestingly, CNT-polymer composites, could be tougher and more scratch-resistant than any other materials [139–142].

Recently, CNTs have been used as field-emission electron sources [143, 144]. This technology finds applications in the construction of flat panel displays and X-rays to microwave generators [145–148].

Finally, storage of hydrogen on CNTs could represent a great development on fuel-cells and a milestone toward energy-clean systems. However, despite the exciting potential and the progress made so far, the results are controversial. For example, there have been many reports claiming high and efficient hydrogen storage on CNTs that, however, have often been disputed [149–152]. The highest reported hydrogen storage capacity on SWNTs exceeds 10 *wt. - %* and the smallest values approach zero, with the main reason for these discrepancies being the differences in CNT sample quality (e.g. production method, purification, handling, etc).

2.2.4 Percolation of conductive additives

In selecting a conductive additive, there are three primary considerations: (a) intrinsic conductivity of the additive; (b) loading level; and (c) the geometry of the additive.

For a fixed intrinsic conductivity and geometry, the conductivity (or, inversely, the resistivity) of the compound undergoes a classic curve as a function of loading, as that shown in Fig. 2.8 [153]. At around 30% loading in this example, there is a sudden transition to a conductive compound. The sudden lowering of resistivity with loading is governed entirely by the geometry of the additive (assuming complete dispersion in the host material). For low resistivity, long conductive pathways are required, obtained only when there is a high enough density of particles to touch one another and form chains over long distances. Therefore, the key geometric element is the aspect ratio (length to diameter ratio) of the additive. In order to achieve a given conductivity, a low aspect ratio additive such as carbon black (which is roughly spherical) requires a higher loading (providing that all other matters such as dispersion are equal) than graphite fibres, for example, which have much higher aspect ratios.

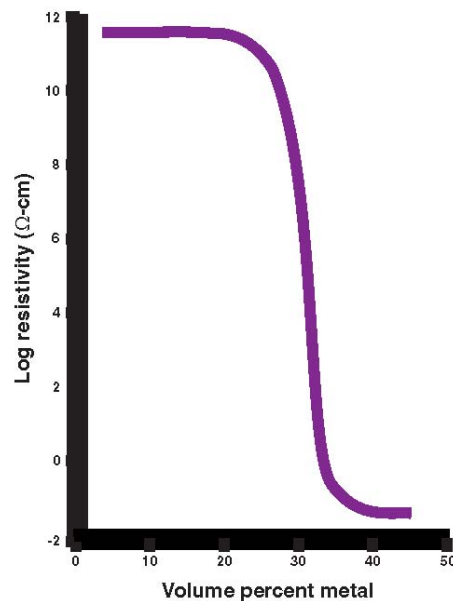


Fig. 2.8: Typical curve demonstrating the behaviour of the resistivity measured as a function of the loading of nanotubes [After Colbert, 2003].

The idea of percolation networks is shown in Fig. 2.9. Below the threshold loading, conductivity is poor, but increases suddenly and significantly above the threshold, as particles form long touching chains [154]. This percolation pathway theory can also be used

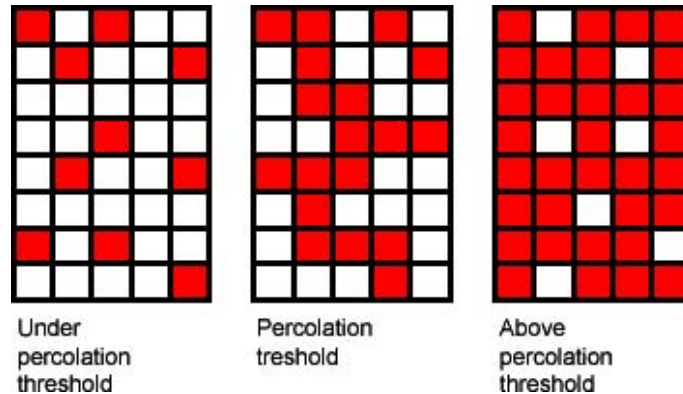


Fig. 2.9: Representation of percolation networks showing the concentration necessary to form a conducting pathway.

to partly describe the electrical conductivity in CNT composites. The basic principle is not about conductivity, but about arrangement and concentrations of CNTs in composite materials. If the insulating polymer is considered to be a matrix in which CNTs are randomly positioned, then the conductivity partly depends on the concentration of CNTs. Considering a red square in Fig. 2.9 as a CNT in the polymer matrix and that the composite (matrix) is supposed to conduct from top to bottom, one can say that, in the situation “below percolation threshold”, CNTs are not connected from top to bottom. In the second case, a sufficient number of CNTs is added to form a conducting pathway in this direction. This is the so-called “percolation threshold”. In the case (“above percolation threshold”), an enormous increase in conductivity is expected when the concentration of CNTs exceeds the percolation threshold. A typical representation for CNTs in composites could be as that depicted in Fig. 2.10.

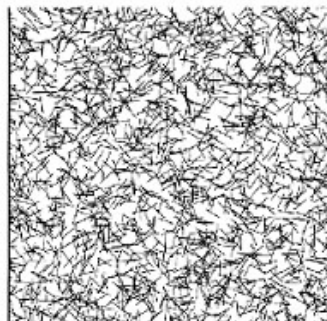


Fig. 2.10: A schematic representation of the surface of a CNT-polymer composite where CNTs percolate.

3. STATE OF THE ART

The literature review presented in this Chapter will familiarize the reader with the depth, breadth and scope of the research topic and establish the body of knowledge that this research will contribute to. It starts reviewing the transparent conductive coatings most studied as transparent electrodes (Section 3.1), paying special attention to coatings prepared by sol-gel techniques (Section 3.1.2). The last part of the Chapter reports the progress made on CNT-based composites and networks (Section 3.2). Finally, the definition of the problematic in the field of this research will serve as the baseline to justify the approach proposed here.

3.1 TCOs

3.1.1 TCO semiconductors for thin-film transparent electrodes

In general, TCO thin films that are in practical use as transparent electrodes are polycrystalline or amorphous (except for single crystals grown epitaxially) and exhibit a resistivity of the order of $10^{-3} \Omega.cm$ or less and an average transmittance above 80% in the visible range [155]. Thus, TCO semiconductors suitable for use as thin-film transparent electrodes should have a carrier concentration of the order of $10^{20} cm^{-3}$ or higher and a band gap energy above approximately 3 eV, i.e., degenerated *n*-type or *p*-type semiconductors. Historically, most research to develop TCO thin films as transparent electrodes has been conducted using *n*-type semiconductors; in practice, TCO thin films used as transparent electrodes are *n*-type semiconductors consisting of metal oxides. On the other hand, many reports have been also reported on *p*-type semiconductor-based thin films [156–159]. Nevertheless, there has been no report on the preparation of a *p*-type TCO thin film suitable for use as a practical transparent electrode.

For the purpose of obtaining lower resistivities, various TCO semiconductor materials

have been developed; *n*-type TCO semiconductors now available for thin-film transparent electrodes both as binary or ternary compounds are listed in Table 3.1, grouped by compound type and associated with their effective dopants [160]. It should be noted that, although the dopants have to be considered in their compound forms, they will be written along this text as they are normally presented in the literature, i.e. in their cation or anion forms (antimony-doped tin oxide, for example, will be written as *Sb* : *SnO*₂ rather than *Sb*₂*O*₃ : *SnO*₂).

One advantage about the use of binary compounds as TCO materials is the easier controlling of the chemical composition in the film depositions, compared to ternary compounds and multicomponent oxides. Up to now, various TCO thin films consisting of binary compounds such as *SnO*₂, *In*₂*O*₃, *ZnO* and *CdO* have been developed, with impurity-doped *SnO*₂ (*SnO*₂ : *Sb* and *SnO*₂ : *F*), impurity-doped *In*₂*O*₃ (*In*₂*O*₃ : *Sn*, known as ITO) and impurity-doped *ZnO* (*ZnO* : *Al* and *ZnO* : *Ga*) films in practical use [161]. In addition, it is well known that highly transparent and conducting thin films can also be prepared using metal oxides without intentional impurity doping [35]. The resulting films are *n*-type degenerated semiconductors with free electron concentrations of the order of 10^{20} cm^{-3} provided by native donors such as oxygen vacancies and/or interstitial metal atoms. However, since undoped oxide films were found to be unstable when used at a high temperature, binary compounds without impurity doping have proved unusable as practical transparent electrodes [162]. The reported effective dopants are also listed in Table 3.1, along with their associated binary compounds.

In addition to binary compounds, ternary compounds such as *Cd*₂*SnO*₄, *CdSnO*₃, *CdIn*₂*O*₄, *Zn*₂*SnO*₄, *MgIn*₂*O*₄, *CdSb*₂*O*₆ and *In*₄*Sn*₃*O*₁₂ have been developed [163–165]. Multicomponent oxides materials consisting of combinations of binary compound TCOs [166] or combinations of ternary compound TCOs have been also reported in the literature [167]. There are only a few reports on the effect of impurity doping, due to the lack of an effective dopant. As a result, TCO films fabricated from these ternary compounds are not in practical use yet.

From Table 3.1, one can see that TCO semiconductors for thin film transparent electrodes in practical use consist on metal oxides containing at least one of the following metal elements: *Zn*, *Cd*, *In* and *Sn*. Although producing a low resistivity thin film, it should be noted that *Cd*-containing TCO semiconductors such as *In*-doped *CdO* (*CdO* : *In*₂*O*₃), *Cd*₂*SnO*₄, *CdSnO*₃ and *CdIn*₂*O*₄ are of no practical use because of the toxicity of *Cd* [168]. For thin-film transparent electrodes, TCO semiconductors such as impurity-doped *ZnO*, *In*₂*O*₃ and *SnO*₂ and multicomponent oxides composed of combinations of these binary

Table 3.1: TCO semiconductors used as thin-film transparent electrodes.

Material	Dopant
<i>SnO₂</i>	<i>Sb, F, As, Nb, Ta</i>
<i>In₂O₃</i>	<i>Sn, Ge, Mo, F, Ti, Zr, Hf, Nb, Ta, W, Te</i>
<i>ZnO</i>	<i>Al, Ga, B, In, Y, Sc, F, V, Si, Ge, Ti, Zr, Hf</i>
<i>CdO</i>	<i>In, Sn</i>
<i>ZnO – SnO₂</i>	<i>Zn₂SnO₄, ZnSnO₃</i>
<i>ZnO – In₂O₃</i>	<i>Zn₂In₂O₅, Zn₃In₂O₆</i>
<i>In₂O₃ – SnO₂</i>	<i>In₄Sn₃O₁₂</i>
<i>CdO – SnO₂</i>	<i>Cd₂SnO₄, CdSnO₃</i>
<i>CdO – In₂O₃</i>	<i>CdIn₂O₄</i>
<i>GaInO₃, (Ga,In)₂O₃</i>	<i>Sn, Ge</i>
<i>CdSb₂O₆</i>	<i>Y</i>
<i>ZnO – In₂O₃ – SnO₂</i>	<i>Zn₂In₂O₅ - In₄Sn₃O₁₂</i>
<i>CdO – In₂O₃ – SnO₂</i>	<i>CdIn₂O₄ - Cd₂SnO₄</i>

compounds are the most suitable candidates for practical use.

3.1.2 TCO films made by the sol-gel technique

TCOs are usually prepared by chemical vapor deposition (CVD), physical vapor deposition (PVD) or by spray pyrolysis techniques [169, 170]. However, these methods require high manufacturing costs and are not appropriate for large-size substrates, besides presenting a relatively low deposition rate. Sol-gel techniques can be an advantageous alternative in this sense, once they provide a low manufacturing cost, uniform thickness of coating and require low processing temperature [1, 171, 172].

3.1.2.1 *In₂O₃* based coatings

Daoudi and co-authors [173] fabricated ITO multi-layered films by a dip coating process using tin and indium chlorides as precursors. A minimum global resistivity of $2.9 \times 10^{-3} \Omega.cm$ was obtained for 3 layer films annealed at 500 °C while the value of $2 \times 10^{-3} \Omega.cm$ was obtained for 5-layer films annealed at 600 °C. The resistivity of the films obtained by Tomonaga and Morimoto [174] was $2.8 \times 10^{-3} \Omega.cm$ for ITO coatings fired in air on non-alkali glass substrates and $6.2 \times 10^{-4} \Omega.cm$ after annealing in a hydrogen-containing atmosphere. The authors used spin coating for producing the films containing 8 mol – % Sn. Similar results were reported by ITO films produced by dip coating using an ethanol solution of

chlorides and surfactants [175]. Resistivities initially as low as $2 \times 10^{-3} \Omega.cm$ of 60 nm thick films were decreased by approximately one order ($2.5 \times 10^{-4} \Omega.cm$) after annealing in a mixture of N_2 and H_2 . Alam and Cameron [50] have deposited ITO thin films in glasses by sol gel using metal salts precursors ($InCl_3$ and $SnCl_4$) and organic solvents as raw materials. The resistivity of the films containing 10 wt. – % Sn annealed at 600 °C in air is $1.5 \times 10^{-3} \Omega.cm$. The films present an optical transparency up to 93% from 400 to 900 nm and have an absorption edge at approximately 300 nm. Later, the same group [176] studied the influence of the annealing of the films in different atmospheres and found that the resistivity of the films had a minimum value of 8.5×10^{-4} , 9.8×10^{-4} and $8.0 \times 10^{-4} \Omega.cm$ with a Sn content of 10 wt. – % when annealed at 500 °C in air, oxygen and nitrogen, respectively. Shigeno and co-workers [177] have used indium dipropionate monohydroxide to produce ITO films by dip coating on glass substrates. In the field of dip coating and spin coating, a coating solution composed of a metal salt of an organic acid dissolved in organic acid seems to be unique. The minimum resistivity obtained after annealing was $3.1 \times 10^{-4} \Omega.cm$ for a film containing 6.9 at. – % Sn, which is compatible with the dip-coated films obtained by other authors ($3.3 \times 10^{-4} \Omega.cm$) [178].

Deposition of ITO in plastic substrates by sol-gel methods has also been published [179], using hydrolyzed silane as a binder. Resistivities not lower than $9 \times 10^{-2} \Omega.cm$ were observed in 570 nm thick films with transparency of 87% at 580 nm.

The transparency and resistivity properties of ITO films prepared by sol-gel methods are comparable to those prepared by other methods like CVD and sputtering. The application of those films in practical use, however, possess problems because of the relatively high annealing temperature required in order to obtain a high conductivity.

3.1.2.2 SnO_2 based films

Lee *et al.* [180] prepared tin oxide films by spin, dip and spray coating from a stable tin (IV) isopropoxide solution, obtaining transmittance higher than 90% in the visible range of light and resistivity as low as $1 \times 10^{-2} \Omega.cm$.

Sb : SnO_2 (ATO) coatings have been also prepared by sol-gel [181, 182]. Similar results of undoped tin oxide were obtained by Goebbert and co-authors [51], who prepared antimony-doped tin oxide (ATO) coatings on glass and plastic substrates by spin and dip coating, obtaining the lowest resistivity value of $1.7 \times 10^{-2} \Omega.cm$ at sintering temperature of 550 °C. ATO films have also been deposited on glass substrates by spray coating [183]. The properties of the coatings are similar to those obtained by dip coating [33], with a

thickness of up to 120 nm, resistivity of $2 \times 10^{-2} \Omega.cm$ and transmission around 85% in the visible. The resistivity values are, however, higher than those obtained by sputtering, spray pyrolysis and CVD processing. On the other hand, Giraldi *et al.* [184] have recently produced ATO films from the polymeric precursor method using spin coating technique, and a resistivity as low as $6.5 \times 10^{-3} \Omega.cm$ for a 988 nm thick film and transparency in the order of 80% was obtained.

Sol-gel fabrication of $F : SnO_2$ (FTO) films has been also reported [185] and an optimum F/Sn atomic ratio of 10.8% has yielded the minimum resistivity value of $\sim 1 \Omega.cm$. This value is lower than that obtained by Cachet *et al.* [186] ($\sim 20 \Omega.cm$) but higher than reported by Ray and co-authors [187] ($\sim 10^{-2} \Omega.cm$). The lowest value of resistivity of $9.1 \times 10^{-2} \Omega.cm$ was achieved by FTO films with compositions of $Sn : F = 97.5 : 2.5$, prepared by dip coating on soda lime silica glass [188].

The resistivities presented by SnO_2 -based coatings prepared by sol-gel seem to remain unchanged in the last years, laying in the order of $10^{-2} \Omega.cm$. Such electrical properties are still much inferior than that presented by ITO systems.

3.1.2.3 ZnO based films

Undoped ZnO films were produced by the spin coating method [67], and a minimum resistivity of $28 \Omega.cm$ was obtained for a 10-cycle spin-coating film sintered in air at 525 °C. Later, the same group [189] investigated the effects of a post-annealing of the undoped ZnO films in hydrogen atmosphere (350 °C for 3 h) and the film resistivity decreased to $2.2 \times 10^{-1} \Omega.cm$. Lee and Park [190, 191] prepared pure and doped ZnO thin films by sol-gel using Al, In and Sn as dopants. Higher conductivities and transmittances were shown in preferred (0 0 2) oriented films. Undoped ZnO films presented the lowest resistivity of $9.9 \times 10^{-2} \Omega.cm$ after a second heat treatment at 500 °C. Al : ZnO films with 1 at. - %Al reached an electrical resistivity value of $1.1 \times 10^{-2} \Omega.cm$ and transmittance over 90% in the visible range, much promising than others reported in the literature [192].

Aluminium doped zinc oxide (AZO) films have been prepared by dip coating using an alcoholic non-alkoxide route [193, 194], showing resistivities between 1.3 and $7.2 \times 10^{-3} \Omega.cm$, with transmittance of 80 – 90% within the visible wavelength. Their lowest resistivity was achieved in films containing 2 wt. - % of aluminium, post-heated at 600 °C and annealed at 450 °C in forming gas. Resistivities in the same order of $10^{-3} \Omega.cm$ [195] were obtained by dip coating of 10 layers AZO films in fused silica substrates, sintered in a flux of forming gas (N_2/H_2) at 400 °C for 2 h. Even lower resistivities, in the order of

$10^{-4} \Omega.cm$, have been reported by AZO films prepared by dip coating from zinc acetate and aluminium nitrate (or chloride) precursor solutions [182, 196], with transmittance as high as 90% at 550 nm. These values are comparable to those obtained by ITO films in practical use nowadays.

Films of ZnO doped with gallium (GZO) have been also studied [197, 198]. An optimum doping concentration of 2 at. – % gallium and annealing at 550 °C provided the lowest resistivity of $6.8 \times 10^{-3} \Omega.cm$. The same group [199] studied ZnO mixed with ZrO_2 and the films obtained by drain coating on glass slides presented a minimum resistivity of $7.2 \times 10^{-2} \Omega.cm$ using a doping concentration of 1.5 at. – % Zr.

CdO – ZnO films with above 90% optical transmission in the visible region have been prepared by dip coating on glass slides [200]. The resistivity of pure ZnO films decreased by 4 orders of magnitude with the addition of Cd. The films exhibit an abrupt resistivity decrease from 10^3 to $10^{-1} \Omega.cm$ when varying the content of Cd in the film.

The use of a rare-earth impurity (*Y*) as a dopant in ZnO has been also demonstrated [201]. YZO films obtained by dip coating on corning glass substrates present a minimum resistivity of $3.5 \times 10^{-2} \Omega.cm$ when diethanolamine (DEA) is used as stabilizer. Doping zinc oxide with indium (IZO) was the alternative found by Kim *et al.* [202]. The lowest resistivity achieved was $4.48 \times 10^{-2} \Omega.cm$ for films prepared at 600 °C containing $Zn/(Zn + In) = 0.33$.

3.1.2.4 Ternary compounds coatings

A few TCO coatings consisting of ternary compounds deposited by sol-gel have been reported, such as Cd_2SnO_4 [203, 204], $ZnGa_2O_4$ [205], In_6WO_{12} [206] and Zn_2SnO_4 [207]. Lopez and co-workers [208] have deposited Cd_2SnO_4 films on glass using a dip-coating technique. They obtained films with optical transmission of 78 % with electrical conductivities as high as $2 \times 10^4 (\Omega.m)^{-1}$. Recently, Kurz and Aegerter [165] have reported on the preparation of zinc stannate on glass substrates by spin coating. The coatings have a transmission of 85% in the visible range and a resistivity of 10 $\Omega.cm$ without post-annealing and 3 $\Omega.cm$ after annealing in forming gas for 5 h at 300 °C. Due to the high resistivities presented by ternary compounds coatings, they are not in practical use yet.

3.2 CNT composites and networks

Some years ago, most of the applications of CNTs were related to the use of pure CNTs, not nanocomposites [209–211]. The few reports on the development of nanocomposites using CNTs as reinforcing inclusions in a polymer matrix were probably due to the difficulty in dispersing the nanotubes, which have a non-reactive surface.

The embedding of carbon nanotubes in polymeric matrices such as polythiophene, polystyrene and polyaniline to make various nanocomposite materials is now a popular subject in nanotube research [212, 213]. The research is fuelled by the hope of delivering the properties of CNTs to the composites [214, 215]. Among the various conducting polymers, polythiophene (PT) has always been one of the more likely candidates because of its high stability of doped and undoped states, ease of structural modification and controllable electrochemical behaviour. The highly substituted thiophenes, in particular, have been the subject of intense research and development as candidate material in the areas of microelectronics, electrode materials, opto-electronics and sensors [216–218].

The general methods used to prepare polymer-carbon nanotube composites are:

- (a) ultrasonication of carbon nanotubes or surface functionalized of carbon nanotubes in the presence of matrix polymers;
- (b) *in situ* polymerization of monomers of matrix polymer in the presence of carbon nanotubes; and
- (c) polymerization of the matrix polymer from the surface of the nanotube.

Carbon nanotubes functionalized with polymers were found to produce a good dispersion of carbon nanotubes in the polymer matrices of nanocomposites [219, 220]. Lin and co-workers [221] reported that the use of polymers that are structurally close to the matrix polymer for functionalization of CNTs is a good approach for the development of polymeric nanocomposites.

Kaiser *et al.* [222] have used conductive CNTs as fillers in a polymer matrix to enhance conductivity, but the resulting nanocomposites exhibited little or no transparency in the visible range. Coleman *et al.* [223] and Curran *et al.* [214] reported conjugated polymer-CNT composites using multi-walled CNTs where the percolation concentration of the CNTs exceeded 5 *wt. %*. The resulting nanocomposites were black with no transparency in the visible region. Shaffer and Windle [224] reported the conductivity of a

multi-walled CNT/poly(vinyl alcohol) composite with percolation above 5 wt. – % nano-tube loading, resulting in a black nanocomposite. The same group [225] reported another multi-walled CNT composite with an epoxy resin, which achieved percolation below 0.04 wt. – %. An optical micrograph of the CNT/epoxy resin composite was reported: the CNT phase was separated from the epoxy resin and several millimetres of resin-rich domains are revealed, indicating that the dispersion of CNTs in this material was very poor. Preliminary measurements of the conductivity of a CNT/poly(methyl methacrylate) (PMMA) composite were measured on a fiber [226]. The level of conductivity was relatively high ($1.18 \times 10^{-3} S.cm^{-1}$) at 1.3 wt. – % SWNT loading. However, the optical transparency in the visible range was not determined for the fiber sample. The mechanical properties of these fibers were much lower than the predicted value, which implies that the CNTs were not fully dispersed. Connel *et al.* [227] have studied different ways to redisperse CNTs into polymer matrices, obtaining more promising results when the polymers were synthesized in the presence of the CNTs. The nanocomposites showed high retention of optical transparency in the visible range, electrical conductivity and high thermal stability, meeting the requirements for the use in aerospace applications.

Several reports are found describing the production of electrically conducting films containing CNTs in loading levels varying from 0.01 [228–230] to 4 wt. – % [231–234]. In most cases, the electrical conductivity obtained is not sufficient for the use in flat panel displays, but only in electrostatic charge mitigation applications [130]. To improve the conductivity, films fabricated from SWNT solutions have also been investigated [235]. In previously published work, SWNTs were first dispersed in aqueous solutions, then thin films were fabricated by wet coating techniques [236,237] or filtering through membrane and transferring to substrates thereafter [238,239]. Thin films made by these methods (normally referred as networks) show much better conductivity than the CNT-based composites, although 30% transmission at a wavelength of 3 μm were reported. Since SWNTs are insoluble in most organic solvents and water, a surfactant (such as Triton X-100 or SDS) has to be used in order to provide a stable SWNT solution. However, the surfactant adsorbed on the surface of SWNTs will greatly affect the electrical properties of the networks. Washing away the surfactant has been reported, although this process is not easy to be scaled up and the bonding between the SWNT networks and the substrate is quite weak. In most reports of CNT used as transparent conductive films, nothing is mentioned about the adhesion of the films to the substrate.

Recently, the use of single-walled carbon nanotube films as the transparent anode in a solar cell was also claimed [135]. However, the transparency of the CNT films was

low (around 45% for a sheet resistance of $282 \Omega/sq$) and the device configuration was suboptimal, using an active absorber layer 800 nm thick. The performance of the resulting cells was significantly below efficiencies achieved in similar cells using ITO.

3.3 Sum up of the literature review: Identification of the problematic

With respect to transparent conductive oxides, although the obtainable electrical properties of coatings are strongly dependent on the deposition method as well as on the deposition conditions, TCO films with a low resistivity of the order of $10^{-5} \Omega.cm$ can only be prepared with impurity-doped binary compounds. For thin-film transparent electrodes, TCO semiconductors such as impurity-doped ZnO , In_2O_3 and SnO_2 and multicomponent oxides composed of combinations of these binary compounds are the most suitable candidates for practical use. Specially ITO thin films prepared by magnetron sputtering (MSP) with a resistivity of the order of $10^{-4} \Omega.cm$ are commercially available at present, although resistivities of the order of $10^{-5} \Omega.cm$ are also possible to obtain using higher temperatures and/or pulsed laser deposition (PLD) methods. The minimum resistivities obtained by SnO_2 and In_2O_3 films have essentially remained unchanged in the past twenty years. All tentatives to produce transparent conductive materials with a high conductivity as that presented by ITO have failed, except for some reports on AZO films. Their preparation, however, requires high temperatures and post-annealing in reducing atmospheres, what enhances the costs prices and complicates large-scale production of the films. This set of factors motivates the study of alternative materials for opto-electronic devices which are not based on semiconductor oxides and that require lower curing temperatures.

Carbon nanotubes, on the other hand, have been recently explored as additional conductive structures in composites and are promising candidates for transparent conductive systems due to their small diameters, high aspect ratio and high conductivity. In most cases, however, the electrical conductivity obtained by networks and composites is much inferior than that of ITO films, only sufficient for application in electrostatic charge mitigation. Many challenges for integration of this unique nano-material include uniform dispersions and the proper removal of the surfactant in CNT networks. Moreover, the adhesion of the networks to the substrates has to be considered for an appropriate comparison with ITO films, although most networks reported in the literature have shown poor adherence

to the substrates. Therefore, there is a need to improve the fabrication processes so as to achieve CNT thin films with improved electrical and optical transmission properties.

4. OBJECTIVE

Considering the limitations of ITO such as the scarcity of indium, its high cost and brittleness of the films, it was the objective of this work to study new alternative materials which could be used as transparent conductive coatings in opto-electronics devices. For this purpose, materials with excellent transparency in the visible range and high electrical conductivities are required. Taking advantage on the high aspect ratio and high electrical conductivity of carbon nanotubes, the potential of these nanomaterials in the form of networks as well as in composites with both conducting and insulating matrices for the obtention of transparent conductive devices was investigated in this work. The tentatives reported in the literature failed in obtaining high electrical conductivity, what has been mainly attributed to inefficient dispersion of the CNTs in the matrix. In this work, an alternative surfactant to sodium dodecyl sulphate (SDS) normally reported for the dispersion of nanotubes was studied (hexadecyltrimethyl ammonium chloride, HDTAC), due to its longer carbon chains in comparison with SDS. In addition, a high shear processing after the ultrasonication of the dispersions was applied as a tentative to obtain finer dispersions. Focusing on cost benefits multi-walled carbon nanotubes (MWNTs) were investigated, due to their lower cost in comparison with SWNTs.

The three CNT-based systems investigated were:

1. Networks of MWNTs deposited on borosilicate glass substrates, with and without the addition of adhesion promoters in the dispersion used as precursor for the networks. Parameters such as the behaviour of the sheet resistance with the concentration of CNTs and the temperature of sintering were studied and analyzed. The performance of the networks was compared with others presented in the literature and with ITO.
2. Antimony-doped tin oxide (ATO) and ATO/MWNT composites deposited on borosilicate glass substrates. ATO is one of the most studied TCO materials for replacement of ITO, but seems to have reached its physical limits with respect to electrical prop-

erties. Since this water-based material has a high transparency in the visible range but still suffers from inferior electrical properties in comparison with ITO, it was the objective of this part of the work to improve its conductivity by the addition of CNTs. New ATO/CNT composites were developed and their performance was compared to the ATO matrix and to ITO.

3. A titanium dioxide-based sol normally used for the production of films with high refractive index [240] was investigated as a matrix for CNT-based composites since this sol produces high transparent films in the visible range. In this part of the work, the electrical conductivity provided by the CNTs to the initially insulating matrix was studied.

Aspects such as the sheet resistance, resistivity, adhesion of the coatings to the substrate and transparency in the visible range were studied. The structural characterization of the powders and films was performed by different techniques such as transmission electron microscopy, scanning electron microscopy, white light interferometer, atomic force microscopy and Raman spectroscopy. The dispersions were characterized by ultrafine particle analysis and zeta potential measurements. Electrical properties of the coatings i.e. sheet resistance were measured by the four points techniques and the thickness was determined by profilometry and/or ellipsometry. The transmittance of the coatings in the visible range was determined by UV-VIS spectroscopy.

5. EXPERIMENTAL

This Chapter describes the detailed experimental work carried out in this research. It is divided in 3 Sections: MWNT Networks (5.1), ATO/MWNT nanocomposites (5.2) and TiO_2 /MWNT nanocomposites (5.3). Each Section describes the experiments realised for the study of the different systems, including the preparation and characterization of powders, sols and coatings. Technical data (chemicals, apparatus) are written along the text, but are also summarized in Tables listed in the Appendix (Chapter 9).

5.1 MWNT networks

The study of MWNT networks was motivated by the interesting properties of CNTs, mainly their high aspect ratio and high electrical conductivity. The formation of adherent and conducting CNT networks on different substrates could open new venues in the transparent electronics industry. SWNT networks studies have been recently presented in the literature, as already pointed out in Section 3.2. In this work, however, MWNTs were chosen as materials of study due to their lower price in comparison with SWNTs.

5.1.1 Characterization of the MWNT powder

As-received very thin (10 nm outer diameter) MWNTs (Nanocyl S.A.) were investigated by different techniques. The morphology of the powder was examined with a scanning electron microscope (JSM 6400F, JEOL). The second electron image was formed by exciting the sample with a primary electron beam under 10 kV accelerating voltage. To obtain a charge free surface imaging, the sample was sputtered with a gold film with the SCD 030 (Balzers) using a current of 25 mA for 40 s. The structure and morphology of the MWNTs were also studied using high resolution transmission electron microscopy (HRTEM: CM 200 FED, Philips). Investigation was carried out at an accelerating voltage of 200 kV and

structure imaging was recorded.

Raman spectroscopy (LabRAMAN ARAMIS, Version 010, DILOR/Jobin HORIBA/Yvon equipment) accoupled with a CCD Detector, *He Ne* Laser 632.8 nm was used in this work to identify the MWNT in the networks. This technique has been appointed in the literature as an effective tool for the study of nanotubes, specially SWNTs, since it provides the diameter, chirality, type, and the aggregation state of nanotubes [241].

The thermal analysis of the powder was performed by Thermogravimetric Analysis (TG) [242] using a thermal analyzer STA 999C Jupiter (Netzsch)). For the measurement, 40 mg of the MWNT powder were placed in a Al_2O_3 crucible and then heated from room temperature to 1100 °C at a heating rate of 10 °C/min under synthetic air atmosphere.

Finally, X-Ray powder diffraction (XRD) was performed in order to verify the possible graphite crystal phase in the MWNT powder. The analysis was performed with a D500 model diffractometer (Siemens, radiation $CuK\alpha_1$) operating at 40 kV.

5.1.2 Surfactant-assisted dispersion of MWNTs

Although CNTs have remarkable electronic and mechanical properties, their potential applications can be limited to their insolubility in many solvents, due to strong intertube van der Waals interactions, as presented in Section 2.2.2. A good dispersion of CNTs is of most importance so as to prevent precipitation and hence allow the fabrication of homogeneous films with optical quality. The attachment of functional groups to the nanotubes sidewall could allow a more efficient dispersion of CNTs in liquids. Therefore, as-received functionalized MWNTs ($-COOH$ and $-NH_2$ functionalization groups) were investigated in this work.

The surfactant of choice was hexadecyl trimethyl ammonium chloride (HDTAC), which possess a longer carbon chain length than sodium dodecyl sulphate (SDS), the surfactant normally investigated in the literature for the dispersion of CNTs. Such hexadecyl chain is expected to provide a more efficient dispersion of CNTs in water than a shorter dodecyl chain. The concentration of SDS in water often used for the dispersion of CNTs is 1 wt.-% [85], while the concentration of nanotubes in the surfactants is 0.5 mg/ml [243]. In this work, however, a higher amount of MWNTs in the surfactant was studied, ranging from 1 – 10 mg/ml. The intention was to study the influence of the concentration of MWNTs in the properties of the networks formed. Consequently, the concentration of HDTAC in water utilized was also higher than that presented in the literature, varying from 1 to 5 wt.-%, since more surfactant molecules are necessary to properly maintain the

MWNTs suspended in water.

Stirring and ultrasonic mixing were applied for 10 *min* each. Subsequently, the suspension was ultrasonically dispersed for 20 *min* with an ultrasonic disintegrator Branson Sonifier®450, operating for 15 *min* with duty cycle of 40% and output control 9. In this method, the liquid jet streams resulting from ultrasonic cavitation overcome the van der Waals forces between the nanotubes, separating them. Finally, a high shear processor treatment using a Microfluidizer®M110-Y Microfluidics (Fig. 5.1a), pressure of 1500 *Bar* and cylinders of 300 and 87 μm was employed. This high shear fluid processing disperses big agglomerates into uniform smaller particles and forms stable dispersions by utilizing a high-pressure liquid stream that collides at ultra-high velocities in precisely defined diamond micro channels. Combined shear and impact forces act upon the liquid systems to create finer, more uniform dispersions. A schematic showing the equipment is demonstrated in Fig. 5.1b. In order to remove possible agglomerates remaining in the dispersions, filtration using a 10 μm filter was performed. The flow chart in Fig. 5.2 summarizes the MWNT dispersion process.

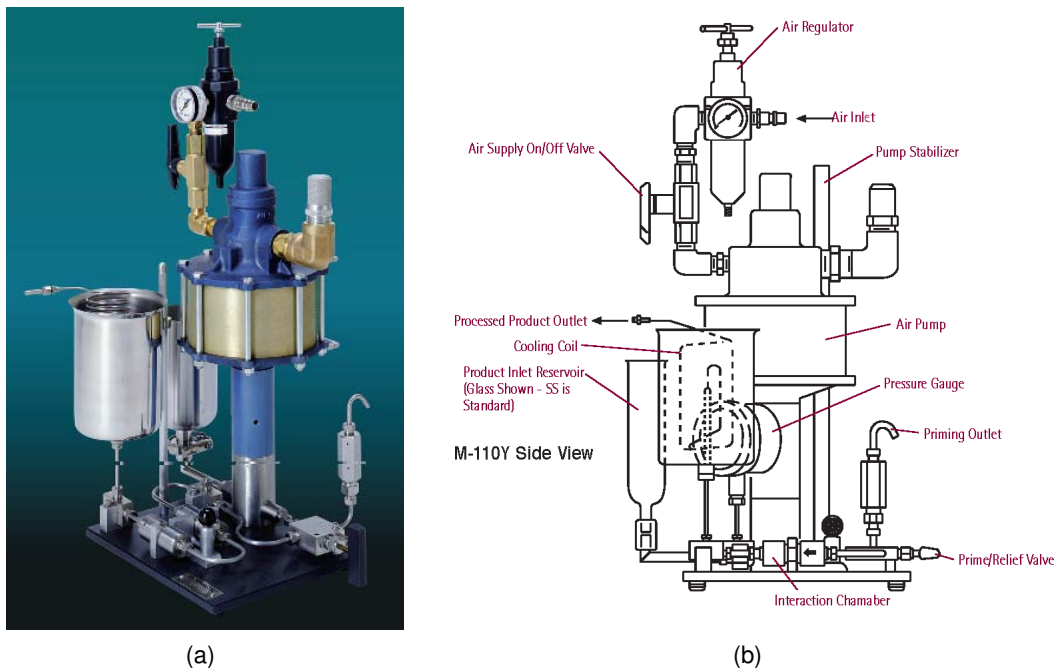


Fig. 5.1: High shear processor. (a) M110-Y Microfluidizer processor and (b) its schematic view.

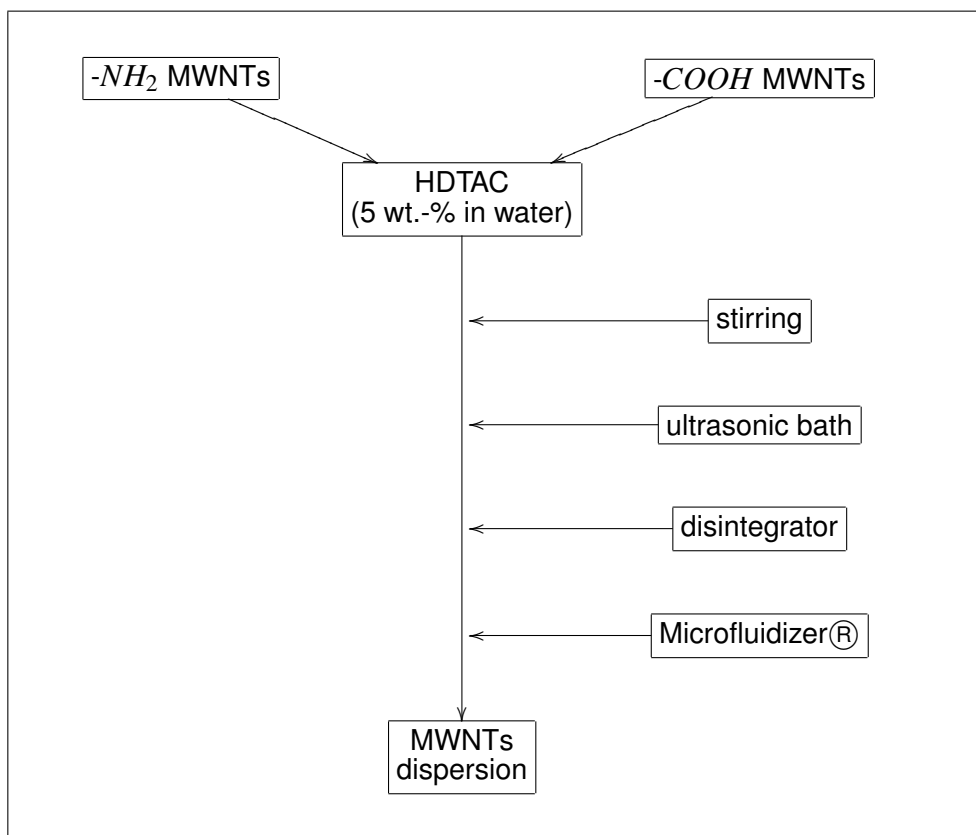


Fig. 5.2: Flow chart of the dispersion of MWNTs in HDTAC.

5.1.3 Characterization of the dispersion

Besides the difficulty in obtaining stable and homogeneous dispersions of CNTs, another complication is finding a valid method to evaluate their state of dispersion. Techniques such as atomic force microscopy (AFM) seem not to be representative of the whole sample; others like transmission and scanning electron microscopies (TEM and SEM, respectively) require pre-treatment with gold or carbon sputtering, which might cause a defect in the original pattern of the composite. Also characterization methods such as ultrafine particle analysis (UPA) and dynamic light scattering (DLS) are not appropriate, since CNTs are not spherical particles. Therefore, zeta potential measurements were performed in this study as an effective way to determine the stability of the MWNTs in the surfactant. Generally, particles tend to avoid coagulation by electrostatic repulsion above certain surface potentials, usually 25 mV . Thus, by knowing the magnitude of the net surface potential, one can predict the possible aggregation behaviour of CNTs. For example, a high surface

charge on a CNT surface will indicate a preference for considerable electrostatic repulsion within nanotube aggregates. A low nanotube surface charge will be insufficient to overcome the van der Waals' forces between tubes, and will lead to a high degree of nanotube aggregation. For the measurement of the absolute zeta potential, MWNTs dispersed in HDTAC (5 wt.-% in water) with concentration of 3 mg/ml were investigated at Malvern facilities, using a Zetasizer Nano System from Malvern Instruments.

5.1.4 Preparation of the networks

MWNT networks were prepared by spin coating the dispersion of MWNTs in HDTAC on borosilicate glass substrates.

The glass substrate of choice was Borofloat33® (Schott). It is a highly chemically resistant borosilicate glass with low thermal expansion produced by the float process. It has a mirror surface like quality, high thermal resistance and transmission. Moreover, it does not contain alkaline earth elements in its composition. The composition of the glass was determined using atomic emission spectroscopy with inductively coupled plasma (ICP-AES, Ultima 2, Horiba Jobin Yvon). 30 mg of the glass in powder form were dissolved in 3 ml concentrated HNO_3 and 1 ml concentrated HF at 150 °C for 5 h. After cooling down to room temperature, the solution was diluted with deionized water and analyzed.

Spin coating (spin coater model 1001 CPS II, Convac) was chosen as deposition method because it is a fast technique which requires only a small amount of sol in order to form the coatings. A final speed of 2500 rpm for 15 s was used during the deposition. The sintering of the coatings deposited on borosilicate was carried out in a furnace in air (Carbolite) at temperatures varying from 150 to 400 °C for 5 to 30 min. In order to improve the adherence of the networks to the glass substrate, 0.5 vol.-% of an adhesion promoter prepared from Glycidyloxypropyl-triethoxysilane (GPTES) and Levasil®200S/30 (1:1) [244] was added to the coating sol.

5.1.5 Characterization of the networks

The MWNT networks deposited on borosilicate were examined by transmission electron microscopy (JEM 200CX, JEOL) accoupled with energy dispersive X-ray spectrometry (EDX, Noran Instruments), for a quantitative element analysis. High-resolution scanning electron microscope (SEM) equipped with a field emission gun (FEI Strata DB 235) at 5

kV acceleration voltage was used in the investigation of the surfaces. The topography of the networks was also analyzed by atomic force microscopy (AFM), using a Digital Instruments Multimode Nanoscope IIIa. The roughness of the networks was characterized with a White Light Interferometer (WLI), Zygo New View 5000. It is a 3D surface profiler that images surface detail and provides accurate measurements without contacting the surface. The measurements were carried out using a white light beam, divided within an optical objective. One portion is reflected from the tested part and the other from a high quality flat reference. A MetroPro software was used to convert the intensities into images.

The transmittance of networks with different MWNT concentrations was measured in the visible range by UV-VIS-Spectroscopy, using a CARY 5E UV-VIS-NIR spectrophotometer (Varian). The measurements were carried out at room temperature within the range 300 to 3000 *nm*. The transmission (*T*) was measured at normal incidence against air as reference.

The sheet resistance (R_{sq}) of the films was measured by the four-points technique (Napson Corporation, Model RT-70/RG-7S). The final results presented were the average value of at least 5 measurements in different parts of the surface. The results were correlated with different parameters such as the concentration of MWNTs in the network and the temperature of sintering.

Mechanical adhesion is an important property which is related with the durability of the coatings. Therefore, the adhesion of the MWNT networks in the substrates was examined. The procedure follows standard tape test [245] and consists of a visual observation after pulling off of a tape from the substrate. The layer is classified as either completely removed, partially removed or left on the substrate.

The surface hardness of the networks was evaluated through the pencil test [246]. First, the films are placed on a firm horizontal surface. Then, a pencil of known hardness is held firmly against the film at a 45° angle and pushed away from the operator in a 6.5 *mm* stroke. The process is initiated with the hardest pencil and continued down the scale of hardness until the pencil that will not damage the film. The classification of the drawing lead meets the following scale:

$$\frac{6B - 5B - 4B - 3B - 3B - B - HB - H - 2H \dots 6H}{\text{softer} \dots \dots \dots \text{harder}}$$

5.2 ATO/MWNT nanocomposites

Antimony doped tin oxide (ATO) films are known to present a low resistivity and high transparency at room temperature. Such films can find potential application in electro-optical systems. However, their electrical properties, mainly their electrical conductivity, are still inferior than that presented by ITO. The objective of this part of the work was to improve the electrical conductivity of ATO systems, which are less expensive alternatives to ITO. The approach used was the addition of CNTs as additional conductive particles to the ATO matrix. The experimental details for producing the new nanocomposites are described below.

5.2.1 Preparation of the $SnO_2 : Sb$ (ATO) powder

The ATO powder was prepared following a recipe from Goebbert *et al.* [33, 34] whereby a solution of tin (IV) chloride pentahydrate (10 g) in ethanol (100 ml) containing 2 mol-% of $SbCl_3$ (0.137 g) was added dropwise to an aqueous ammonia solution (20 ml) containing 10 wt.-% (with respect to the oxide) of a surface modifying agent, β -alanine (2.89 g). The ATO suspension was treated at 150 °C for 3 h under hydrothermal conditions. The resulting powder (3.2 g) was isolated by centrifugation (4000 rpm, 15 min), washed with bi-distilled water for the elimination of Cl^- ions and then dried at 60 °C. The preparation of the powder is illustrated in Fig. 5.3.

5.2.2 Characterization of the ATO powder

For the chemical analysis of ATO, 30 mg of the powder were dissolved in 2 ml of concentrated H_2SO_4 at 200 °C for 5 minutes. The solution was diluted and analysed using atomic emission spectroscopy with inductively coupled plasma (ICP-AES) for the determination of the elements antimony and tin.

X-ray powder diffraction (XRD) was used to identify the crystal phase of the ATO powder. The samples were analysed by a D500 model diffractometer (Siemens, radiation $CuK\alpha_1$) operating at 40 kV. The structure and morphology of the ATO powder were studied with high resolution TEM (HRTEM: CM 200 FED, Philips) at an accelerating voltage of 200 kV. Energy dispersive X-ray spectrometry (EDX, Noran Instruments) was applied for a quantitative element analysis.

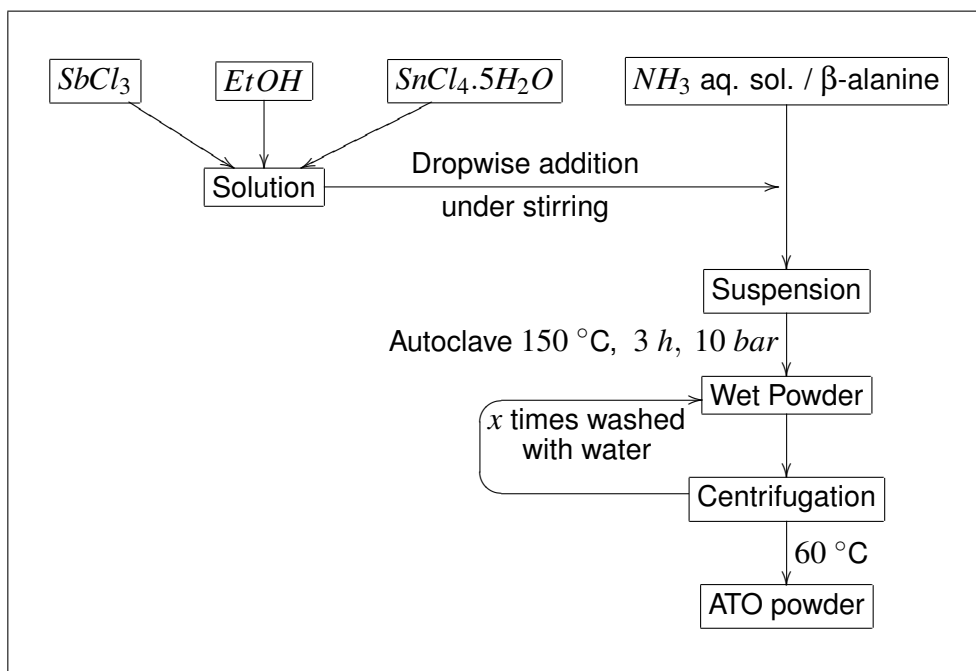


Fig. 5.3: Flow chart of the preparation of antimony-doped tin oxide powder [After Goebbert *et al.*, 1999].

5.2.3 Preparation of the ATO suspension

Colloidal suspensions from the ATO powders were prepared by dispersing them in water at $pH = 11$ using 0.78 mol.l^{-1} tetramethyl ammonium hydroxide (TMAH) as a base. The choice of this pH was based in the original report for the preparation of the ATO powder used in this work [33]. The concentration of the solutions prepared with ATO powder varied from 5 to 25 *wt. - %*. After powder addition, the resulting suspensions were ultrasonicated for 3 – 5 *min.* In order to remove possible remaining agglomerates, the final dispersions were filtered using a 0.2 *mm* thick filter. The preparation of the ATO suspension is summarized in Fig. 5.4.

5.2.4 Characterization of the ATO solution

The hydrodynamic particle size distribution of the ATO suspension was determined with a Grimm UPA 400 ultrafine particle analyser (UPA). The measurement takes 60 seconds and was repeated 3 times. The refractive index of 1.80 and particle density of 6.80 gm/cc were used, in accordance with the literature. The source of the incident light is a laser diode with

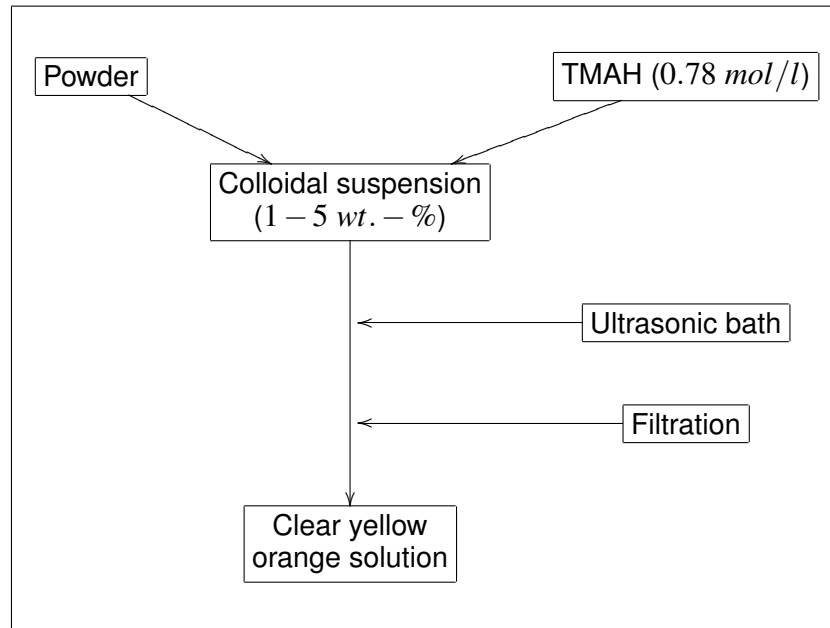


Fig. 5.4: Flow chart of the preparation of ATO suspension [After Goebbert, 1999].

780 *nm* wavelength and a power of 3 *mV*. The equipment determines the Doppler shift of the scattered light caused by the moving particles. Smaller particles cause a greater shift in the frequency than larger particles. The difference in the frequency of the scattered light is used to determine the size of the particles.

5.2.5 Preparation of the ATO/MWNT nanocomposite solutions

The nanocomposites of ATO and MWNTs (hereafter written as ATO/MWNT) were prepared according to the flow chart presented in Fig. 5.5. The MWNTs redispersed in surfactants (Section 5.1) were added to the ATO sol (Section 5.2.3) in different concentrations, varying from 1 to 50 *vol. - %*. Ultrasonic bath treatment of the solutions was applied for 15 minutes. Finally, the sols were filtered using a pre-filter (10 μm).

5.2.6 Preparation of the coatings

The preparation of 1 – 5 layers ATO and ATO/MWNT coatings in borosilicate substrates was the same described for the preparation of MWNT networks in Section 5.1.4. The procedure is shortly described in Fig. 5.6.

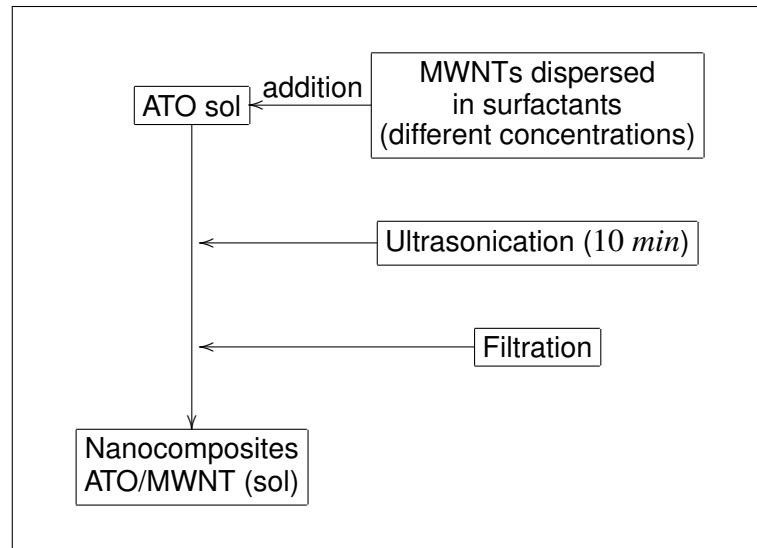


Fig. 5.5: Flow chart of the preparation of ATO/MWNT nanocomposite sols.

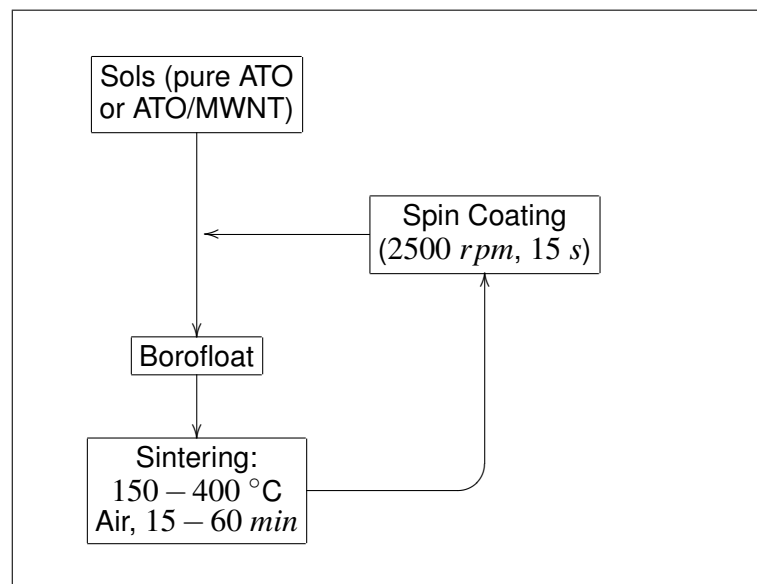


Fig. 5.6: Flow chart of the preparation of ATO and ATO/MWNT coatings.

5.2.7 Characterization of the ATO and ATO/MWNT coatings

The same methods previously described in Section 5.1.5 for the characterization of MWNT networks were applied for the study of ATO and ATO/MWNT coatings. Here, however, not only the sheet resistance of the films was measured, but also their resistivity. The sheet resistance (R_{sq}) of the films was measured by the four-points technique (Napson Corporation, Model RT-70/RG-7S). The resistivity (ρ) was calculated by:

$$\rho = R_{sq} \times t \quad (5.1)$$

where t is the thickness of the coating.

The film thickness was measured by profilometry using a Tencor P-10 surface profilometer. The surface of the samples was scanned by a diamond stylus through an uncoated part of the substrate, obtained by etching the coating with a mixture of zinc powder and hydrolic acid. The stylus registers the vertical motion at the etched edges and thereby allows determining the thickness of the coatings. The thickness was also measured by ellipsometry (Spectroscopic ellipsometer ESGV, Sopra). The method consists of measuring and interpreting the change of polarization state that occurs when a polarized light beam is reflected at non-normal incidence from a film surface. The light source is first made monochromatic, collimated, and then linearly polarized. Upon passing through the compensator (usually a quarter-wave plate), the light is circularly polarized and then impinges on the specimen surface. After reflection, the light is transmitted through a second polarizer that serves as the analyser. Finally, the light intensity is judged by eye or measured quantitatively by a photomultiplier detector. The polarizer and analyser are rotated until light extinction occurs. The extinction readings enable the phase difference and amplitude ratio of the two components of reflected light to be determined. From these, either the film thickness or the index of refraction can be obtained.

5.3 TiO_2 /MWNT nanocomposites

In this part of the work, MWNTs were dispersed in a TiO_2 -based insulating matrix developed at the INM facilities, normally used in the fabrication of films with high refractive index [240] and new TiO_2 /MWNT nanocomposites were developed. The efficiency of the MWNTs as conductive additives in the composite was evaluated and parameters such as

sheet resistance, resistivity, transparency and adhesion of the coatings were studied.

5.3.1 Dispersion of MWNTs in the TiO_2 -based sol

$-NH_2$ functionalized MWNTs were added to the as-received TiO_2 -based sol in different concentrations varying from 1 – 10 mg/ml . The detailed preparation of this sol consisting on 3% TiO_2 in a mixture of 2-propanol and 1-butanol is described in Appendix 9.6. The sols containing MWNTs were stirred for 15 *min* and ultrasonicated for 20 *min*. In order to obtain finer dispersions, the solutions were also submitted to a high shear processor. The details of the dispersions follow the same procedure already described in Section 5.1.

5.3.2 Preparation of the coatings

Also in this part of the study, spin coating technique was chosen as deposition method for the coatings. The details were already described in Section 5.1.4.

5.3.3 Characterization of the TiO_2 /MWNT coatings

The techniques utilized in the characterization of TiO_2 /MWNT coatings are the same already described in Section 5.1.5 for the characterization of the MWNT networks.

6. RESULTS AND DISCUSSION

The results obtained in this work are presented and discussed in the following chapter. The different systems investigated were divided in three sections: MWNT networks in Section 6.1; ATO/MWNT nanocomposites in Section 6.2; and TiO_2 /MWNT nanocomposites in Section 6.3. At the end of each Section, the results are summarized and compared with other studies reported in the literature.

6.1 MWNT Networks

6.1.1 Characterization of the MWNT powder

The MWNTs were investigated by SEM and by TEM and the results are shown in Fig. 6.1. Since the images obtained by both $-COOH$ and $-NH_2$ functionalized powders were very similar, only those related to $-NH_2$ MWNTs were reported here. Fig. 6.1a shows that the powder consists of agglomerations of MWNTs, what is expected due to van der Waals attractions among the tubes. In Fig. 6.1b, it is possible to see the individual MWNTs, each one with approximately 10 nm outer diameter. Their curly-like structure could be an indication of the presence of defects in their structure. Moreover, one can detect residues of catalytic particles encapsulated in the nanotubes during the CVD synthesis process, as indicated by narrows in this Figure. A precise length of the nanotubes is difficult to predict, although it seems to remain in the tens of micrometer range. It is important that the nanotubes are long in length in order to enable their electrical and mechanical properties.

Raman spectra of the MWNTs with $-NH_2$ and $-COOH$ functionalizations are shown in Fig. 6.2. The so-called D-band associated to the presence of defects is shown between 1250 – 1350 cm^{-1} . In $-NH_2$ functionalized nanotubes, this peak appears at 1322 while in $-COOH$ functionalized MWNTs, it is evident at 1326 cm^{-1} . Their second harmonic D* (or G') are presented between 2500 – 2700 cm^{-1} . The G-band, characteristic of most

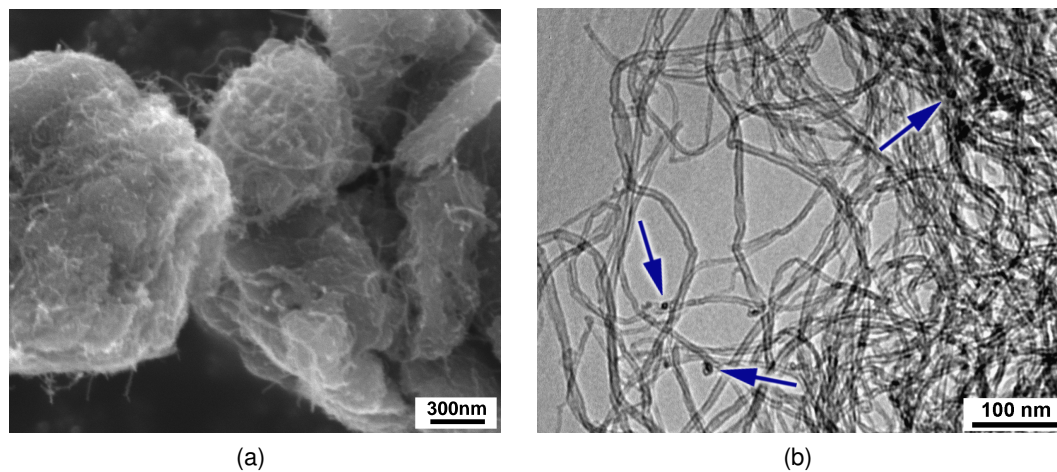


Fig. 6.1: (a) SEM images of as-received $-NH_2$ functionalized MWNTs and (b) TEM images of the same MWNTs, revealing an outer diameter of 10 nm.

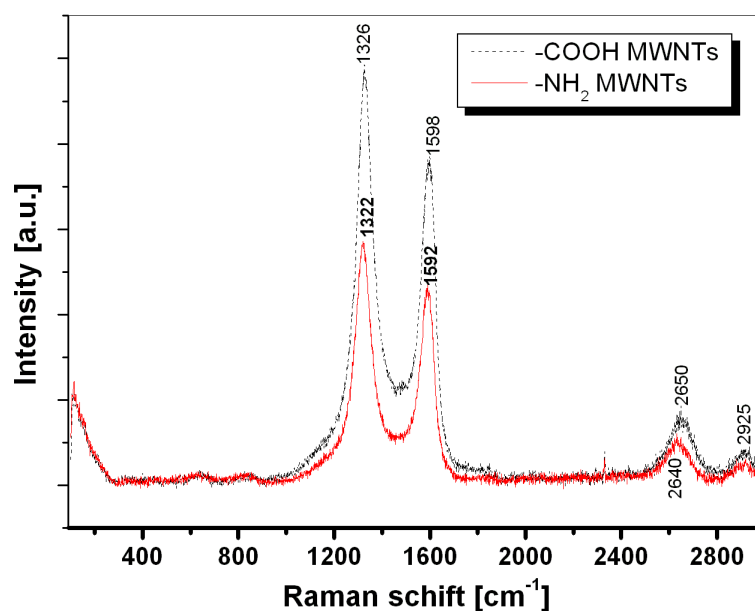


Fig. 6.2: Raman spectra of $-NH_2$ and $-COOH$ functionalized MWNTs.

carbonaceous materials due to elongations of $C - C$ bonds, is evident at 1592 ($-NH_2$) and 1596 ($-COOH$) cm^{-1} [247]. The high intensity of the D-band in comparison with the G-band in both analyzed materials is due to the presence of defects in the nanotube structure or to the presence of other impurities, such as amorphous carbon or the metal catalysts highlighted in Fig. 6.1b. Comparing the D-band with its respective G-band, MWNTs containing $-NH_2$ functionalization seem to present higher purity than $-COOH$ functionalized ones.

This observation is also supported by TG investigations performed in both powders. The concentration of metal catalysts remaining after the thermal treatment was higher in $-COOH$ functionalized samples than in the $-NH_2$ functionalized MWNT powder. In the last case, 1.8 g were observed against 3.2 g in $-COOH$ samples. Nevertheless, since only a small amount of MWNTs is used in the TG measurements, one should be aware of using the results observed as representative of the samples as a whole. The thermal degradation behaviour of both MWNT powders under synthetic air atmosphere (10 °C/min) is illustrated in Fig. 6.3. It is clear that the oxidation of $-NH_2$ MWNTs in this atmosphere starts at 440 °C and they burn completely at temperatures higher than 670 °C (almost 100% weight loss). In the case of $-COOH$ samples, however, the weight loss starts at much lower temperatures, what was attributed to evaporation of H_2O . From 440 °C, a considerable change in the overall mass of the powder is observed, which is related to the oxidation of the MWNTs themselves. These values are consistent with others reported in the literature [76, 248–250]. They could be used as an evidence of the “purity” of the sample, i.e., that the powder consists of MWNTs and not of other kind of nanotubes (SWNTs) or amorphous carbon, which starting oxidizing at different temperatures. Knowing the behaviour of the nanotubes with the increase of the temperature is of key importance, once this parameter will be taken in consideration during the sintering process of the networks.

The remaining powders after thermal treatment of MWNTs at 1000 °C were investigated and the results are shown in Fig. 6.4. Similar results were obtained by $-COOH$ and $-NH_2$ functionalized nanotubes, therefore only the ones related to $-NH_2$ will be shown. Particle sizes ranging from 60 – 100 nm are observed (Fig. 6.4a) and have been identified by EDX as consisting of *Co* and *Fe* oxides (Fig. 6.4b), which are catalysts commonly used in the synthesis of CNTs [70].

X-ray investigations of the powders are shown in Fig. 6.5. A crystalline graphite-like structure is revealed with peaks shifted to smaller 2θ values due to the presence of impurities (i.e. catalysts) in the samples.

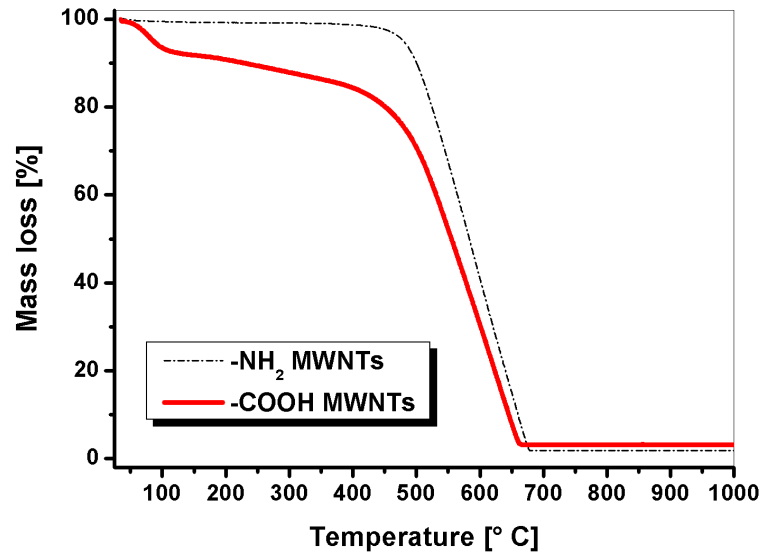


Fig. 6.3: TG curves showing the behavior of $-COOH$ and $-NH_2$ functionalized MWNTs with the increase of the temperature under synthetic air.

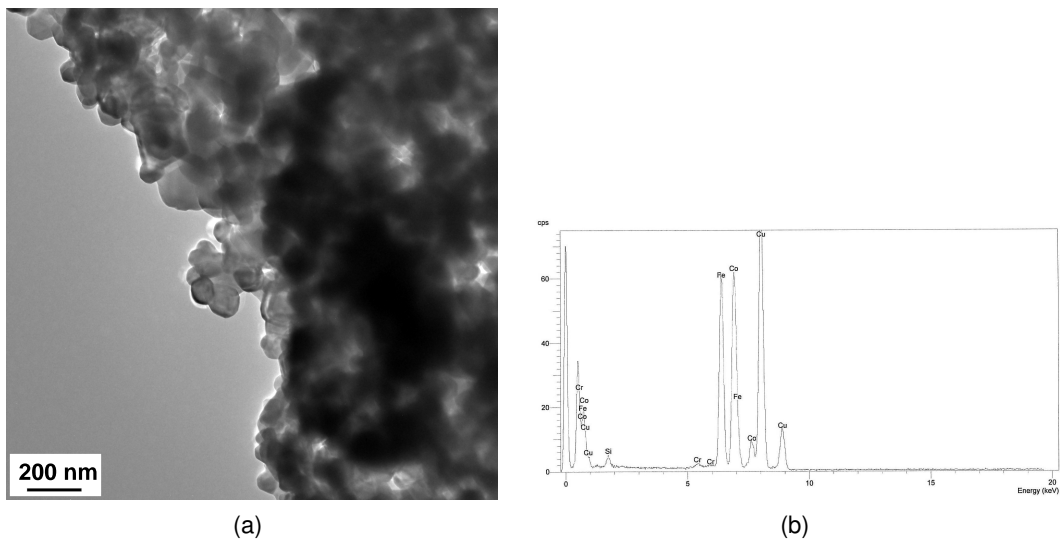


Fig. 6.4: Investigation of the metal catalyst particles present in the $-NH_2$ MWNT powder by (a) TEM and (b) EDX methods.

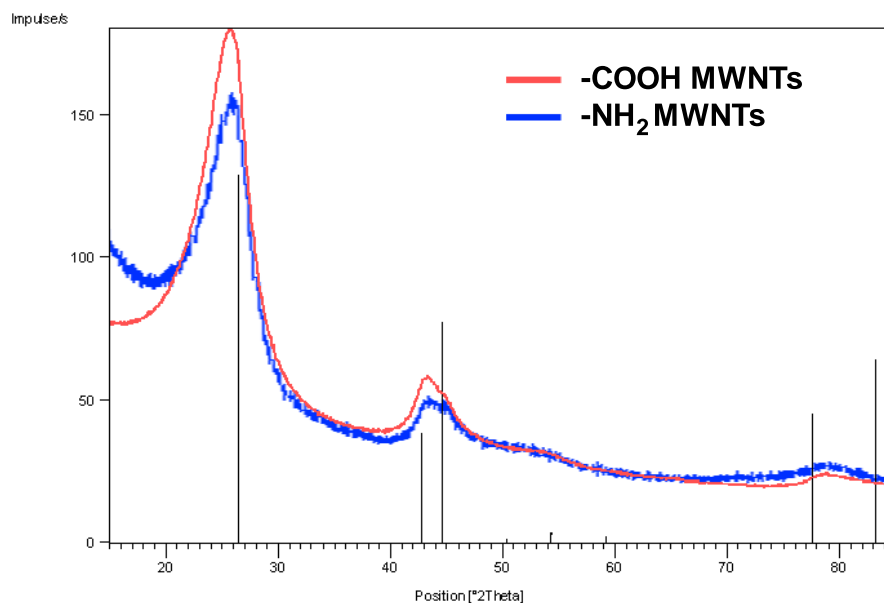


Fig. 6.5: X-ray spectra of functionalized MWNT powders. The inserted lines correspond to graphite structure.

6.1.2 Characterization of the MWNT dispersion in HDTAC

Fig. 6.6 shows the zeta potential (ζ) distribution of $-COOH$ MWNTs dispersed in HDTAC (5 wt.-% in water) with concentration of 3 mg/ml. The existence of only one peak suggests that the particles are monodispersed and an absolute ζ of 57 mV was observed. Traditionally, if the absolute value of ζ is smaller than ~ 25 mV, the repulsive force is not strong enough to overcome the van der Waals attraction between the particles, and hence the particles begin to agglomerate. Therefore, the results obtained suggest that the nanotubes are well dispersed in HDTAC. Such a surfactant with long tail groups and unsaturated C-C bonds can greatly contribute to the stabilization of CNT dispersions, since the increase in the number of carbon-carbon double bonds per surfactant tail decreases the size of the CNT agglomerate. Similar results were obtained by $-NH_2$ MWNTs (58.5 mV) and are in accordance with others reported in the literature for the dispersion of SWNTs [251].

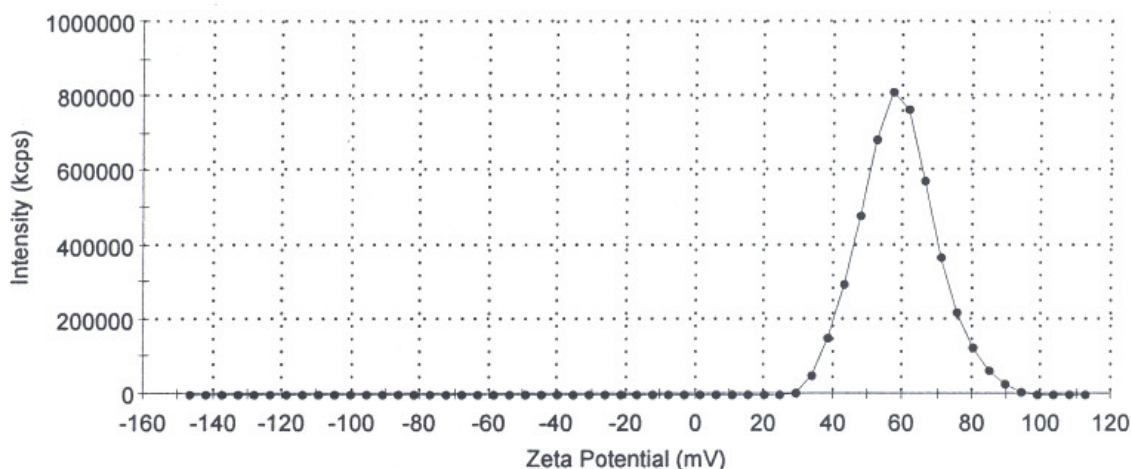


Fig. 6.6: Zeta potential distribution of MWNTs dispersed in HDTAC (5 wt.-% in water) with concentration of 3 mg/ml.

6.1.3 Characterization of the MWNT networks deposited on borosilicate substrates

Due to the presence of less impurities in the $-NH_2$ nanotube samples, as revealed in the last Section, dispersions containing this powder were used in the preparation of the MWNT networks. Therefore, all following results presented in the study of MWNT networks are related to $-NH_2$ functionalized MWNTs.

In order to facilitate the reading, MWNT networks prepared with (0.5 vol.-%) and without an adhesion promoter (see Chapter 5, Section 5.1.4) will be hereafter written as MWNT-NET-Si and MWNT-NET, respectively. All networks were prepared on borosilicate substrate. Analysis by ICP-AES has detected 0.603 ± 0.011 wt.-% CaO , 0.004 ± 0.001 wt.-% MgO and 5.220 ± 0.021 wt.-% Na_2O in the substrates.

Fig. 6.7 shows TEM images of both MWNT-NET and MWNT-NET-Si deposited on borosilicate substrates and sintered at 300 °C for 20 min. In Fig. 6.7a, the MWNTs are easily recognized, while in Fig. 6.7b their visualisation is obstructed by the presence of SiO_2 nanoparticles of 20 nm. The peaks related to these particles were highlighted by EDX measurements and are shown in Fig. 6.8. The Cu peaks come from the grid used during the preparation of the sample for the TEM measurements.

The surfaces of both networks were examined by SEM and the results are depicted in Fig. 6.9. In MWNT-NET (Fig. 6.9a), the MWNTs are randomly oriented and in contact with each other, suggesting that a percolation path has been established. However, in MWNT-

NET-Si networks, a completely different surface morphology is revealed, as shown in Fig. 6.9b. It is a more compact structure where many SiO_2 particles were sintered together, impeding the visualisation of the MWNTs. A AFM image of the MWNT-NET examined in Fig. 6.9a is presented in Fig. 6.10, confirming the porous structure observed by SEM.

The average roughness of MWNT-NET heated in different temperatures was determined with the help of a white light interferometer (WLI) and is shown in Fig. 6.11. The surface roughness decreases as a function of the temperature and reaches its lowest value at 350 °C, temperature above which the average roughness of the surface starts increasing. This behavior is strongly related to the oxidation of the MWNTs in air in this temperature range, according to the results presented in Fig. 6.3. The overall surface morphology of MWNT-NET and MWNT-NET-Si sintered at this optimum temperature is revealed by the WLI images shown in Fig. 6.12.

The band gap of CNTs has been predicted to decrease with increasing tube diameter [252]. The smallest diameter nanotubes can act as insulators, and, as the diameter of the CNTs increases, they can become semiconductors or even exhibit metallic properties, acting as conductors. Therefore, the MWNTs studied in this work (which are larger than SWNTs) are expected to show metallic rather than semiconducting behaviour at room temperature (see Appendix 9.4).

The sheet resistance of MWNT-NET was studied as a function of the concentration of MWNTs in the dispersion used for the preparation of the networks. Networks with different densities were treated in air at 300 °C (for the preservation of the MWNTs) for 20 min and the sheet resistance measured for each concentration was plotted in Fig. 6.13. The values vary from 100 – 15 $k\Omega/sq$ when the concentration of nanotubes increases from 5 to 10 mg/ml . High concentrated dispersions lead to higher conductive networks since more nanotubes are in contact. An important parameter to be considered in this case is the transparency in the visible range of the higher density networks. Since more nanotubes are present, a low transmittance of these networks in the visible range is expected, due to strong light absorption. However, even networks prepared from a dispersion containing 10 mg/ml MWNTs have shown relatively high transparencies in the visible range, ranging between 75 – 80% (Fig. 6.14). This can be related to the MWNT's diameter size of 10 nm, which is smaller than the wavelength of light, allowing the formation of concentrated, conductive and transparent networks in the substrate.

The sheet resistance of MWNT-NET was also studied as a function of the heating temperature. The behaviour is illustrated in Fig. 6.15. It is clear from this graphic that

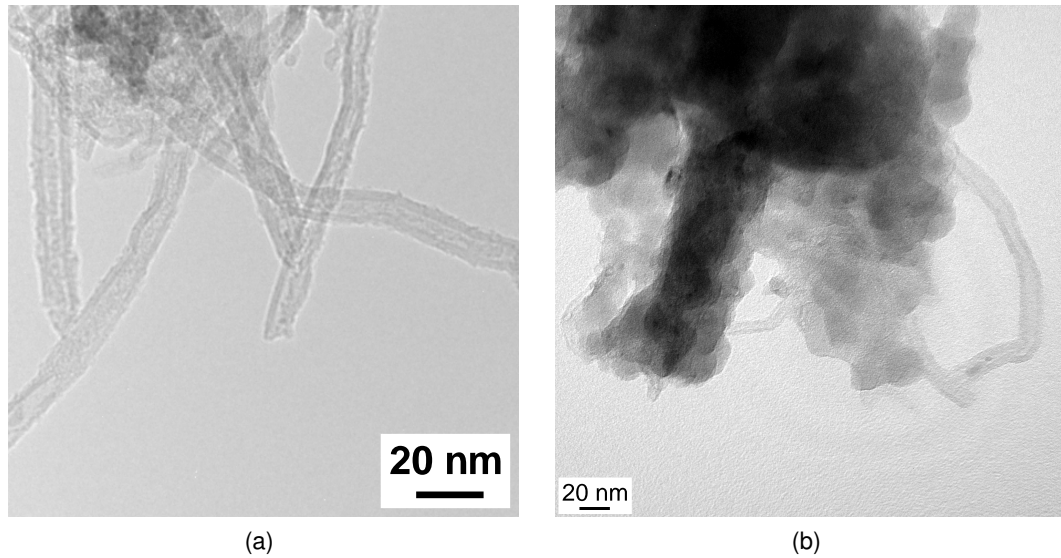


Fig. 6.7: TEM micrographs of (a) MWNT-NET and (b) MWNT-NET-Si deposited on borosilicate substrates and sintered at 300 °C for 20 min.

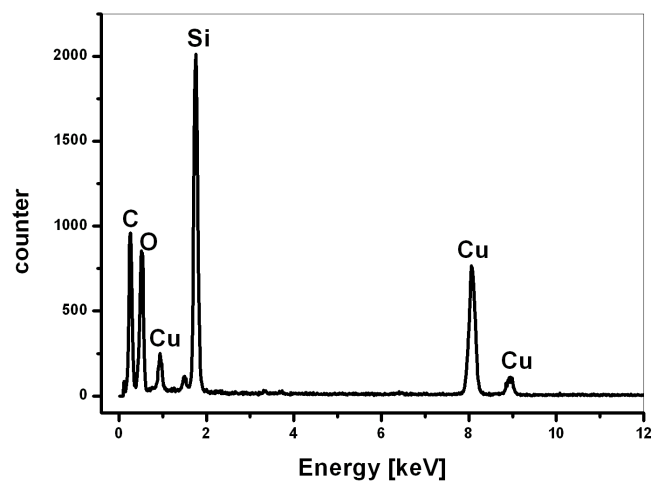


Fig. 6.8: EDX spectrum of MWNT-NET-Si deposited on borosilicate and sintered at 300 °C for 20 min

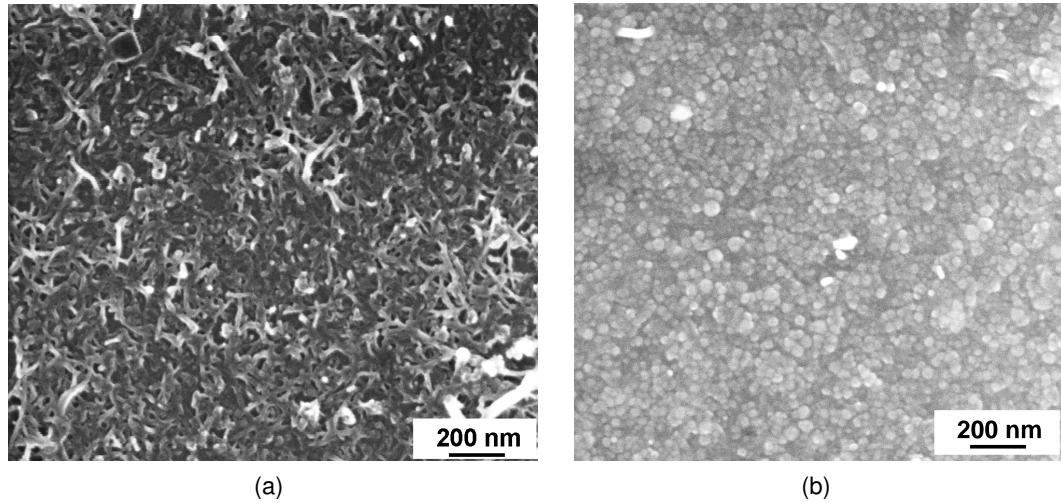


Fig. 6.9: FESEM images of (a) MWNT-NET and (b) MWNT-NET-Si deposited on borosilicate substrates and sintered at 300 °C for 20 min.

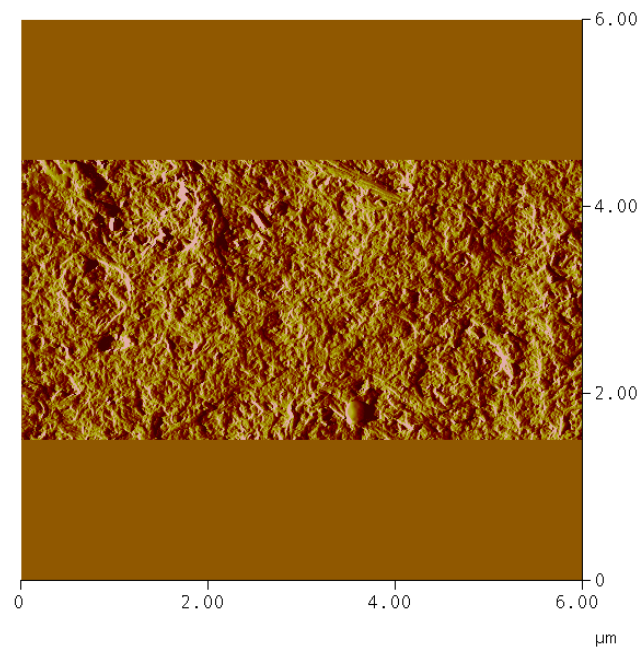


Fig. 6.10: AFM image of MWNT-NET deposited on borosilicate and sintered at 300 °C for 20 min.

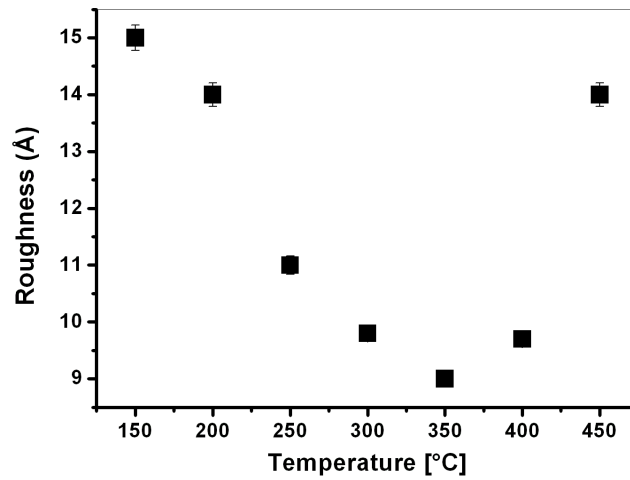


Fig. 6.11: Average roughness of MWNT-NET as a function of the heating temperature.

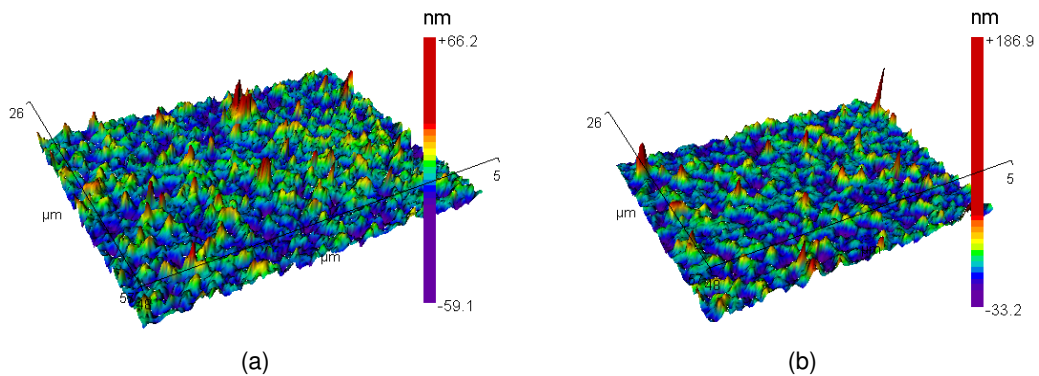


Fig. 6.12: WLI image of (a) MWNT-NET; and (b) MWNT-NET-Si, both sintered at 350°C for 20 min.

lower sheet resistances are obtained when heating the networks between 200 – 400 °C, although the values measured for networks treated at 150 and 450 °C are not much higher than that. Indeed, it is expected that the sheet resistance of MWNT-NET will start increasing at temperatures higher than 400 °C due to the oxidation of the nanotubes (Fig. 6.3). On the other hand, heating temperatures lower than 400 °C (i.e. in which the structure of CNTs is preserved) seem not to be a significant limiting factor in the sheet resistance presented by the networks and, in principle, any temperature lower than that could be chosen as ideal for the preparation of conductive networks. However, taking in consideration that smoother surfaces were obtained when treating the networks at 350 °C (6.11), this tem-

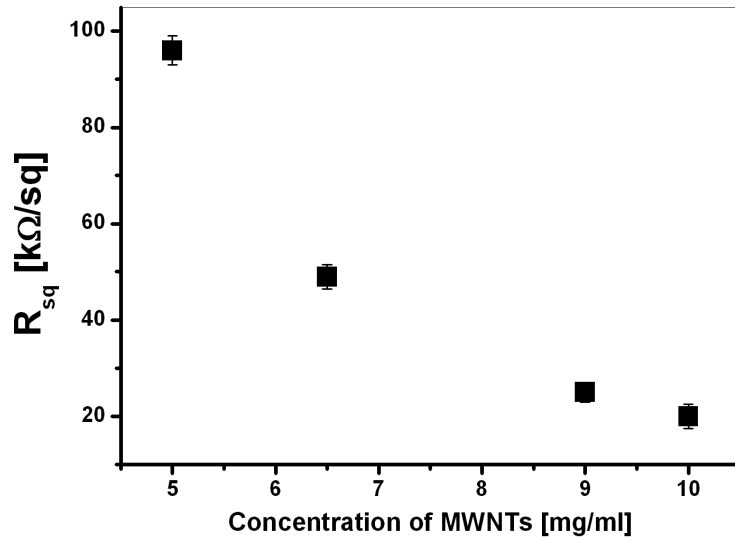


Fig. 6.13: Variation of the sheet resistance of MWNT-NET prepared at 300 °C for 20 min with the concentration of nanotubes.

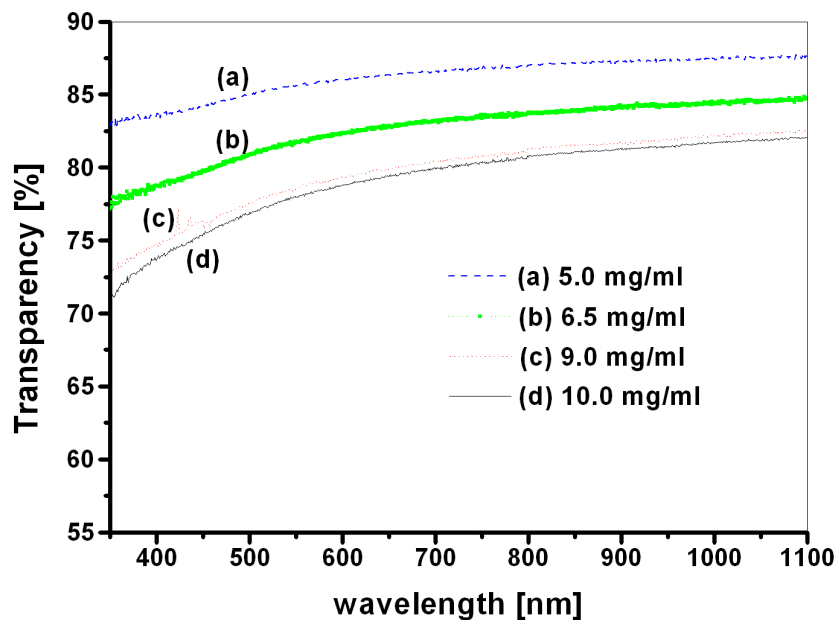


Fig. 6.14: Transmittance of MWNT-NET containing different concentrations of MWNTs heated at 300 °C for 20 min.

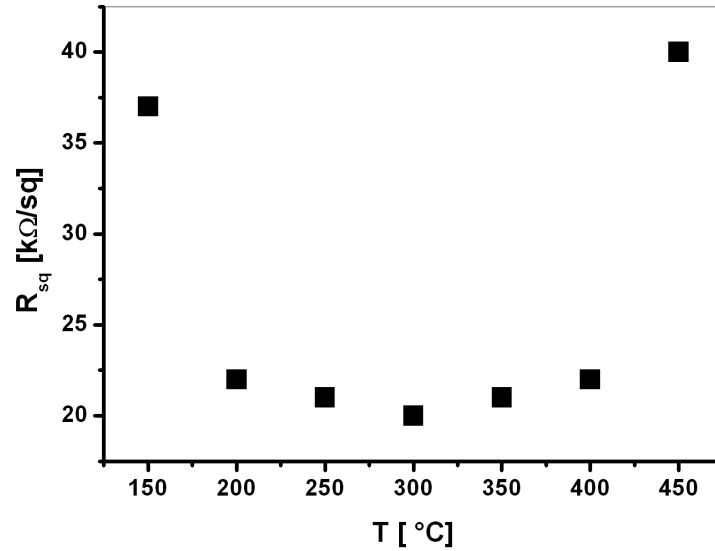


Fig. 6.15: Variation of the sheet resistance of MWNT-NET (10 mg/ml) with the heating temperature.

perature can be chosen as optimal for the fabrication of conductive, smooth networks in this work. Another important observation from Fig. 6.15 is that networks treated at 150 °C present sheet resistances as low as 37 kΩ/sq, suggesting that the networks investigated in this work could be applied in the preparation of conductive films in plastic substrates where normally low sintering temperatures are required [253].

Having defined 10 mg/ml as an optimum concentration of the nanotubes for the preparation of transparent (78 %) networks and 350 °C as an appropriate temperature for obtaining conductive (20 kΩ/sq) and smooth networks, MWNT-NET-Si were also prepared in these conditions. However, it has to be said that, in this case, the temperature is expected to play an important role in the sintering of the SiO₂ nanoparticles and, consequently, on the sheet resistance presented by the networks.

The sheet resistance of MWNT-NET-Si was evaluated as a function of the concentration of the adhesion promoter used in the preparation of the networks and the tendency is presented in Fig. 6.16. A significant increase of the sheet resistance is observed as the concentration of SiO₂ particles in the networks increases. Clearly the electrical properties of the MWNTs are influenced by the presence of the insulating SiO₂ particles in the surface of the coatings, which decreases the electrical conductivity response of the networks. The transparency of the coating, however, is preserved, as depicted in the photograph shown

in Fig. 6.17 comparing MWNT-NET and MWNT-NET-Si.

Besides, the presence of the adhesion promoter in the solution used for the preparation of the MWNT-NET-Si networks significantly improves the mechanical properties of the networks. As one can see from Table 6.1, MWNT-NET show a low adhesion on glass, being classified as “totally removed from the substrate” after the tape test procedure [245]. A SEM image is provided in Fig. 6.18, demonstrating the area obtained after the removal of the tape from the substrate. On the other hand, the addition of at least 0.5 *wt. - %* of a water based inorganic-organic monomer to the MWNT dispersion used in the preparation of the networks considerably enhanced the adhesion of the networks to the substrate. The MWNT-NET-Si were therefore classified as “left on the substrate” after pulling off the tape. In addition, the hardness of the networks has also raised from “6B” to “B”, enhancing even to “2H” when prepared with higher concentrations of adhesion promoter. The mechanical characterization of both MWNT-NET and MWNT-NET-Si is summarized in Table 6.1.

Table 6.1: Classification of MWNT-NET and MWNT-NET-Si deposited on borosilicate after standard mechanical tests.

System	Tape test classification	Pencil test classification
MWNT-NET	Totally removed	6B
MWNT-NET-Si	Left on the substrate	B – 2H

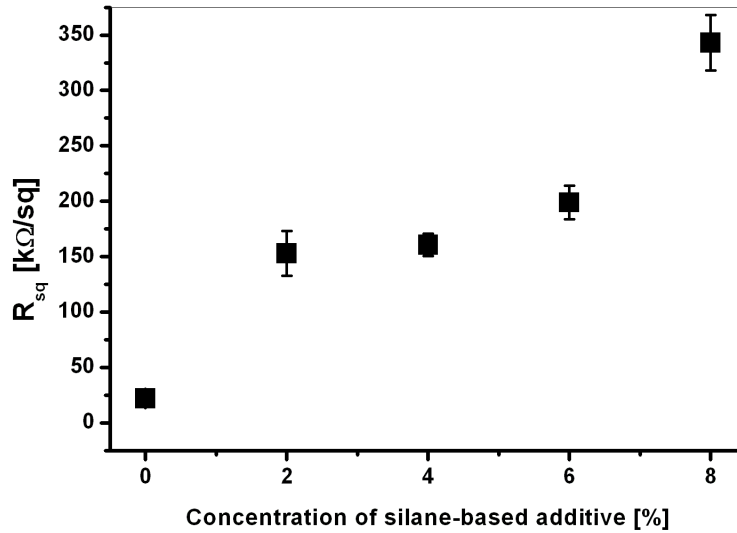


Fig. 6.16: Variation of the sheet resistance of MWNT-NET (10 mg/ml in HDTAC) with the increase of the concentration of adhesion promoters during the preparation of MWNT-NET-Si.



Fig. 6.17: Photograph comparing the optical transparency of MWNT-NET (left) and MWNT-NET-Si (right) deposited on borosilicate glass at 350 °C.

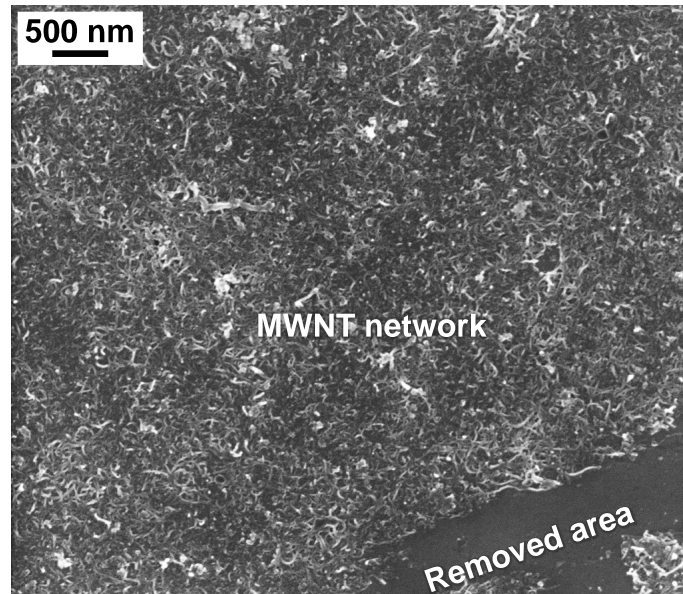


Fig. 6.18: SEM image of MWNT-NET after the performance of the tape test.

6.1.4 Conclusion of the MWNT network studies

MWNT networks were successfully obtained on borosilicate substrates. Different parameters were investigated in order to find the optimum concentration of MWNTs in the networks, temperature of heat treatment, transparency in the visible range and mechanical durability. It turns out that the combination of the optimum parameters can lead to MWNT networks which:

- contain 10 *mg/ml* of MWNTs in their composition;
- present transparency of 78% in the visible range;
- were sintered at 350 °C;
- are smooth; and
- present sheet resistances as low as 20 *kΩ/sq*.

The drawbacks presented by these networks consist on their poor mechanical response. Such networks are not hard nor adherent to the substrate, having failed standard test procedures for the determination of hardness and adhesion of coatings to the substrate. The addition of low concentrations of an adhesion promoter to the dispersion

of nanotubes used in the preparation of the networks can significantly improve such mechanical properties. However, this implies on the production of networks with higher sheet resistances (i.e. lower electrical conductivity) on the substrate with preserved transparency in the visible range. A minimum sheet resistance of $150 \text{ k}\Omega/\text{sq}$ can be obtained by adherent MWNT-NET-Si against $20 \text{ k}\Omega/\text{sq}$ presented by MWNT-NET with comparable transparency at 550 nm . Moreover, the low sheet resistance presented by networks treated at low temperatures as $150 \text{ }^\circ\text{C}$ encourages their application in plastic substrates which do not withstand higher temperatures of curing.

It has been established in the community studying carbon nanotube networks that a direct comparison of sheet resistance results can be made when considering the transmittance measured in a defined wavelength [237]. As a matter of fact, the measurement of thickness in carbon nanotubes networks leads to relatively high scale bar errors due to their very small nanometer size, therefore, resistivity does not apply in this case. Although it is predicted that MWNTs can cause a decrease in the transmittance of films due to the higher absorption related to their high diameters, MWNTs of 10 nm outer diameter used in these work presented high transparency in the visible range, compared with that obtained by SWNTs [236, 237, 254] or even superior to others presented by SWNT [255, 256] and MWNT networks [237], as demonstrated in Fig. 6.19. The sheet resistance results were also promising for MWNTs systems and performance similar to that obtained by SWNTs networks [255, 257] was presented. The advantage in the MWNT networks studied in this work remain on their lower cost in comparison with SWNT networks.

Although the studied networks did not meet the requirements necessary for a properly substitution of ITO in opto-electronic devices in terms of electrical conductivity, their optical and electrical response as well as their low cost and simplicity of preparation allow them to be employed in other applications where the high conductivity of ITO is not a requirement, such as in antistatic materials [258].

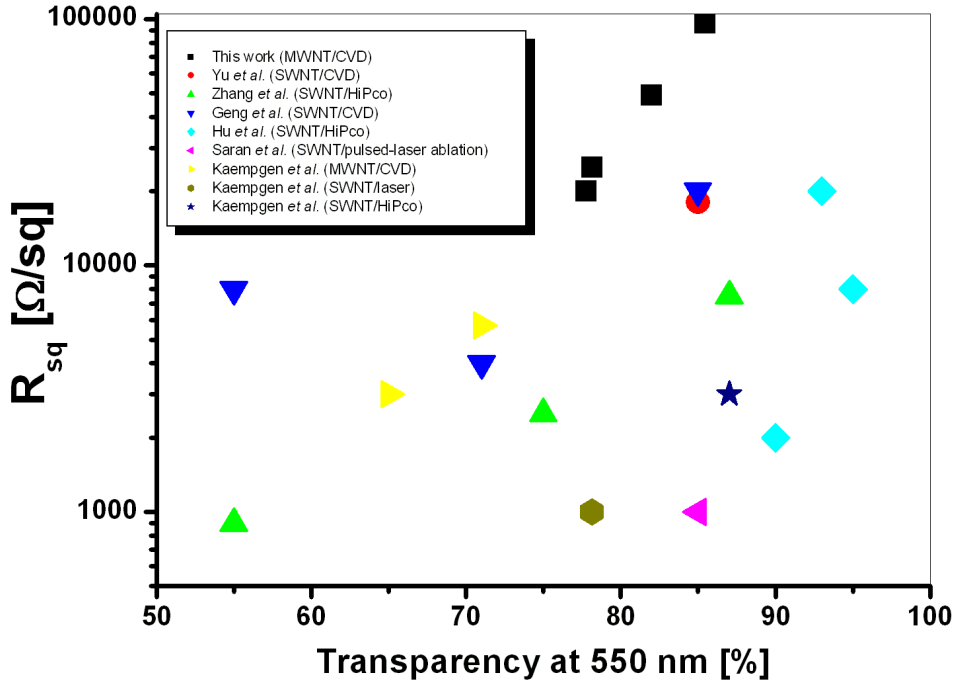


Fig. 6.19: Comparison of the sheet resistance of MWNT networks obtained in this work with others reported in the literature as a function of their transparency measured at $\lambda = 550 \text{ nm}$.

6.2 ATO/MWNT nanocomposites

6.2.1 Characterization of the ATO powder

The X-Ray diffraction pattern of the ATO powder prepared according to [33] is shown in Fig. 6.20. The sharpness of the peaks evidences the crystallinity of the particles, which were identified as the cassiterite form of SnO_2 (PDF-Nr. 03-0439). It is also observed that all peaks are slightly shifted to smaller 2θ values, indicating a change of the cell parameters by the presence of the dopant (Sb), consistent with Vegard's law applicable for mixed oxides [259].

The crystalline structure of the nanoparticles was also confirmed by HRTEM. In Fig. 6.21, one can clearly see the lattice planes of the nanoparticles, with diameter sizes ranging from 2 to 5 nm. The EDX analysis of the powder shown in Fig. 6.21b gives evidence of the presence of the elements Sn , Sb , Cu , Cl , O and C (Cu and C come from the C-

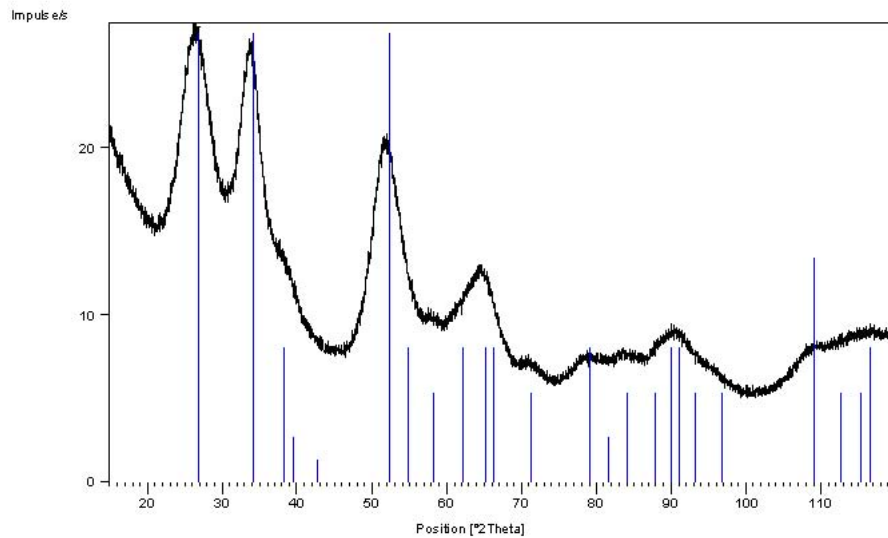


Fig. 6.20: X-ray diffraction of nanoscaled, crystalline $\text{SnO}_2 : \text{Sb}$ powder prepared under hydrothermal conditions (150°C for 3 h) [After Goebbert *et al.*, 1999]. The inserted lines correspond to the cassiterite form of SnO_2 .

sputtered Cu -net necessary for the microscopic investigation). The amount of Sb detected by EDX was about $5\text{ at.}\%$. Elemental analysis of the powder through AES shows as result $1.18 \pm 0.01\text{ wt.}\%$ of Sb and $57.85 \pm 0.59\text{ wt.}\%$ of Sn .

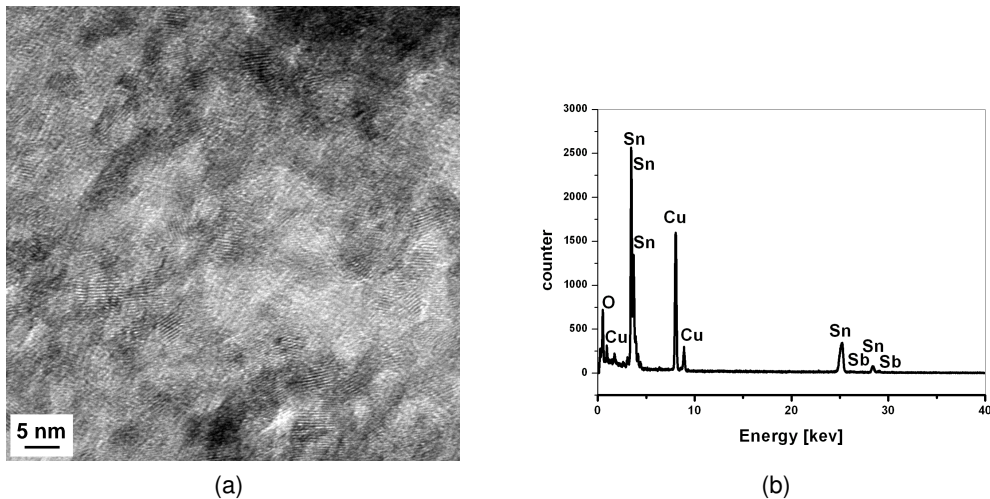


Fig. 6.21: Investigations of ATO nanopowder obtained by hydrothermal crystallization at 150°C for 3 h [After Goebbert *et al.*, 1999]. (a) HRTEM evidencing overall particle diameter of 3 nm ; (b) EDX analysis of the powder.

6.2.2 Characterization of the sols used in the ATO/MWNT studies

The dispersion of ATO particles in TMAH (25 *wt. – %*) was investigated by TEM, as depicted in Fig. 6.22). It is a clear, orange-colour sol, where no visible agglomeration of particles is verified, as shown in the inset. Individual particles of 3 – 4 *nm* in diameter (in accordance with Fig. 6.21a) can be seen in the TEM micrograph, indicating the suitability of the dispersing agent (TMAH) and the pH chosen (11) in the preparation of stable ATO suspensions. No precipitation of particles was seen for at least 1 year. UPA investigations confirm the results, as one can see in Fig. 6.23. The monomodal distribution shows that 90% of the particles have diameters lower than 12 *nm* and 10% lower than 5.1 *nm*. Since most aqueous colloidal systems are stabilized by electrostatic repulsion, the larger the repulsive forces between particles, the less likely they will be to come close together and form aggregates. Therefore, the results obtained evidence that colloidal ATO suspensions prepared with TMAH at pH 11 lead to high repulsive forces between the ATO nanoparticles.

The sols prepared by addition of MWNT dispersion to the ATO suspensions will be hereafter written as ATO/MWNT sols. ATO/MWNT sols prepared with 1 – 50 *vol. – %* MWNT dispersions were clear, with a grey-like colour and stable for at least 2 months, although less concentrated solutions presented a clearer aspect and remained free of precipitations for longer times. The clear solutions obtained, specially in less MWNT-concentrated cases, indicate the absence of powder agglomerates, what can be related to an efficient dispersion of the MWNTs in the ATO matrix with the help of the cationic surfactant.

6.2.3 ATO and ATO/MWNT coatings

In the first part of this Section, ATO coatings and nanocomposites prepared by the addition of 10 and 20 *vol. – %* of dispersions of MWNTs to the ATO sol will be examined. These concentrations correspond to final concentrations of 0.05 and 0.1 *wt. – %* (respectively) of MWNTs in the composite with respect to the ATO particles from the matrix. The ATO particles were prepared with concentration of 5 *wt. – %* in the TMAH.

The sintering temperature of 400 °C was chosen so as to preserve the structure of MWNTs in the composite (see Section 6.3 for the thermal behaviour of the MWNTs in air). Also pure ATO coatings were sintered at this temperature, in order to enable appropriate comparisons with the ATO/MWNT composites.

In order to facilitate the reading, the nomenclature presented in Table 6.2 is adopted in

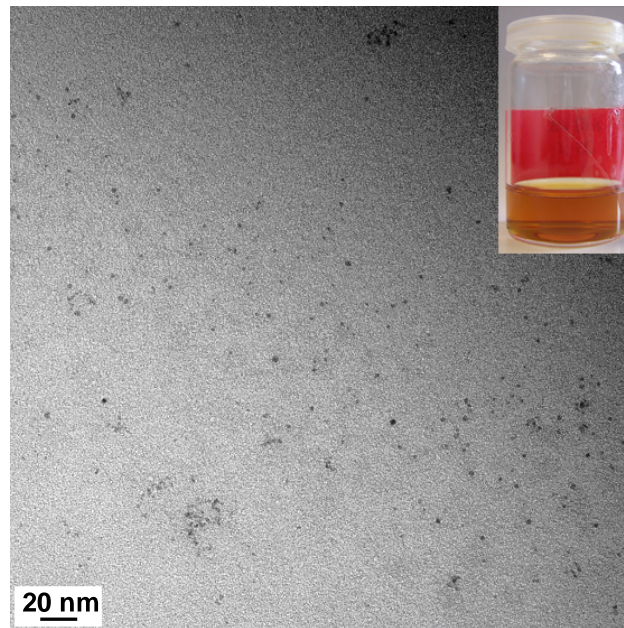


Fig. 6.22: TEM micrograph of ATO sol (25 wt. – % in TMAH) after Goebbert *et al.* 1999. A picture of the sol is depicted in the inset.

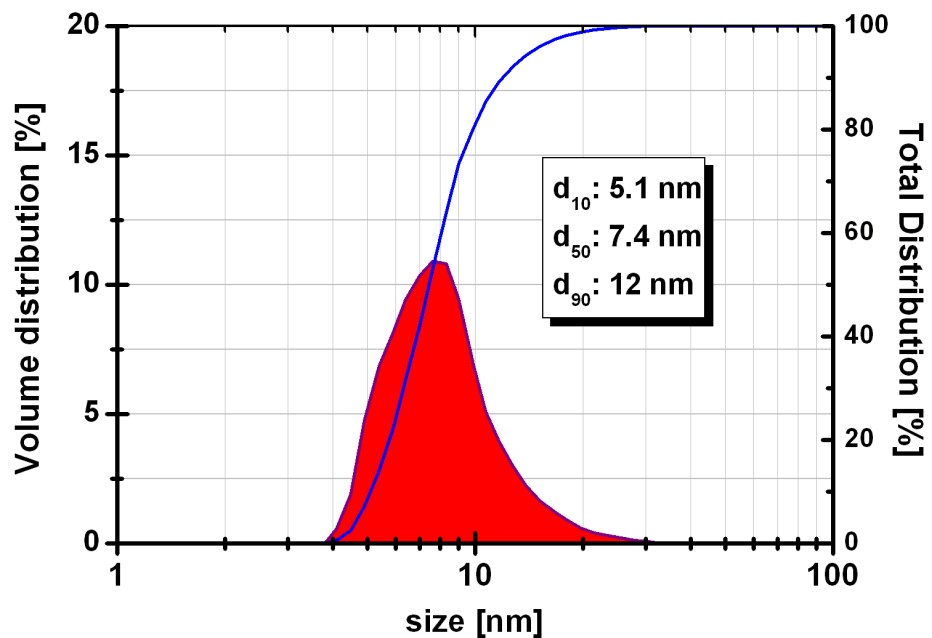


Fig. 6.23: Ultrafine particle size analysis of ATO sol (25 wt. – % in TMAH 0.78 M) after Goebbert *et al.* 1999.

this Section.

Table 6.2: Nomenclature adopted for the different coatings studied in Section 6.2.3

Composition of the Coating	Nomenclature adopted
5-layers ATO coating	S_ATO
5-layers (ATO : 10 <i>vol.</i> – % <i>NH</i> ₂ -MWNT)	S_NH2_10
5-layers (ATO : 10 <i>vol.</i> – % <i>COOH</i> -MWNT)	S_COOH_10
5-layers (ATO : 20 <i>vol.</i> – % <i>NH</i> ₂ -MWNT)	S_NH2_20
5-layers (ATO : 20 <i>vol.</i> – % <i>COOH</i> -MWNT)	S_COOH_20

6.2.3.1 Structural characterization

Fig. 6.24 shows HRTEM micrographs of a 3-layers spin coated ATO film deposited on borosilicate substrate at 400 °C for 30 *min.* It is an homogeneous coating consisted of well defined layers (~ 33 *nm*) and with a thickness of 100 *nm*, as one can see in Fig. 6.24a. This thickness was also confirmed by ellipsometry measurements. In magnified Fig. 6.24b, it is possible to see the ATO particles of diameter of ~ 5 *nm*, in accordance with results shown in 6.21. From the EDX analysis shown in Fig. 6.25, it was calculated that about 3 *at.* – % *Sb* and 97 *at.* – % *Sn* are present in the coating. The *Si* peak is related to the glass substrate while the *C* peak comes mainly from the glue used in the preparation of the sample for the TEM investigations.

Fig. 6.26 shows TEM micrographs of S_NH2.20 coating. The visualization of the nanotubes in the matrix is difficult, since they are present in very low concentrations (Fig. 6.26a). Therefore, a magnified picture originated from Fig. 6.26a was edited in order to facilitate the visualization. The result is shown in Fig. 6.26b. The film consists basically on ATO particles of 4 *nm* in diameter. A single MWNT of about 8 *nm* diameter is highlighted in Fig. 6.26c.

The SEM images present in Fig. 6.27 indicate that the addition of the MWNTs to the ATO matrix (Fig. 6.27b) do not change the overall morphology of the original coating (Fig. 6.27a). This is strongly related to an effective dispersion of the nanotubes in the ATO matrix with the help of the HDTAC surfactant, which might lead to individually separated and coated nanotubes. Comparative studies were performed using an anionic and a non-ionic

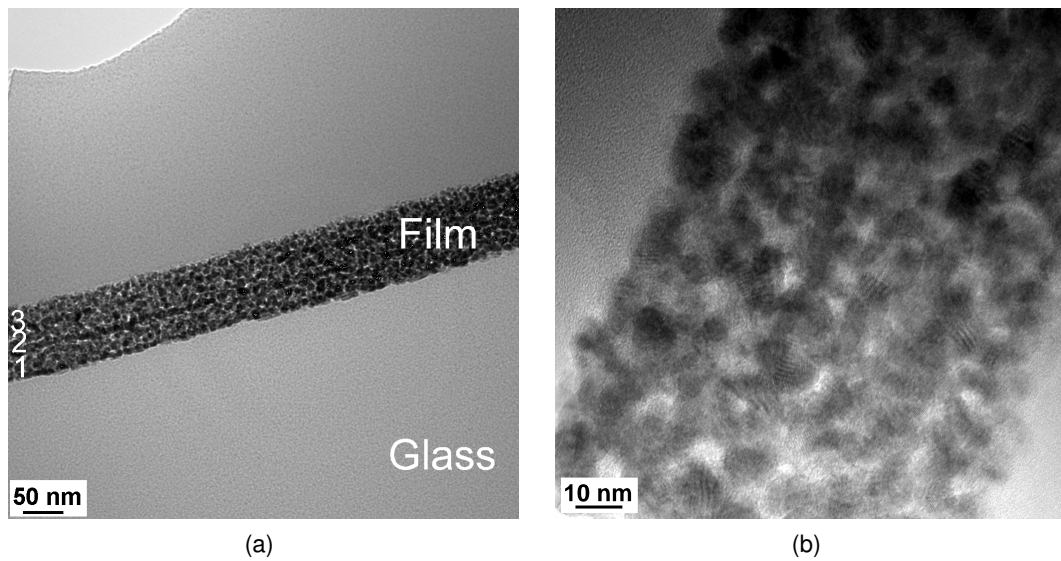


Fig. 6.24: HRTEM investigations of 3-layers ATO coating on borosilicate sintered at 400 °C for 30 min. (a) Cross-section view of the 3 layers; and (b) magnified micrograph highlighting the ATO particle size.

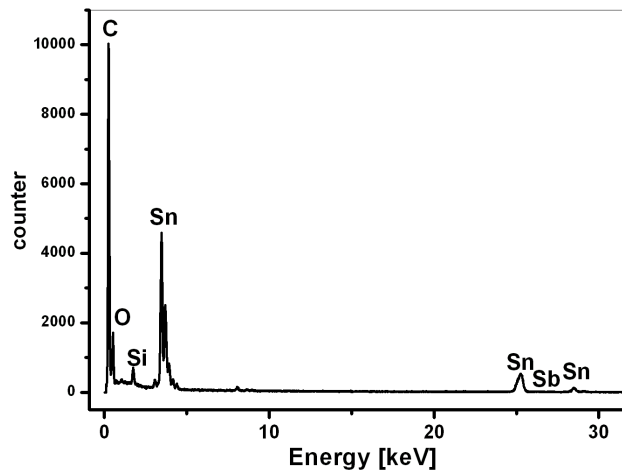


Fig. 6.25: EDX spectrum of 3-layers ATO coating deposited on borosilicate at 400 °C for 30 min.

surfactant in order to support this affirmation. As a matter of fact, addition of MWNT dispersions in sodium dodecyl sulphate (anionic) and TritonX-100 (non-ionic) surfactants to the ATO sol (prepared in the same conditions as MWNTs in HDTAC) has lead to coatings with a very different surface than those presented in Figure 6.27. The aggregative behav-

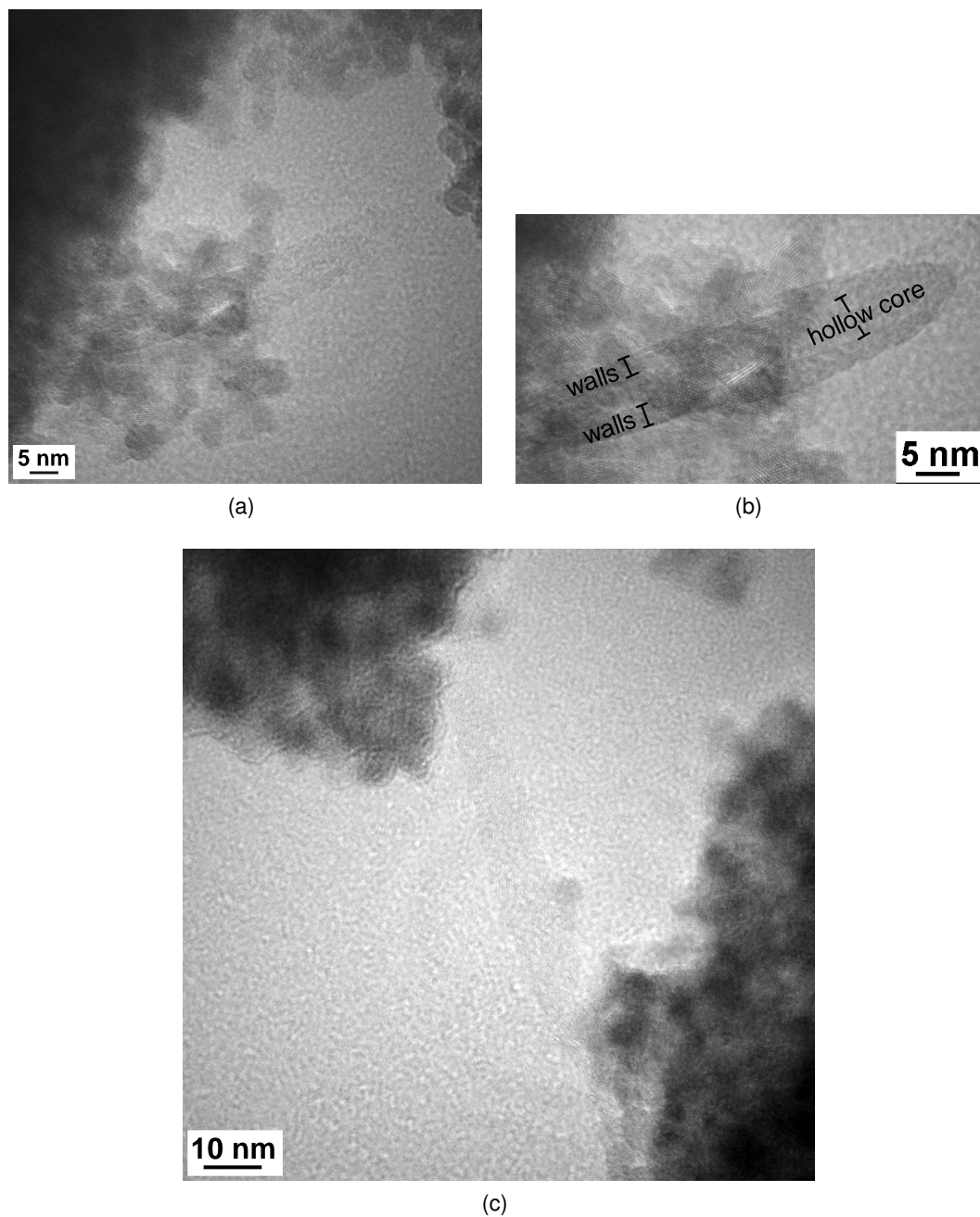


Fig. 6.26: TEM micrographs of S_NH2_20 (ATO/MWNT coatings).

ior observed denotes the ineffective dispersion provided by these surfactants (see SEM images in Appendix 9.5).

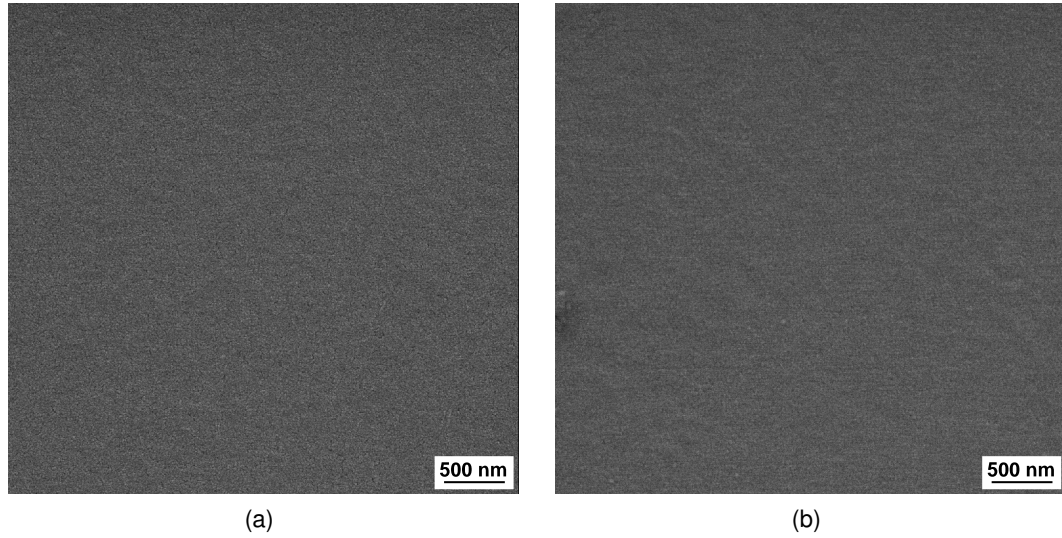


Fig. 6.27: SEM micrographs of (a) S_ATO and (b) S_NH2.20, sintered at 400 °C in air for 15 minutes.

6.2.3.2 Electrical properties

Thickness (t), resistance (R_{sq}) and resistivity (ρ) values measured for the different systems studied are summarized in Table 6.3. All coatings containing MWNTs present lower resistivity in comparison with S_ATO. It is an evidence that the nanotubes can improve the conductivity of ATO coatings due to an efficient dispersion of the nanotubes in the matrix with the help of the HDTAC surfactant. Moreover, one can see from this table that the carbon nanotubes containing $-COOH$ functionalization provided relatively lower resistivity values in comparison with coatings prepared with $-NH_2$ functionalized MWNTs. S_COOH_20 was the coating with higher conductivity. Its resistivity is 16 times smaller than that of pure ATO [260].

Table 6.3: Thickness, resistance and resistivity values obtained for ATO and ATO/MWNT coatings.

System	t (nm)	R_{sq} (k Ω)	ρ ($\Omega.cm$)
S_ATO	84 ± 2	117.45	9.9×10^{-1}
S_NH2.10	83 ± 3	42.67	3.5×10^{-1}
S_COOH_10	86 ± 2	20.73	1.8×10^{-1}
S_NH2.20	65 ± 5	23.06	1.5×10^{-1}
S_COOH_20	51 ± 4	12.15	6.2×10^{-2}

On the other hand, it has to be emphasized that higher temperatures of treatment of ATO coatings can lead to higher electrical conductivities as a consequence of a more efficient sintering process, which increases the contact between the conductive nanoparticles. As one can see from Fig. 6.28, the sheet resistance of ATO films decreases from $3\text{ M}\Omega/\text{sq}$ to $4\text{ k}\Omega/\text{sq}$ by enhancing the sintering temperature from 130 to $550\text{ }^\circ\text{C}$. However, when the same study is performed with ATO/MWNT composites containing $0.48\text{ wt.}\%$ MWNTs, it is clear that, at temperatures higher than $400\text{ }^\circ\text{C}$, the nanotubes are playing no role on the electrical properties of the coatings, since resistances similar to that obtained by pure ATO coatings at such high temperatures are measured. At lower temperatures, the sheet resistances obtained by ATO/MWNT nanocomposite are slightly lower than the measured by ATO coatings prepared at the same temperatures, suggesting the the nanotubes can contribute for the enhancing of the electrical properties and that an efficient dispersion of the MWNTs can be achieved in the matrix with the help of surfactants. However, at higher temperatures, the nanotubes are oxidized and, therefore, all contribution regarding electrical conductivity comes exclusively from sintered ATO nanoparticles.

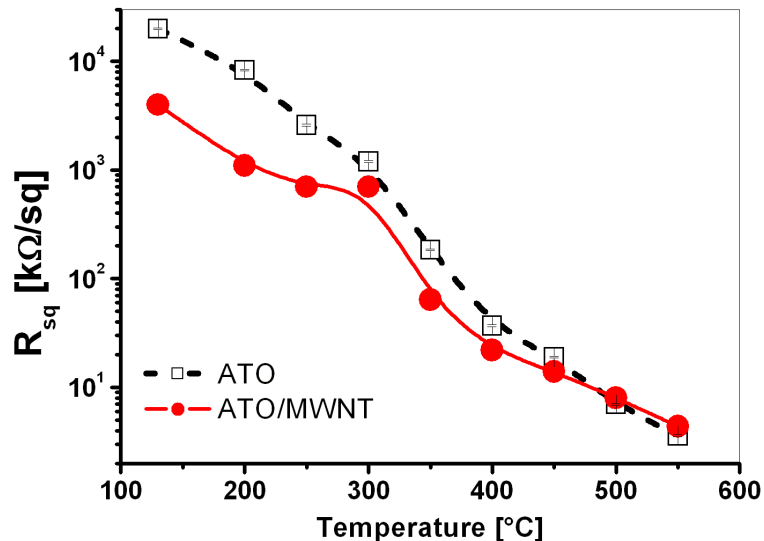


Fig. 6.28: Sheet resistance of ATO and ATO/MWNT coatings as a function of the sintering temperature.

Nevertheless, comparing the resistivity values obtained for S-COOH_20 with most of that presented by ATO coatings in the literature, films with similar electrical properties can be obtained. The advantage of the films demonstrated in this work is that lower sintering

temperatures and less ATO nanoparticles are needed therefore. Normally, since electric conductivity results from direct contact between powder particles, it is necessary for the conductive powder, e.g. ATO, to be present in the dry film in a large proportion (usually more than 50 *wt. – %*) in order to provide the film with adequate electric conductivity. This increases the costs of a conductive film made by the wet process and leads to losses of physical, mechanical and thermal properties of the coating [261].

Once lower resistivity values were obtained with composites containing *–COOH* MWNTs, these nanotubes will be the material of consideration hereafter in this section.

The decrease on the thickness observed in Table 6.3 is due to the presence of less ATO particles in coating provenient from the addition of MWNTs to the matrix. The tendency on thickness decrease of ATO/MWNT coatings as the MWNTs are added to the matrix can be observed in Fig. 6.29. In this case, the composites were prepared with higher concentrated ATO suspension (25 rather than 5 *wt. – %* in TMAH) in order to allow the measurement with more precision.

The resistivity of such thicker ATO/MWNT coatings was also studied as a function of different concentrations of *–COOH* MWNTs in their composition, varying from 1 – 50 *vol. – %* and the behavior was plotted in Fig. 6.30. At the 0% position, only ATO particles are present in the coating and, consequently, only ATO contributes for the electrical conductivity of the film. At the positions 1% and 5%, corresponding to 0.03 and 0.15 *wt. – %* of MWNTs in the composite, the resistivity increases in comparison with pure ATO. At these positions, less ATO particles are in contact and the concentration of MWNTs present is not yet sufficient to allow the formation of a percolation path in the coating. Both situations lead to a increase of the resistivity in these films. In the range 10 – 20%, however, a different behavior is observed. The resistivity in this range is lower than that presented by pure ATO in position 0%. Probably at these concentrations (0.3 – 0.6 *wt. – %* of MWNTs), there exist enough MWNTs in contact, allowing electrical conductivity through the nanotubes. It is also an indication of an appropriate dispersion of the MWNTs in the ATO matrix. There must be a competition between the MWNTs and ATO for the contribution to electrical conductivity in the composites at these compositions. At concentrations higher than 25 *vol. – %* MWNTs (i.e. 0.75 *wt. – %*), the resistivity increases to higher values than presented by pure ATO. This behaviour can be strongly related to inefficient dispersions of MWNTs in the ATO matrix at higher concentrations, according with the results shown in Section 6.2.2.

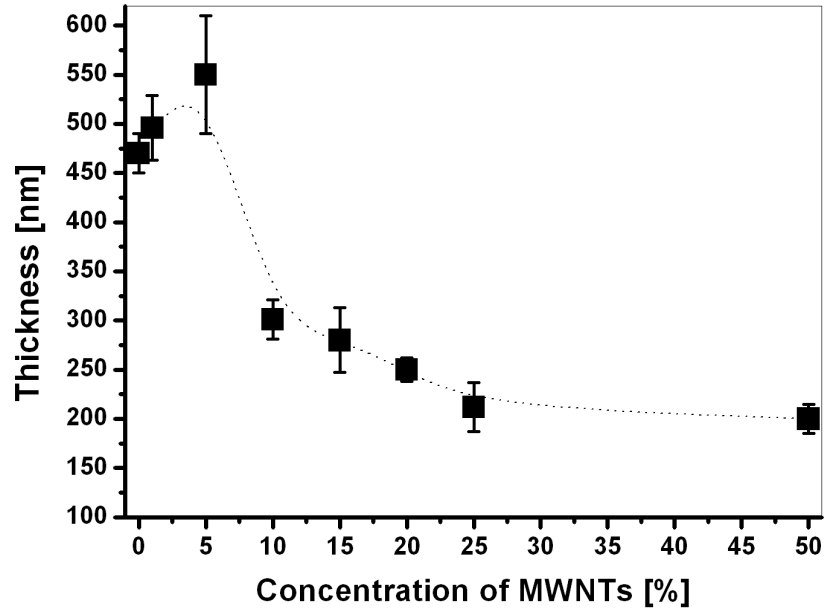


Fig. 6.29: Thickness of ATO/MWNT nanocomposites with different compositions.

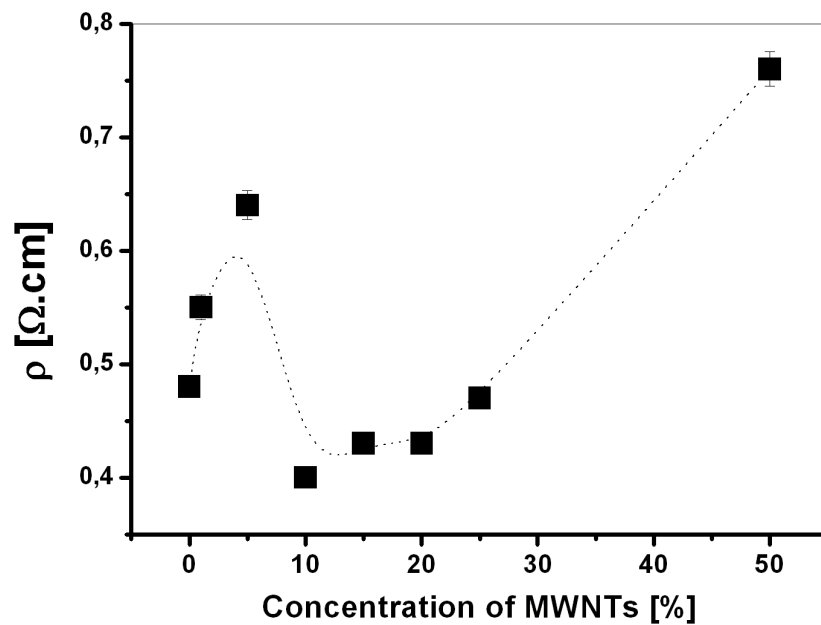


Fig. 6.30: Resistivity of ATO/MWNT coatings as a function of the concentration of MWNT dispersion in the matrix precursor.

6.2.3.3 Transmittance in the visible range

The coatings presented in Table 6.2 present high transparency in the visible range, with values between 87 – 88% measured at $\lambda = 550 \text{ nm}$. A photograph is showing the appearance of the coatings in Fig. 6.31. Apparently S_ATO and S_COOH_20 are not different, although the resistivity of S_COOH_20 is superior.

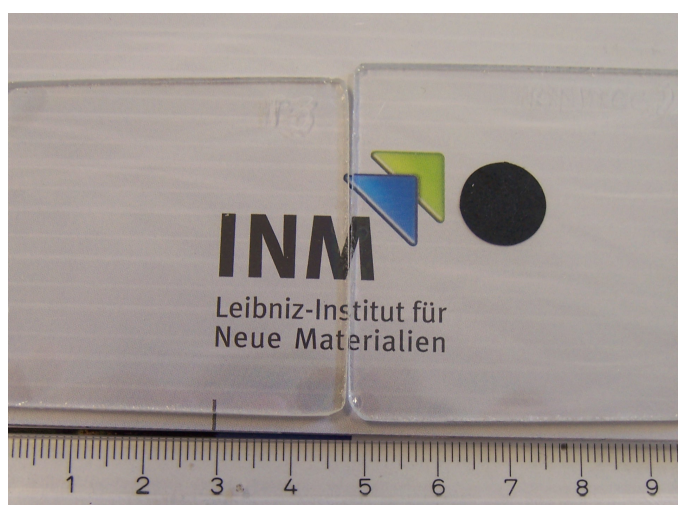


Fig. 6.31: Photograph illustrating the transparency of S_ATO (left) and S_COOH_20 (right).

ATO films show a strong absorption in the upper part of the visible and the near infrared range, related to a free charge carrier absorption (Fig. 6.32). When less ATO particles are present as in the case of the ATO/MWNT composites, the transmission of the films significantly increases in the visible range. Since less ATO particles are present, there is a decrease in the charge carrier density leading to a shift of the plasma absorption band towards the IR. As a result, the absorption does not occur in the visible and the obtained films are colorless.

6.2.3.4 Mechanical Properties

The decrease of the content of ATO particles was also expected to influence on the mechanical properties of the coatings. After the adhesion test using the tape test procedure [245], both ATO as ATO/MWNT composites were classified as “left on the substrate”, suggesting that the nanotubes are well dispersed in the matrix. It also evidences that the presence of nanotubes in the coating does not negatively affect the mechanical perfor-

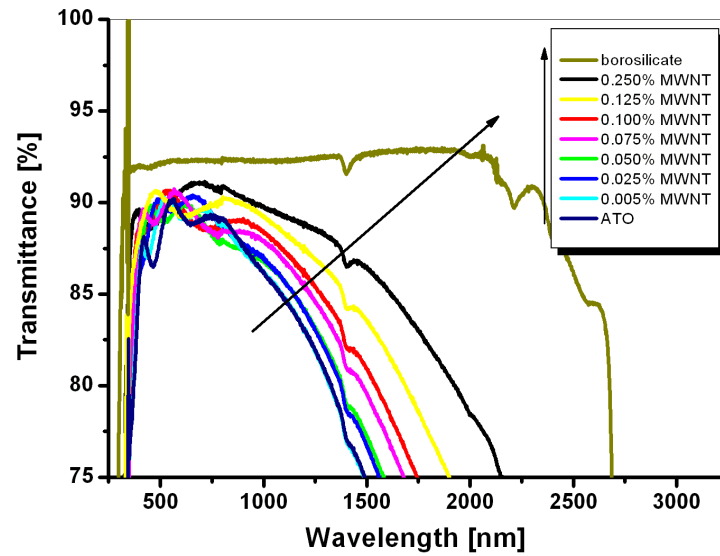


Fig. 6.32: Transparency of ATO and ATO/MWNT coatings.

mance of ATO. Contrarily, the addition of MWNTs has increased the hardness of the ATO coatings from H to $2H - 6H$, depending on the concentration of nanotubes. The mechanical characterization of both MWNT-NET and MWNT-NET-Si is summarized in Table 6.4.

Table 6.4: Classification of ATO and ATO/MWNT coatings deposited on borosilicate after standard mechanical tests.

System	Tape test classification	Pencil test classification
ATO	Left on the substrate	HB
ATO/MWNT	Left on the substrate	$2H - 4H$

6.2.4 Conclusion of the ATO/MWNT nanocomposites studies

ATO and ATO/MWNT coatings were successfully deposited on borosilicate substrates. The addition of MWNTs to the ATO matrix has led to improved electrical properties of the coatings. This behavior was observed when MWNT dispersions in HDTAC (preparation reported in Section 5.1.2) were added to the precursor ATO sol in concentrations varying from 10 – 25 *vol.%*. The lowest resistivity of 6.2×10^{-2} was obtained for coatings prepared with ATO containing 0.1 *wt.-%* of MWNTs and sintered at 400 °C. Although this resistivity is still lower than that performed by ITO, this value is in the same order of magnitude of ATO coatings prepared by sol-gel presented in the literature [33, 180, 183]. The high transparency of 88 % in the visible range is also comparable or superior to other studies of ATO coatings produced by sol-gel already reported [184]. The advantages of the ATO/MWNT developed in this work is that films with the same resistivity and transparency in the visible range as the ones reported in the literature can be obtained at temperatures lower than 550 – 600 °C using less ATO nanoparticles. It is evident that ATO itself produces electrical transparent films. In this case, however, in order to impart electrical conductivity, the amount of powder employed exceeds 50 *wt.-%* and, therefore, a decrease in the strength and the transparency of the film can not be avoided. The nanotubes used in this investigation have diameters of 10 nm, what reduces scattering of visible light and prevents a decrease in the transparency, associated with the presence of less ATO particles in the composition of the film. Furthermore, the addition of MWNTs leads to increased hardness of the ATO coatings (from *HB* to *2H – 4H*) [262].

6.3 TiO_2 /MWNT nanocomposites

6.3.1 TiO_2 sol and TiO_2 /MWNT dispersions

The TiO_2 -based sol [240] is a clear, yellowish, stable sol (no precipitation observed in at least 2 years) which is shown in Fig. 6.33. The addition of MWNTs to this sol leads to the production of dark, black solutions. The higher the concentration of nanotubes in the sol, the faster the visible sedimentation of the carbon nanotubes.



Fig. 6.33: TiO_2 -based sol developed at INM facilities [After Mennig *et al.*, 2003].

6.3.2 TiO_2 /MWNT coatings

6.3.2.1 Structural properties

Micrographs obtained by HRTEM of TiO_2 /MWNT coatings containing 5 mg/ml nanotubes are shown in Fig. 6.34. The very good contrast with the TiO_2 matrix allows an easy observation of the MWNTs, as demonstrated in Fig. 6.34a. Outer diameters ranging from 5-8 nm are recognized. The narrows indicate typical defects in the structure of the MWNTs prepared by the CVD process, which can significantly influence on other properties of the material. In Fig 6.34b, one can see that the MWNTs present typical curved end-caps, also expected for CVD-made nanotubes, as indicated by the narrows. It is also possible to predict the number of concentric tubes in the MWNTs from the depicted area, as shown

in 6.34c. The concentric tubes vary from 3 to 7 nanotubes. In this Figure, a bare scale was built in order to facilitate the visualization of 6 concentric walls. Fig. 6.34d shows the EDX spectrum obtained for this coating. It has mainly detected *Ti* element present in the matrix, while the *Cu* peaks are related to the grid used in the preparation of the samples for HTEM investigations.

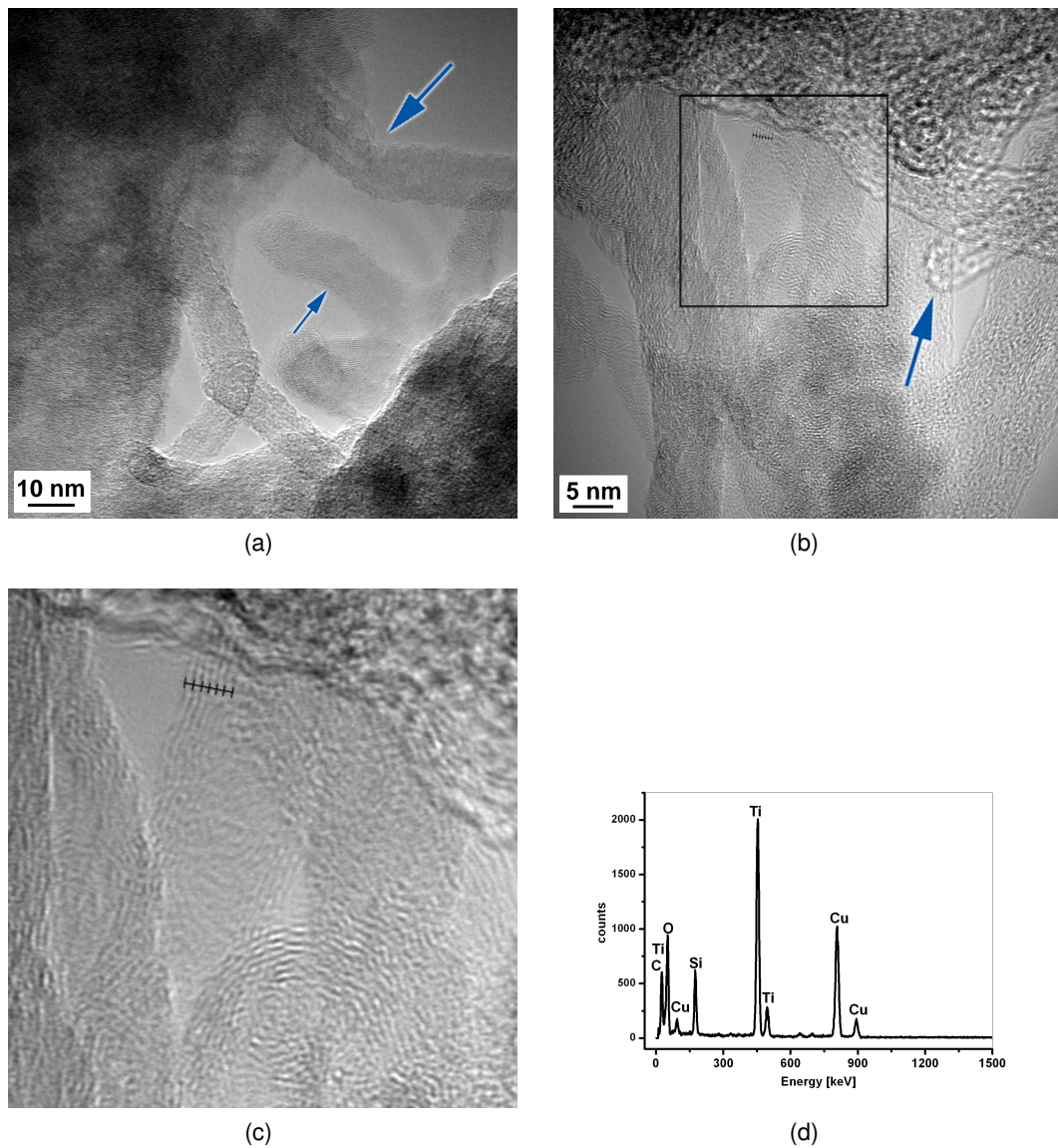


Fig. 6.34: HRTEM images of $TiO_2/MWNT$ (5 mg/ml) with different magnifications. (a) Defects on the structure of the MWNTs; (b) curved end-caps of MWNTs; (c) a MWNT containing 6 inner nanotubes; and d) the EDX spectrum of the coating.

Investigations of the morphology of TiO_2 coatings deposited on borosilicate were also performed and are shown in Fig. 6.35. No crystalline structure of TiO_2 has been observed by HRTEM in coatings sintered at $400\text{ }^\circ\text{C}$ (Fig. 6.35a). This is due to the sintering temperature used, which was not sufficient to promote the crystallization of an anatase or rutile phase of TiO_2 . The results were supported by X-Ray investigations shown in Fig. 6.35b, where no crystalline phase is identified.

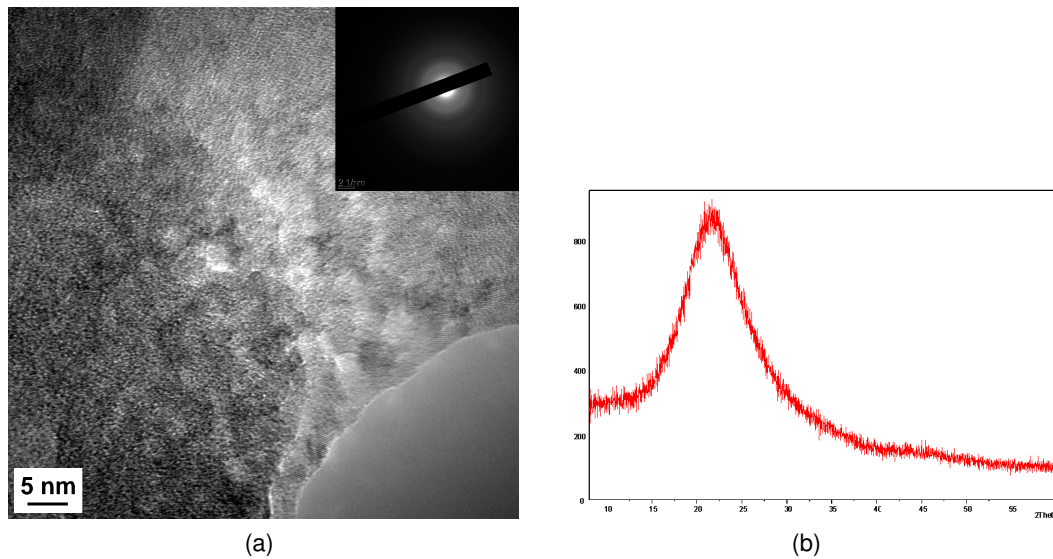


Fig. 6.35: Investigations of TiO_2 coatings deposited on borosilicate and sintered at $400\text{ }^\circ\text{C}$. (a) HRTEM image shows that no crystalline phase is present; (b) X-Ray investigations confirms the observation.

Raman investigations of TiO_2 /MWNT composites (5 mg/ml MWNTs) are shown in Fig. 6.36. Also here, no sign of anatase TiO_2 crystalline structure is detected at lower Raman shifts [263], as shown in the inset. On the other hand, the peaks related to the presence of MWNTs are easily recognized between 2500 and 2700 cm^{-1} (D^* band) and at 1324 cm^{-1} (D band). The G-band is revealed at 1596 cm^{-1} . The higher intensity of the D-band in comparison with the G-band quite typical for MWNTs prepared by CVD process denotes defects in the structure of the tubes, as pointed out in Fig. 6.34a.

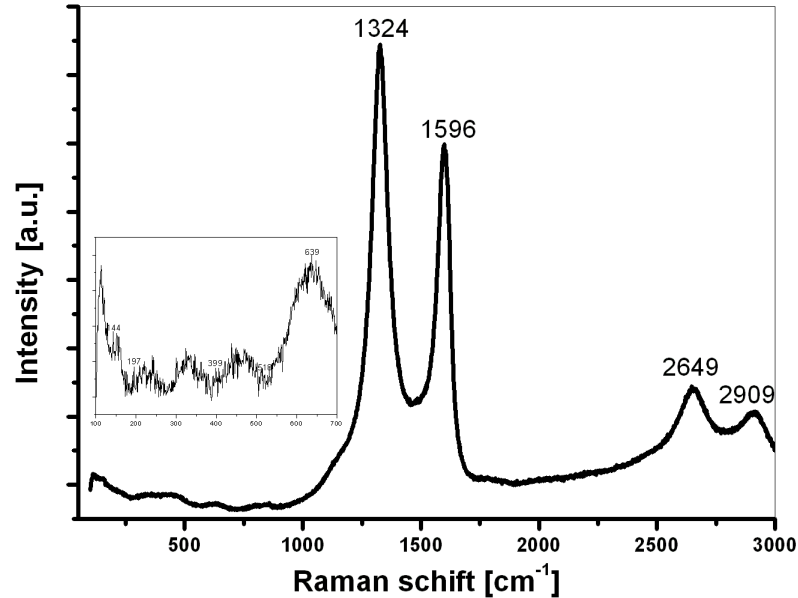


Fig. 6.36: Raman spectrum of TiO_2 /MWNT coatings containing 5 mg/ml MWNTs

FESEM images of TiO_2 and TiO_2 /MWNT composites prepared with different concentrations of MWNTs are shown in Fig. 6.37. Clearly, the introduction of MWNTs into the matrix dramatically changes the overall morphology of TiO_2 coatings. Films containing MWNTs have a very inhomogeneous surface in comparison with pure TiO_2 coatings (6.37a). This can be an indication of the presence of MWNTs at the surface of the coating and also of a low dispersion of the nanotubes in the matrix. Films containing 1.0 mg/ml MWNT (Fig. 6.37b) seem to present poor connections among nanotubes, while films prepared with 3.0 (Fig. 6.37c) and 5.0 mg/ml MWNTs (Fig. 6.37d) reveal a more efficient connective network of nanotubes. The topography of this last coating is shown in Fig. 6.38. It is important that the nanotubes are in contact to each other forming a percolation path in order to provide the coating electrical conductivity.

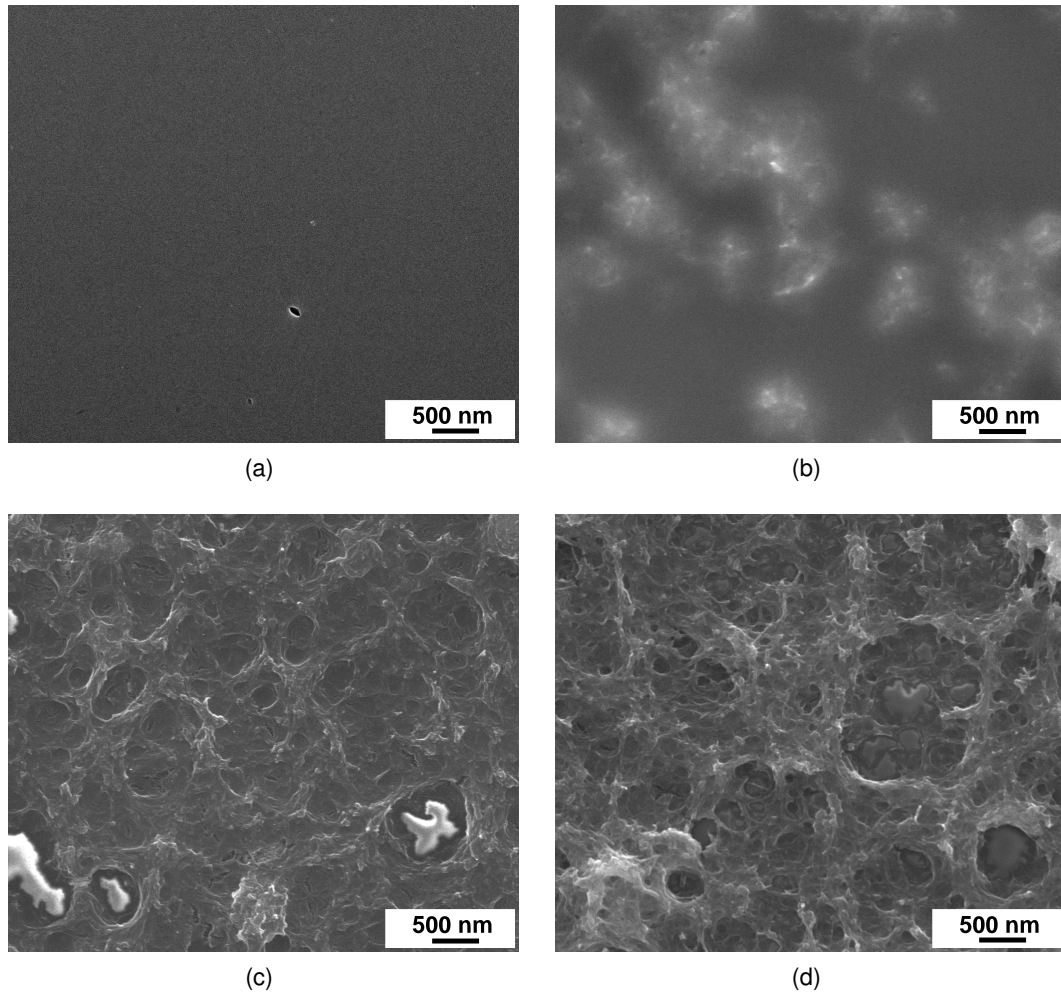


Fig. 6.37: FESEM micrographs of (a) TiO_2 and TiO_2 /MWNT coatings containing (b) 1, (c) 3, and (d) 5 mg/ml MWNTs.

6.3.2.2 Electrical properties

The presence of a connective network of CNTs within the insulating TiO_2 matrix was characterized by sheet resistance measurements using the 4-points technique. The sheet resistance of coatings containing different concentrations of MWNTs is shown in Fig. 6.39.

The results confirm the FESEM observations: the percolation of nanotubes is reached when MWNTs are present in a concentration of 3.0 mg/ml or higher [264]. At concentrations lower than that, the MWNTs are not efficiently connected to each other, while at concentrations higher than 3.0 mg/ml , a significant decrease of the sheet resistance of the films (from some $M\Omega$ to just a few $k\Omega$) is observed due to strong connections be-

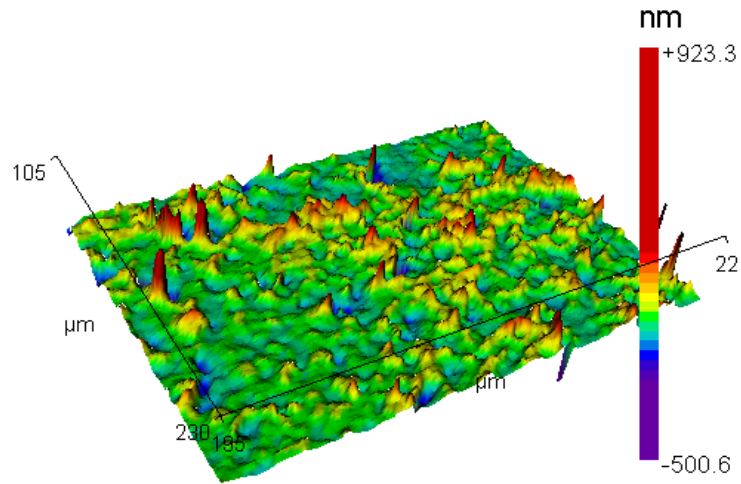


Fig. 6.38: WLI image of TiO_2 /MWNT coating (5 mg/ml MWNTs) deposited on borosilicate glass.

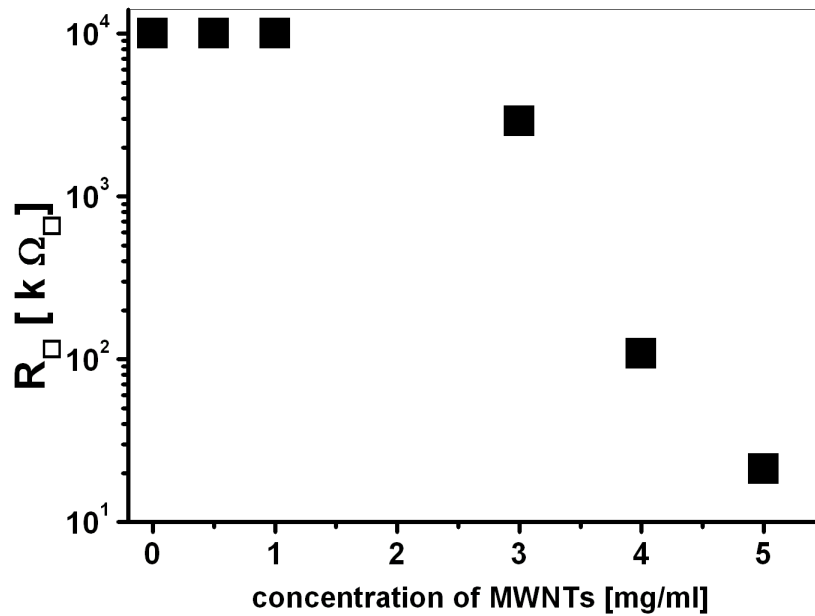


Fig. 6.39: Variation of the sheet resistance of TiO_2 /MWNT composites as a function of the concentration of MWNTs in the coatings.

tween the nanotubes. It has been suggested in the literature that this behaviour can be attributed to an increase of the concentration of free electrons in the conducting band of TiO_2 by the presence of CNTs, thus promoting electron transfer through the $TiO_2/MWNT$ coating [265, 266]. Considering films prepared with 5.0 mg/ml MWNT (80 nm thick), the resistivity calculated was $2.0 \times 10^{-1} \Omega.cm$.

The lowest concentration of 3 mg/ml observed in order to have carbon nanotubes percolating in the film can be considered as too high. A low efficient dispersion of the nanotubes in the TiO_2 -based sol could be the explanation for that. Another possibility is that the high-shear process used in order to obtain finer dispersions had cut the nanotubes in length, diminishing their aspect ratio. This behaviour, however, was not observed by MWNTs dispersed in HDTAC and submitted to the same high-shear process, as presented in Section 6.1.

6.3.2.3 Transmittance in the visible range

The coatings containing at least 3 mg/ml nanotubes present a low transparency in the visible range, at the best 52% , as depicted in Fig. 6.40. This can be related to a poor dispersion of the nanotubes within the matrix. The addition of MWNTs to the TiO_2 coating has significantly affected its transmittance. A lowering from 72 to 37% can be observed when MWNTs are added in concentrations of 5 mg/ml . A picture was taken in order to compare the coatings and is shown in Fig. 6.41. Although the nanocomposites present a low transparency in the visible range, they have a clear appearance and no visible agglomerations of MWNTs are observed in the surface of the coating.

6.3.2.4 Mechanical properties

The presence of the MWNTs in the TiO_2 sol negatively affects the mechanical properties of the TiO_2 coating (Table 6.5). The films, originally classified as “left on the substrate”, have performed “partially removed from the substrate” after the tape test. Additionally, the hardness of the TiO_2 coating severely decreased from $2H$ to $6B$. These results confirm that a poor connection was established between the nanotubes and the TiO_2 matrix.

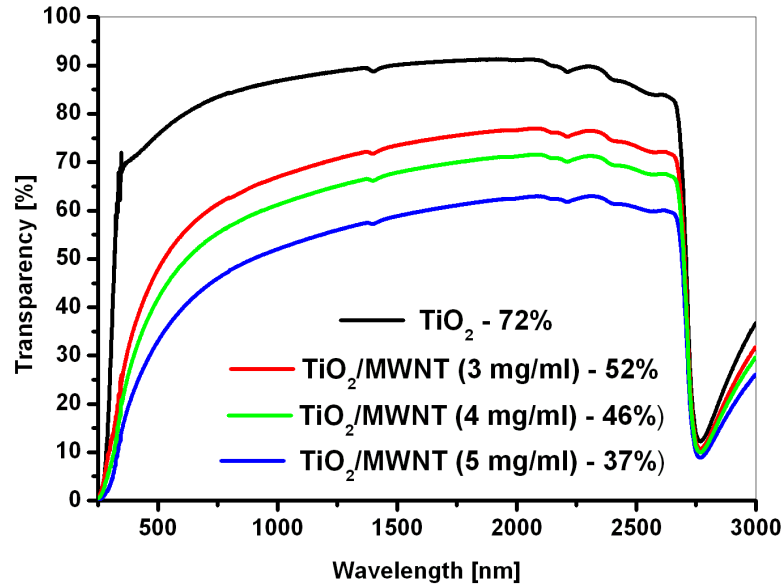


Fig. 6.40: Transmittance of TiO_2 and TiO_2 /MWNT coatings prepared with different concentrations of MWNTs.



Fig. 6.41: Photograph comparing the transparency of TiO_2 (left) and TiO_2 /MWNT nanocomposites containing 3 mg/ml MWNTs (right).

Table 6.5: Classification of TiO_2 and $TiO_2/MWNT$ coatings deposited on borosilicate after standard mechanical tests.

System	Tape test classification	Pencil test classification
TiO_2	Left on the substrate	2H
$TiO_2/MWNT$	Partially removed from the substrate	6B

6.3.3 Conclusion of the $TiO_2/MWNT$ nanocomposite studies

$TiO_2/MWNT$ nanocomposites with resistivity as low as 2.0×10^{-1} were obtained. The transmission of conductive coatings in the visible range was lower than 52%. This result limits the use of such coatings in applications where a high transmittance at 550 nm is required. A comparison with ITO coatings is not possible to be made, since the nanocomposites do not show the transmittance and resistivity required for applications in optoelectronic devices.

MWNTs presented a detrimental effect on the composite properties such as load-transfer mechanism failure resulting in inferior composite mechanical properties and poor appearance due to an inefficient dispersion in the TiO_2 matrix. Comparing the results obtained in this part of the study with the MWNT networks and ATO/MWNT composites presented in the previous sections, it can be said that an efficient dispersion of the carbon nanotubes is achieved when an appropriate concentration of surfactant is present. In the $TiO_2/MWNT$ studies, CNTs did not overcome the van der Waals attractions. Therefore modifications are required in the composition of the dispersion or in the surface of the nanotubes in order to enhance the electrostatic/repulsive forces and promote efficient dispersions.

7. SUMMARY AND CONCLUSIONS

Conductive coatings based on multi-walled carbon nanotubes (MWNTs) have been developed in this work by sol-gel spin coating technique as possible alternative materials for transparent and conductive devices.

MWNTs (Nanocyl S.A.) were chosen as material of choice due to their lower cost in comparison with other kind of nanotubes available in the market (see Appendix 9.7). Their lower prices are related to the synthesis process of the nanotubes: MWNTs are easier and less expensive to produce because current synthesis methods for SWNTs result in major concentrations of impurities that require removal by acid treatment.

Functionalized MWNTs were investigated in order to enable good dispersions of the MWNTs in the solvents studied. It turns out that $-COOH$ functionalized MWNTs are less stable during heat treatment in air than $-NH_2$ functionalized nanotubes, what can be related to evaporation of water from the surface of those MWNTs. Catalysts metals (Co and Fe) were encapsulated in both kinds of nanotubes. A huge D-band in comparison with the G-band was detected by Raman spectroscopy, indicating the presence of defects in the structure of the powders or the presence of impurities, such as the catalysts metals, in the samples analyzed.

Absolute zeta potentials as high as 57 mV were observed when the MWNTs were dispersed in water containing hexadecyl trimethylammonium chloride (HDTAC), a cationic surfactant. Such high absolute zeta potential obtained indicates that the repulsive forces were strong enough to overcome the van der Waals attraction between the carbon nanotubes, leading to the formation of stable dispersions. This can be related to the long tail groups and unsaturated C-C bonds in the chosen surfactant, which can greatly contribute to the stabilization of CNT dispersions, since the increase in the number of carbon-carbon double bonds per surfactant tail decreases the size of the CNT agglomerate.

MWNTs were studied both as networks as well as embedded in conductive and insulating matrixes. Different techniques were applied in each single study for the characterization of the structural, electrical, optical and mechanical properties of the networks and

coatings.

As networks deposited on borosilicate substrates, concentration of 10 mg/ml of MWNTs dispersion in HDTAC has led to the formation of smooth networks with transparency of 78% in the visible range and sheet resistances as low as $20 \text{ k}\Omega/\text{sq}$, but with poor adhesion to the substrate and hardness. When adhesion promoters are added to the networks, significantly improvement of the mechanical properties are observed. However, the sheet resistance of the networks increases as a function of the presence of the insulating particles originally from the adhesion promoter. Adherent networks present minimum sheet resistance of $150 \text{ k}\Omega/\text{sq}$. The transmittance in the visible range was not affected in this case. The MWNT networks studied in this work present transparency compared with that obtained by SWNTs [236, 237, 254] or superior to others presented by SWNT [255, 256] and MWNT networks [237]. Also the sheet resistances obtained were similar to that presented by SWNTs networks reported in the literature [255, 257]. The advantage in the MWNT networks studied in this work lays on their lower cost in comparison with SWNT networks.

ATO and ATO/MWNT coatings were successfully deposited on borosilicate substrates. The addition of MWNTs to the ATO matrix in concentrations varying from $10 - 25 \text{ vol.}\%$ has led to improved electrical properties of the coatings. A lowest resistivity of $6.2 \times 10^{-2} \Omega \cdot \text{cm}$ was obtained for coatings prepared with ATO containing $0.1 \text{ wt.}\%$ of MWNTs and sintered at $400 \text{ }^\circ\text{C}$. In spite of containing carbon nanotubes, transparency is maintained and 88% is obtained in the visible range. Such values are compared with others reported in the literature for the production of ATO coatings by sol-gel. The advantage on using the coatings developed in this work is that a transparent conductive film using a small quantity of electrically conductive powder is economically advantageous. Moreover, a decrease in the strength and adhesion of the film restrained by large quantities of powder can be prevented. Indeed, the addition of MWNTs has increased the hardness of the coatings from HB to $2H - 4H$, depending on the concentration of nanotubes employed.

TiO_2/MWNT nanocomposites with resistivity as low as $2.0 \times 10^{-1} \Omega \cdot \text{cm}$ were obtained. The transmission of conductive coatings in the visible range was lower than 52%. This result limits the use of such coatings in applications where a high transmittance at 550 nm is required. MWNTs presented a detrimental effect on the composite properties such as load-transfer mechanism failure resulting in inferior composite mechanical properties and poor appearance. Comparing the results obtained in this part of the study with the MWNT networks and ATO/MWNT composites presented in the previous sections, it turns out that an efficient dispersion of the carbon nanotubes is achieved when an appropriate

concentration of the cationic surfactant HDTAC is present. In the TiO_2 /MWNT studies, CNTs did not overcome the van der Waals attractions. Modifications are required in the composition of the dispersion or in the surface of the nanotubes in order to enhance the electrostatic/repulsive forces and therefore promote efficient dispersions.

Commercial applications making use of the bulk properties of CNTs are not yet available as predicted in the past. This will only be possible when a better understanding of CNTs and refinement of their synthesis process will be reached. In a single sample, MWNTs differ in diameter, number of walls and length. Moreover, different methods of productions lead to different levels of defects and byproducts. The application of CNTs in electronic devices is strongly dependent upon the reproducibility of individual CNTs on the large scale. However, precise control of nanotube morphology has yet to be realized. In addition, challenges remain in identifying appropriate dispersion protocols that can be used in economically attractive large-scale manufacturing.

Although the studied coatings did not meet the requirements necessary for a properly substitution of ITO in opto-electronic devices, their optical and electrical response as well as their low cost and simplicity of preparation allow them to be used in other applications where the high conductivity of ITO is not a requirement, such as in transparent antistatic layers [258].

8. OUTLOOK

1. The flexible electronics industry is growing fast, and consequently, plastic materials are promising to substitute glass in many fields. Therefore, the deposition of MWNT networks in plastic substrates would be also of great interest. Preliminary studies were conducted on polycarbonate (PC) substrates [267] and the results are shown in Appendix 9.8.
2. A subsequent patterning of the coatings studied would lead to functional structures and allow the creating of low-cost electronic devices. Different patterning techniques could be used for structuring the coatings presented in this work. Studies of direct laser interference patterning were recently performed [268] and are shown in Appendix 9.9.
3. The sintering of the networks and coatings in a reducing atmosphere could eventually lead to lower resistivities. In the case of networks, for example, a carbon atom from the carbon nanotube structure could be substituted by a nitrogen atom provenient from the atmosphere. The thermal degradation of the carbon nanotubes was performed under forming gas atmosphere and it was found out that their structure is preserved at temperatures much higher than 400 °C (see Appendix 9.10). In addition, preliminary studies on TiO_2 /MWNT networks sintered in forming gas at 400 °C for 30 *min* have shown that the sheet resistance of the coatings decreases from 40 to 15 $k\Omega/sq$.
4. The TiO_2 /MWNT coatings studied are not transparent in the visible range and therefore could not be used in applications where transparency is necessary. Nevertheless, the influence of the carbon nanotubes in the TiO_2 matrix could be studied for other applications, such as in photo-degradation efficiency of the coatings or improvement of the photocurrent [269,270].

9. APPENDIX

9.1 List of abbreviations

Table 9.1: List of abbreviations

AFM	Atomic force microscopy
ATO	Antimony-doped tin oxide
CNT	Carbon nanotubes
TG	Thermogravimetry
EDX	Energy-dispersive X-ray spectroscopy
FESEM	Field emitting scanning electron microscopy
GPTES	Glycidoxypropyl-triethoxysilane
GPTS	3-Glycidyloxypropyl-trimethoxysilane
HRTEM	High resolution transmission electron microscopy
HDTAC	Hexadecyl trimethyl ammonium chloride
ITO	Indium tin oxide (tin-doped indium oxide)
MWNT	Multi-walled carbon nanotubes
R_{sq}	Sheet resistance
SDS	Sodium dodecyl sulphate
SEM	Scanning electron microscopy
SWNT	Single-walled carbon nanotubes
TCO	Transparent conductive oxide
TCC	Transparent conductive coating
TEM	Transmission electron microscopy
TMAH	Tetramethyl ammonium hydroxide
WLI	White light interferometer
XRD	X-ray diffraction

9.2 List of used chemicals

Table 9.2: Chemicals used in the preparation of ATO powder

Starting Material	Molecular formula and molecular weight	Purity	Supplier
Tin (IV) chloride pentahydrate	$SnCl_4 \cdot 5H_2O$, 350.58	+98%	Aldrich
Antimony (III) chloride	$SbCl_3$, 228.11	> 99%	Fluka
Ammonia solution	NH_4OH , 35.04	p.a.	Ridel-de H�en
β -alanine	$C_3H_7NO_2$	> 99%	Fluka
Tetramethyl ammonium hydroxide	$C_4H_{13}NO$, 91.15	p.a.	Acr�s Organics

Table 9.3: Surfactants used for the dispersion of MWNTs

Surfactant	Molecular formula and molecular weight	Supplier	CMC in water at 298 K
Sodium dodecylsulphate salt	$C_{12}H_{25}NaO_4S$, 288.38	Merck	8.1 mM
Triton X-100	$C_4H_{22}O(C_2H_4O)_n$	Merck	$0.22 - 0.24 \times 10^{-3} \text{ mol/l}$
Hexadecyl trimethylammonium chloride	$CH_3(CH_2)_{15}N(CH_3)_3Cl$, 320.01	Aldrich	0.0032 mM

9.3 List of instruments and equipment used

- Autoclave: Teflon 250ml, DAH 904, Berghof
- Centrifuge Megafuge: 2.05, Heraeus
- Diffractometer 320 SII Seiko Instr.
- Dishwashing machine G7795/1 IR6001, Miele Aqua Purificator
- Film thickness: Profilometer P10 surface profilometer, Tencor
- High resolution transmission electron microscope (HRTEM): CM 200 FEG, Philips
- Microfluidizer Microfluidics Corp.
- Photon correlation spectrometer (PCS): ALV5000 DLS and SLS; ALV-Laser
- Scanning electron microscope (SEM): JSM 6400F, Jeol
- Sheet resistance: 34401A multimeter, Hewlett Packard
- Spectrophotometer Cary 5E Varian
- Spin Coater Model 1001, CPS II control system, CONVAC
- Substrate cleaning: Rinsing machine, professional IR 6001, Miele
- Transmission electron microscope (TEM): JEM-200CX, Jeol
- Ultrafine particle analyser (UPA): UPA 400, Grimm
- White lite interferometer (WLI) Zygo New View 5000
- X-ray diffractometer: D500, Siemens
- X-ray diffractometer: X'Pert MRD; Philips

9.4 Metallic behavior of MWNTs

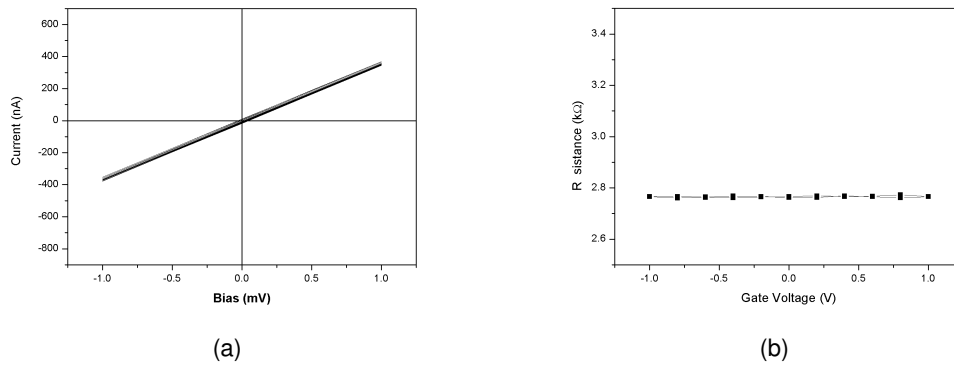


Fig. 9.1: Typical behavior of MWNTs: (a) source drain current through the MWNTs measured as a function of the bias voltage; and (b) derived resistance as a function of the gate voltage. MWNT networks show no gate action.

9.5 ATO/MWNT coatings prepared with MWNTs dispersed in anionic and non-ionic surfactants

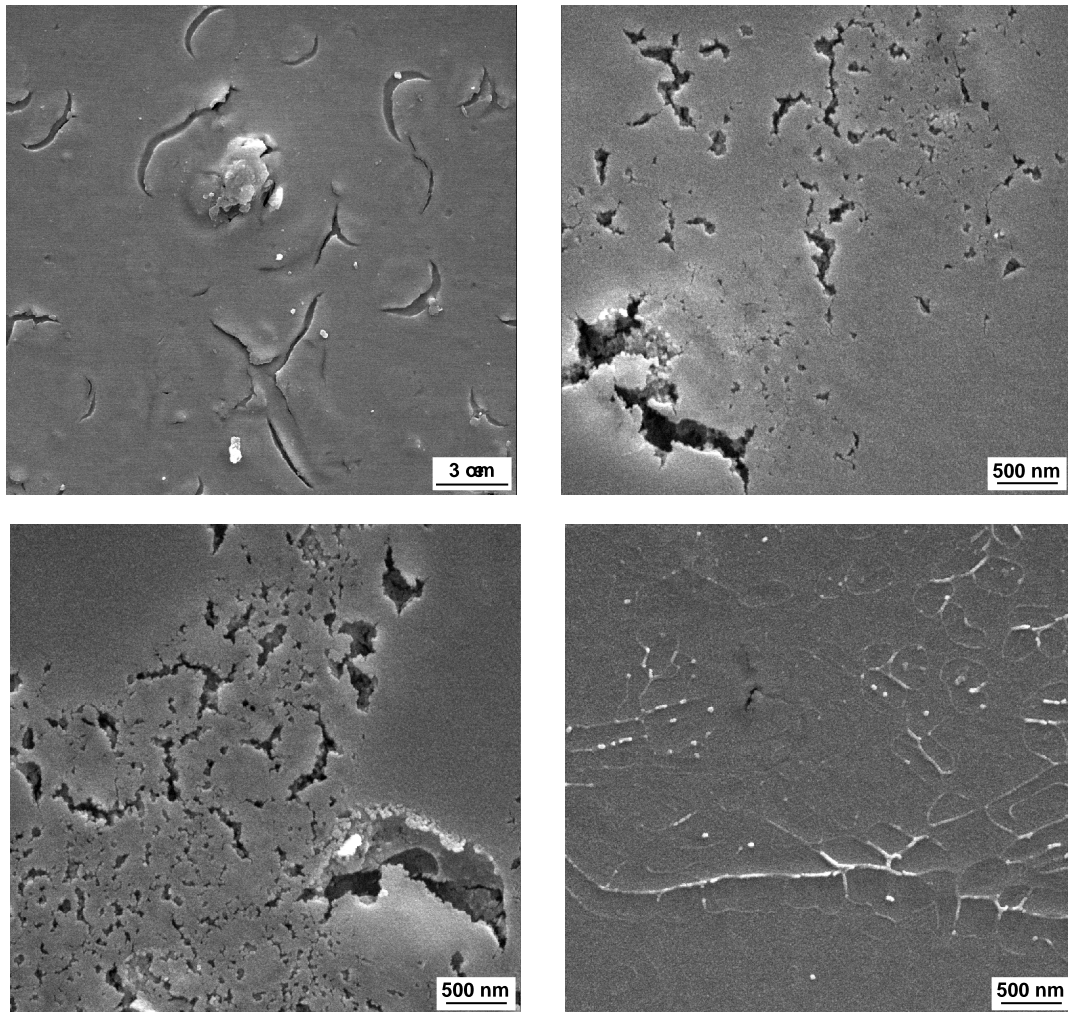


Fig. 9.2: Scanning electron microscopy micrographs of ATO/MWNT coatings prepared with $-NH_2$ MWNTs dispersed in (a) sodium dodecyl sulphate and (b) Triton X-100; and $-COOH$ MWNTs also dispersed in (c) sodium dodecyl sulphate and (d) Triton X-100. The poor appearance denotes aggregation of nanotubes in the cited surfactants.

The inefficient dispersion of functionalized MWNTs in sodium dodecyl sulphate and Triton X-100 was also reflected in the electrical properties of the coatings: the resistivities obtained were higher than that presented by pure ATO coatings.

9.6 Preparation of TiO_2 -based sol used as a matrix for the dispersion of MWNTs.

Preparation of TiO_2 -based sol [240]

Basic sols:

a. Synthesis of the *Ti*-containing sol (TIPOT)

176.3g (9.62mol) tetra-isopropyl-orthotitanate were added to 1276.6g 2-propanol. 62.0g (0.62mol) acetylacetone were added under stirring. After 15 minutes stirring at room temperature, a solution consisting of 17.22g water and 41.22g *HCl* 37% were slowly added. The mixture was stirred at room temperature for 24h and stored in a refrigerator (4 °C).

b. Synthesis of *Si*-containing sol (TEOS-hydrolysate)

494.35 g (2.37 mol) tetraethoxysilane and 362.5 g water were stirred at room temperature. 6.88 g *HCl* 37% were added. The mixture was stirred continuously until it was clear. After about 5 minutes, the sol became turbid for a few seconds. After this, the reaction starts. The sol becomes clear again and the temperature increases. After the reaction has been started, 638.3 g ethanol was added and stirred again for 2 hours. The sol was stored at room temperature.

c. Synthesis of the GPTS-hydrolysate

326.34 g (1 mol) 3-Glycidyloxypropyl-trimethoxysilane and 27.0 g 0.1 N *HCl* were stirred for 24 h at 40 °C. The resulting methanol has to be removed by vacuum distillation (50 mbar, 1 h, 45 °C). The hydrolysed sol was stored at room temperature.

Synthesis of sol for spin coating:

2002.0 g TIPOT was added under stirring to 829.4 g 2-propanol. 104.1 g TEOS-hydrolysate, 207.33 g 1-butanol and 2.14 g GPTS-hydrolysate were added and the mixture was stirred for 5 minutes.

9.7 Prices of commercially available carbon nanotubes.

Table 9.4: Prices of different commercially available CNTs.

Company	Type of Nanotubes	Price per gram
Apex Nanomaterials (USA)	Purified SWNTs (CVD and arc grown)	250 U\$
Bucky (USA)	Purified MWNT and SWNT	150 U\$ (MWNT) and 750 U\$ (SWNT)
Carbol ex (USA)	SWNT	100 U\$
Carbon Nanotechnologies Inc. (USA)	Different types of SWNT HiPCo	500-2000 U\$
n-TEC (Norway)	Arc discharge MWNTs	40 €
Nanocyl S.A. (Belgium)	CVD purified MWNTs and SWNTs	65-100 € (MWNT) and 200-450 € (SWNT)
NANOLAB (USA)	CVD SWNT purified	110-165 U\$
Nanoledge (France)	60% pure SWNT	145 €
Sun Nanotech China	Purified MWNT-acetylene and MWNT_liquid petroleum gas	3 U\$
Timesnano / Chinese Academy of Science	Purified SWNT and MWNT	3-10 U\$ (MWNT) and 30-50 U\$ (SWNT)

Prices from September 2007
source: Companies' homepages

9.8 Coatings deposited on polycarbonate (PC) substrate

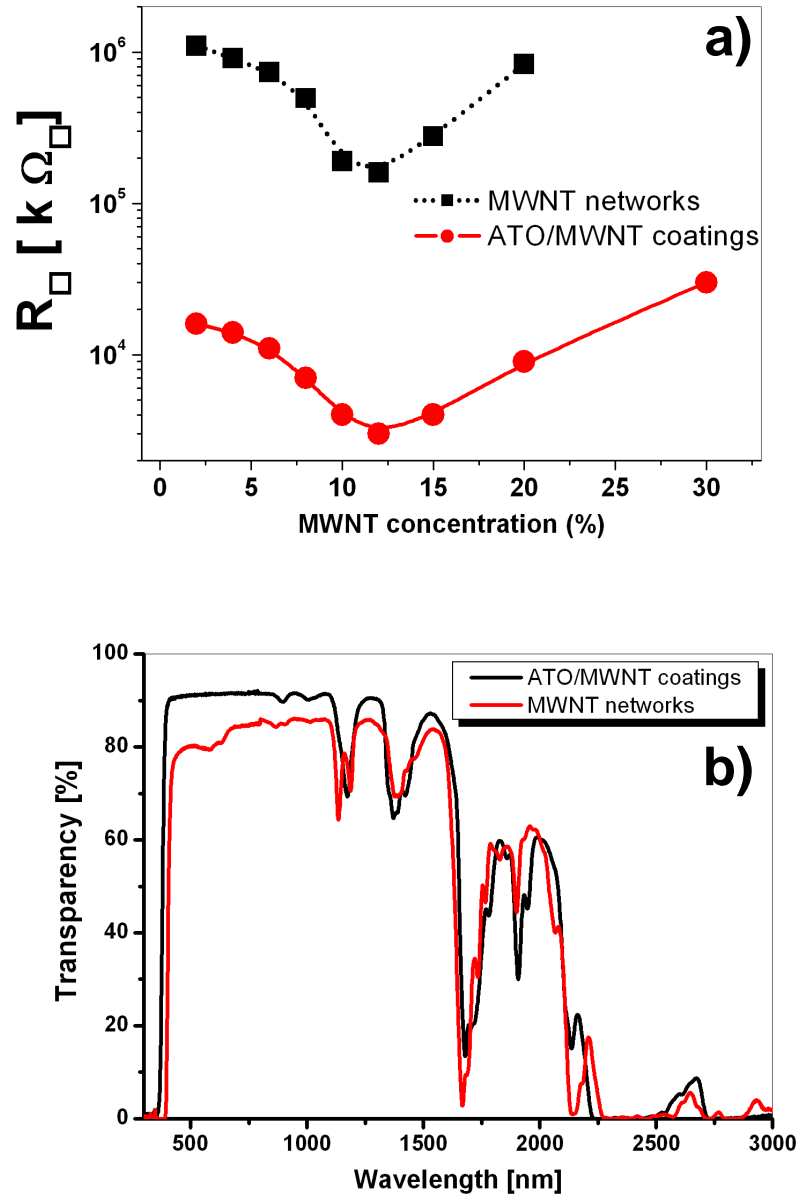


Fig. 9.3: Preliminary studies of the deposition of ATO/MWNT and MWNT networks on polycarbonate (PC) substrates. (a) Sheet resistance as a function of the concentration of MWNTs; and (b) transparency of the coatings. Both ATO/MWNT and MWNT networks were deposited by spin coating and sintered in air at 130 °C for 3 h.

9.9 Direct laser interference patterning of the coatings

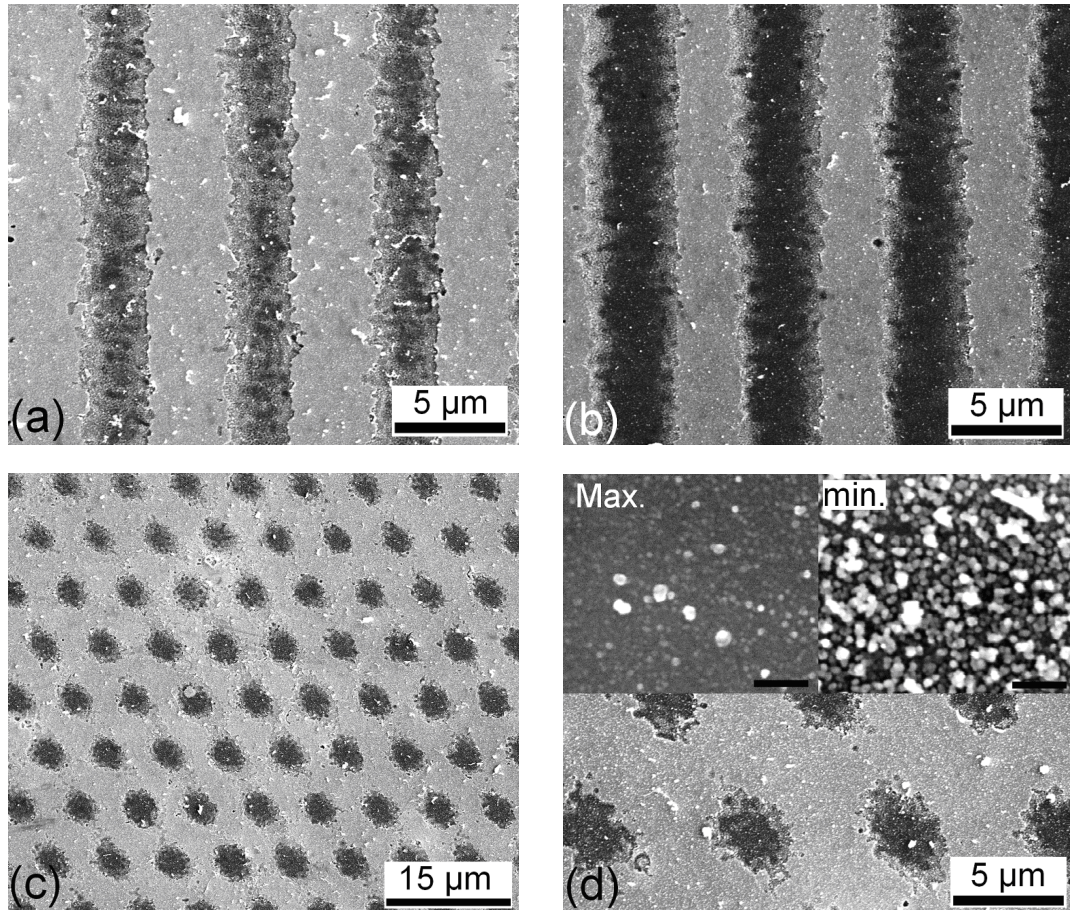


Fig. 9.4: Scanning electron microscope micrographs of irradiated ATO/MWNT coatings with (a, b) two and (c, d) three laser beams interference patterns: (a) Laser fluence = 207 mJ/cm^2 ; (b) Laser fluence = 483 mJ/cm^2 ; (c, d) Laser fluence = 644 mJ/cm^2 . The insert in (d) shows the surface morphology at the interference maximum (Max.) and minimum (min.). The scale bar in the insert of (d) is 200 nm . Well defined arrays of conductive nanostructures can be fabricated in one single laser pulse.

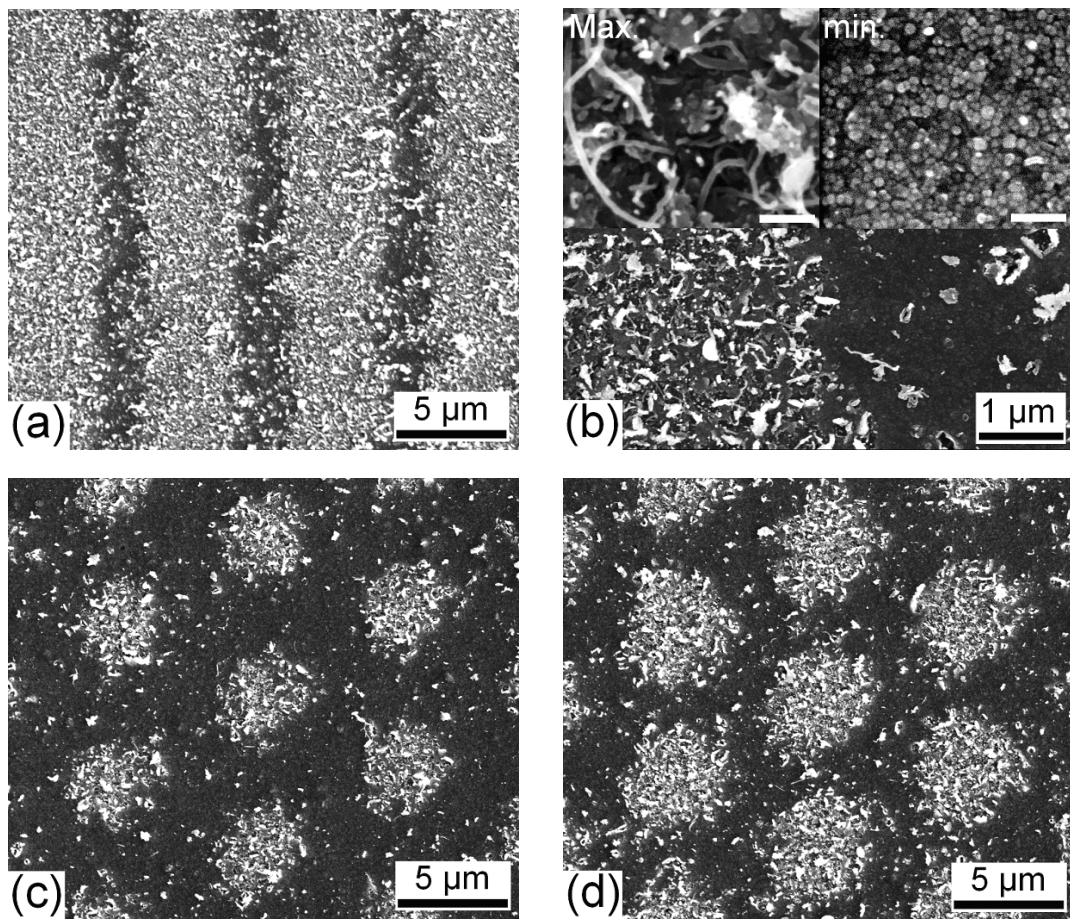


Fig. 9.5: Scanning electron microscope micrographs of irradiated MWNT-NET-Si with (a, b) two and (c, d) three laser beams interference patterns. The laser fluences were (a) 272, (b) 251, (c) 163, and (d) 211 mJ/cm^2 . The insert in (b) shows the surface morphology at the interference maximum (Max.) and minimum (min.). The scale bar in the insert of (b) is 200 nm.

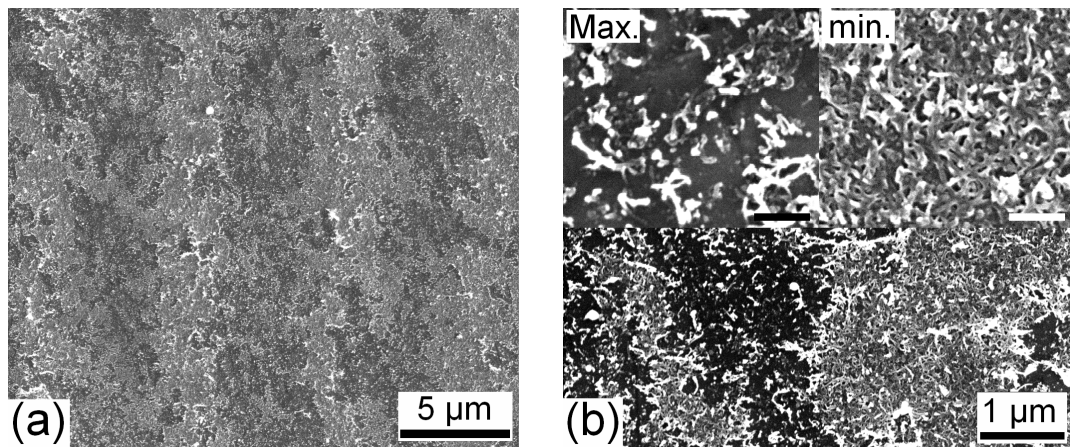


Fig. 9.6: Scanning electron microscope micrographs of low-adherent MWNT-NET irradiated with two laser beam configuration. The laser fluence was $309 \text{ mJ}/\text{cm}^2$. In (a), three laser interference minima are observed. (b) Detail at interference minimum and maximum. The insert in (b) shows the surface morphology at the maxima (Max.) and minima (min.). The scale bar in the insert of (b) is 200 nm .

9.10 Thermogravimetric analysis of MWNTs under forming gas atmosphere

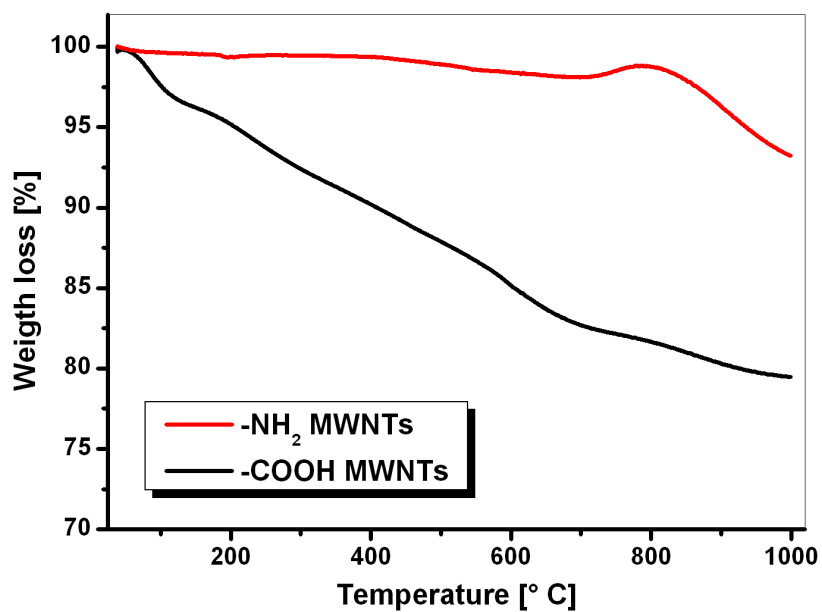


Fig. 9.7: Thermal behaviour of MWNTs under forming gas atmosphere (10 °C/min).

BIBLIOGRAPHY

- [1] H. K. Schmidt. Considerations about the sol-gel process: From the classical sol-gel route to advanced chemical nanotechnologies. *Journal of Sol-Gel Science and Technology*, 40(2):115–130, 2006.
- [2] S. Iijima. Helical microtubules of graphite carbon. *Nature*, 354(6348):56–58, 1991.
- [3] S.M. Sze. *Physics of Semiconductor Devices*. Wiley-Interscience New York, 2007.
- [4] G. Haacke. Evaluation of cadmium stannate films for solar heat collectors. *Applied Physics Letters*, 30:380, 1977.
- [5] J. F. Wager. Transparent Electronics. *Science*, 300(5623):1245–1246, 2003.
- [6] B. G. Lewis and D. C. Paine. Applications and Processing of Transparent Conducting Oxides. *Materials Research Society Bulletin*, 25(8):22–27, 2000.
- [7] C. G. Granqvist. Transparent conductive electrodes for electrochromic devices: A review. *Applied Physics A: Materials Science & Processing*, 57(1):19–24, 1993.
- [8] A. L. Dawar and J. C. Joshi. Semiconducting transparent thin films: their properties and applications. *Journal of Materials Science*, 19(1):1–23, 1984.
- [9] Z. M. Jarzebski and J. P. Morton. Physical Properties of SnO_2 Materials. *Journal of the Electrochemical Society*, 123(10):333C–346C, 1976.
- [10] T. Arai. The Study of the Optical Properties of Conducting Tin Oxide Films and their Interpretation in Terms of a Tentative Band Scheme. *Journal of the Physical Society of Japan*, 15(5):916–927, 1960.
- [11] C. M. Lampert. Heat Mirror Coatings for Energy Conserving Windows. *Solar Energy Materials*, 6(1):1–41, 1981.

- [12] J. Watson. Tin oxide gas sensor and its applications. *Sensors Actuators*, 5(1):29–42, 1984.
- [13] J.-C. Guillaumon, L. J. C. Blet, and F. M. J. B. Guerard. Process for the preparation of an antimony oxide-doped tin oxide pigment with improved electrical conductivity properties, and white and tinted conductive paints containing this pigment which are useful for the removal of electrostatic charges, April 07 1987. US Patent 4655966.
- [14] K. Wakabayashi, Y. Kamiya, and N. Ohta. Oxidation of Propylene over the Tin-Antimony Oxide Catalysts. I. Dependency of Acrolein Formation on the Composition of Catalyst and Calcination Conditions. *Bulletin of the Chemical Society of Japan*, 40(9):2172–2176, 1967.
- [15] W. Dazhi, W. Shulin, C. Jun, Z. Suyuan, and L. Fangqing. Microstructure of SnO_2 . *Physical Review B*, 49(20):14282–14285, 1994.
- [16] D. R. Acosta, W. Estrada, R. Castanedo, A. Maldonado, and M. A. Valenzuela. Structural and surface studies of tin oxide films doped with fluorine. *Thin Solid Films*, 375(1-2):147–150, 2000.
- [17] A. E. Rakhshani, Y. Makdisi, and H. A. Ramazaniyan. Electronic and optical properties of fluorine-doped tin oxide films. *Journal of Applied Physics*, 83:1049, 1998.
- [18] K. C. Mishra, K. H. Johnson, and P. C. Schmidt. Electronic structure of antimony-doped tin oxide. *Physical Review B*, 51(20):13972–13976, 1995.
- [19] E. Shanthi, V. Dutta, A. Banerjee, and K. L. Chopra. Electrical and optical properties of undoped and antimony-doped tin oxide films. *Journal of Applied Physics*, 51:6243, 1980.
- [20] S. A. Nasser. Characterization of boron-doped tin oxide thin films. *Thin Solid Films*, 342(1-2):47–51, 1999.
- [21] E. Shanti, A. Banerjee, V. Dutta, and K. L. Chopra. Electrical and optical properties of tin oxide films doped with F and (Sb+F). *Journal of Applied Physics*, 53:1615–1621, 1982.
- [22] A. Rohatgi, T. R. Viverito, and L. H. Slack. Electrical and Optical Properties of Tin Oxide Films. *Journal of the American Ceramic Society*, 57(6):278, 1974.

- [23] A. F. Carroll and L. H. Slack. Effects of Additions to SnO Thin Films. *Journal of The Electrochemical Society*, 123:1889, 1976.
- [24] C. G. Fonstad and R. H. Rediker. Electrical Properties of High-Quality Stannic Oxide Crystals. *Journal of Applied Physics*, 42(7):2911–2918, 1971.
- [25] E. Shanthi, A. Banerjee, and K. L. Chopra. Dopants Effects in Sprayed Tin Oxide Films. *Thin Solid Films*, 88:93–100, 1982.
- [26] E. Burstein. Anomalous Optical Absorption Limit in InSb. *Physical Review*, 93(3):632–633, 1954.
- [27] W. M. Sears and M. Gee. Mechanics of film formation during the spray pyrolysis of tin oxide. *Thin Solid Films*, 165(1):265–277, 1988.
- [28] S. H. Park, Y. C. Son, W. S. Wills, S. L. Suib, and K. E. Creasy. Tin oxide films made by physical vapor deposition thermal oxidation and spray pyrolysis. *Chemistry of Materials*, 10(9):2389–2398, 1998.
- [29] G. Sanon, R. Rup, and A. Mansingh. Growth and characterization of tin oxide films prepared by chemical vapour deposition. *Thin Solid Films*, 190(2):287–301, 1990.
- [30] A. Czapla, E. Kusior, and M. Bucko. Optical properties of non-stoichiometric tin oxide films obtained by reactive sputtering. *Thin Solid Films*, 182(1-2):15–22, 1989.
- [31] D. W. Lane, J. A. Coath, K. D. Rogers, B. J. Hunnikin, and H. S. Beldon. Optical properties and structure of thermally evaporated tin oxide films. *Thin Solid Films*, 221(1-2):262–266, 1992.
- [32] C. M. Dai, C. S. Su, and D. S. Chuu. Growth of highly oriented tin oxide thin films by laser evaporation deposition. *Applied Physics Letters*, 57:1879, 1990.
- [33] C. Goebbert, R. Nonninger, M. A. Aegerter, and H. K. Schmidt. Wet chemical deposition of ATO and ITO coatings using crystalline nanoparticles redispersable in solutions. *Thin Solid Films*, 351(1-2):79–84, 1999.
- [34] C. Goebbert, M. A. Aegerter, D. Burgard, R. Nass, and H. K. Schmidt. Conducting Membranes and Coatings Made From Redispersable Nanoscaled Crystalline SnO_2 : Sb Particles. *Materials Research Society Symposium Proceedings*, 520:293–304, 1998.

- [35] K. L. Chopra, S. Major, and D. K. Pandya. Transparent conductors – a status review. *Thin Solid Films*, 102(1):1–46, 1983.
- [36] R. L. Weiher and R. P. Ley. Optical Properties of Indium Oxide. *Journal of Applied Physics*, 37:299, 1966.
- [37] J. H. W. de Wit. Electrical properties of In_2O_3 . *Journal of Solid State Chemistry*, 8(2):142–149, 1973.
- [38] J. H. W. De Wit. Structural aspects and defect chemistry in In_2O_3 . *Journal of Solid State Chemistry*, 20(2), 1977.
- [39] I. Hamberg and C. G. Granqvist. Evaporated Sn -doped In_2O_3 films: Basic optical properties and applications to energy-efficient windows. *Journal of Applied Physics*, 60:R123–R160, 1986.
- [40] R. B. H. Tahar, T. Ban, Y. Ohya, and Y. Takahashi. Tin doped indium oxide thin films: Electrical properties. *Journal of Applied Physics*, 83:2631, 1998.
- [41] I. Safi and R. P. Howson. The properties of reactively-sputtered, stoichiometry-controlled and optimum-conductivity transparent indium oxide films as a function of their titanium, aluminium and zinc content; comparisons with the use of tin as a dopant. *Thin Solid Films*, 343:115–118, 1999.
- [42] J. L. Vossen. RF Sputtered Transparent Conductors: The System $In_2O_3 - SnO_2$. *RCA Review*, 32:289–296, 1971.
- [43] C. Nunes de Carvalho, A. M. Botelho do Rego, A. Amaral, P. Brogueira, and G. Lavareda. Effect of substrate temperature on the surface structure, composition and morphology of indium–tin oxide films. *Surface & Coatings Technology*, 124(1):70–75, 2000.
- [44] L. Gupta, A. Mansingh, and P. K. Srivastava. Band gap narrowing and the band structure of tin-doped indium oxide films. *Thin Solid Films*, 176(1):33–44, 1989.
- [45] K. S. Ramaiah, V. S. Raja, A. K. Bhatnagar, R. D. Tomlinson, R. D. Pilkington, A. E. Hill, S. J. Chang, Y. K. Su, and F. S. Juang. Optical, structural and electrical properties of tin doped indium oxide thin films prepared by spray-pyrolysis technique. *Semiconductor Science and Technology*, 15(7):676–683, 2000.

- [46] J. W. Bae, H. J. Kim, J. S. Kim, N. E. Lee, and G. Y. Yeom. Effects of oxygen ion beam plasma conditions on the properties of Indium tin oxide thin films. *Vacuum*, 56(1):77–81, 2000.
- [47] H. J Kim, J. W Bae, J. S Kim, K. S Kim, Y. C Jang, G. Y Yeom, and N. E. Lee. Properties of amorphous tin-doped indium oxide thin films deposited by O_2/Ar mixture ion beam-assisted system at room temperature. *Surface and Coatings Technology*, 131(1):201–205, 2000.
- [48] R. B. H. Tahar, T. Ban, Y. Ohya, and Y. Takahashi. Optical, structural, and electrical properties of indium oxide thin films prepared by the sol-gel method. *Journal of Applied Physics*, 82:865, 1997.
- [49] S. S. Kim, S. Y. Choi, C. G. Park, and H. W. Jin. Transparent conductive ITO thin films through the sol-gel process using metal salts. *Thin Solid Films*, 347(1-2):155–160, 1999.
- [50] M. J. Alam and D. C. Cameron. Optical and electrical properties of transparent conductive ITO thin films deposited by sol–gel process. *Thin Solid Films*, 377:455–459, 2000.
- [51] C. Goebbert, H. Bisht, N. Al-Dahoudi, R. Nonninger, M. A. Aegerter, and H. K. Schmidt. Wet Chemical Deposition of Crystalline, Redispersable ATO and ITO Nanoparticles. *Journal of Sol-Gel Science and Technology*, 19(1):201–204, 2000.
- [52] K. Zhang, F. Zhu, C.H.A. Huan, and A. T. S. Wee. Indium tin oxide films prepared by radio frequency magnetron sputtering method at a low processing temperature. *Thin Solid Films*, 376(1-2):255–263, 2000.
- [53] F. El Akkad, A. Punnoose, and G. Prabu. Properties of ITO films prepared by rf magnetron sputtering. *Applied Physics A: Materials Science & Processing*, 71(2):157–160, 2000.
- [54] R. Mientus and K. Ellmer. Reactive magnetron sputtering of tin-doped indium oxide (ITO): influence of argon pressure and plasma excitation mode. *Surface & Coatings Technology*, 142:748–754, 2001.
- [55] H. L. Hartnagel, A. L. Dawar, A. K. Jain, and C. Jagadish. *Semiconducting transparent thin films*, Institute of Physics Publishing, Bristol and Philadelphia, Ed. Institute of Physics Pub., 1995.

- [56] D. S. Ginley and C. Bright. Transparent conducting oxides. *Materials Research Society Bulletin*, 25(8):15–21, 2000.
- [57] S. J. Pearton, D. P. Norton, K. Ip, Y. W. Heo, and T. Steiner. Recent progress in processing and properties of ZnO. *Superlattices and Microstructures*, 34(1-2):3–32, 2003.
- [58] K. Ueda, H. Tabata, and T. Kawai. Magnetic and electric properties of transition-metal-doped ZnO films. *Applied Physics Letters*, 79:988, 2001.
- [59] T. Minami, T. Yamamoto, and T. Miyata. Highly transparent and conductive rare earth-doped ZnO thin films prepared by magnetron sputtering. *Thin Solid Films*, 366(1-2):63–68, 2000.
- [60] W. W. Wenas, A. Yamada, K. Takahashi, M. Yoshino, and M. Konagai. Electrical and optical properties of boron-doped ZnO thin films for solar cells grown by metalorganic chemical vapor deposition. *Journal of Applied Physics*, 70:7119, 1991.
- [61] E. Eby, R. O’Shaughnessy, and R. Bond. High transmittance, low emissivity coatings for substrates, June 13 2006. US Patent 7,060,359.
- [62] M. Jin, J. Feng, Z. De-heng, M. Hong-lei, and L. Shu-ying. Optical and electronic properties of transparent conducting ZnO and ZnO : Al films prepared by evaporating method. *Thin Solid Films*, 357(2):98–101, 1999.
- [63] H. Nanto, T. Minami, S. Shooji, and S. Takata. Electrical and optical properties of zinc oxide thin films prepared by rf magnetron sputtering for transparent electrode applications. *Journal of Applied Physics*, 55:1029, 1984.
- [64] P. F. Garcia, R. S. McLean, M. H. Reilly, and G. Nunes. Transparent ZnO thin-film transistor fabricated by rf magnetron sputtering. *Applied Physics Letters*, 82(7):1117–1119, 2003.
- [65] M. Krunk and E. Mellikov. Zinc oxide thin films by the spray pyrolysis method. *Thin Solid Films*, 270(1-2):33–36, 1995.
- [66] M. N. Kamalasanan and S. Chandra. Sol-gel synthesis of ZnO thin films. *Thin Solid Films*, 288(1-2):112–115, 1996.

- [67] Y. Natsume and H. Sakata. Zinc oxide films prepared by sol-gel spin-coating. *Thin Solid Films*, 372(1-2):30–36, 2000.
- [68] J. P. Lu. Elastic Properties of Carbon Nanotubes and Nanoropes. *Physical Review Letters*, 79(7):1297–1300, 1997.
- [69] T. W. Odom, J. L. Huang, P. Kim, and C. M. Lieber. Structure and electronic properties of carbon nanotubes. *Journal of Physical Chemistry B*, 104(13):2794–2809, 2000.
- [70] M. S. Dresselhaus. *Carbon Nanotubes: Synthesis, Structure, Properties, and Applications*. Springer, 2001.
- [71] M. Terrones, W. K. Hsu, H. W. Kroto, and D. R. M. Walton. Nanotubes: a revolution in materials science and electronics. *Topics in Current Chemistry*, 199:189–234, 1999.
- [72] P. M. Ajayan and O. Z. Zhou. Applications of Carbon Nanotubes. *Topics in Applied Physics*, 80:391–425, 2001.
- [73] M. S. Dresselhaus and P. Avouris. Introduction to Carbon Materials Research. *Topics in Applied Physics*, 80:1–9, 2001.
- [74] A. Thess, R. Lee, P. Nikolaev, H. Dai, P. Petit, J. Robert, C. Xu, Y. H. Lee, S. G. Kim, A. G. Rinzler, D. T. Colbert, G. E. Scuseria, D. Tomanek, J. E. Fischer, and R. E. Smalley. Crystalline Ropes of Metallic Carbon Nanotubes. *Science*, 273(5274):483, 1996.
- [75] T. W. Ebbesen and P. M. Ajayan. Large-scale synthesis of carbon nanotubes. *Nature*, 358(6383):220–222, 1992.
- [76] C. Journet, W. K. Maser, P. Bernier, A. Loiseau, M. Lamy de La Chapelle, S. Lefrant, P. Deniard, R. Lee, and J. E. Fischer. Large-scale production of single-walled carbon nanotubes by the electric-arc technique. *Nature*, 388(6644):756, 1997.
- [77] A. G. Rinzler, J. Liu, H. Dai, P. Nikolaev, C. B. Huffman, F. J. Rodríguez-Macías, P. J. Boul, A. H. Lu, D. Heymann, D. T. Colbert, R. S. Lee, J. E. Fischer, A. M. Rao, P. C. Eklund, and R. E. Smalley. Large-scale purification of single-wall carbon nanotubes: process, product, and characterization. *Applied Physics A: Materials Science & Processing*, 67(1):29–37, 1998.

- [78] M. Endo, K. Takeuchi, K. Kobori, K. Takahashi, H. W. Kroto, and A. Sarkar. Pyrolytic carbon nanotubes from vapor-grown carbon fibers. *Carbon*, 33:873–881, 1995.
- [79] P. Nikolaev, M. J. Bronikowski, R. K. Bradley, F. Rohmund, D. T. Colbert, K. A. Smith, and R.E. Smalley. Gas-phase catalytic growth of single-walled carbon nanotubes from carbon monoxide. *Chemical Physics Letters*, 313(1-2):91–97, 1999.
- [80] H. Dai. Nanotube Growth and Characterization. *Topics in Applied Physics*, 80:29–53, 2001.
- [81] J. L. Zimmerman, R. K. Bradley, C. B. Huffman, R. H. Hauge, and J. L. Margrave. Gas-Phase Purification of Single-Wall Carbon Nanotubes. *Chemistry of Materials*, 12(5):1361–1366, 2000.
- [82] I. W. Chiang, B. E. Brinson, R. E. Smalley, J. L. Margrave, and R. H. Hauge. Purification and characterization of single-wall carbon nanotubes. *Journal of Physical Chemistry B*, 105(6):1157–1161, 2001.
- [83] J. M. Bonard, T. Stora, J. P. Salvetat, F. Maier, T. Stoeckli, C. Duschl, L. Forro, W. A. de Heer, and A. Chatelain. Purification and size-selection of carbon nanotubes. *Advanced Materials*, 9(10):827–831, 1997.
- [84] S. Bandow, A. M. Rao, K. A. Williams, A. Thess, R. E. Smalley, and P. C. Eklund. Purification of single-wall carbon nanotubes by microfiltration. *Journal of Physical Chemistry B*, 101(44):8839–8842, 1997.
- [85] G. S. Duesberg, M. Burghard, J. Muster, G. Philipp, and S. Roth. Separation of carbon nanotubes by size exclusion chromatography. *Chemical Communications*, (3):435–436, 1998.
- [86] J. N. Coleman, A. B. Dalton, S. Curran, A. Rubio, A. P. Davey, A. Drury, B. McCarthy, B. Lahr, P. M. Ajayan, and S. Roth. Phase Separation of Carbon Nanotubes and Turbostratic Graphite Using a Functional Organic Polymer. *Advanced Materials*, 12(3):213–216, 2000.
- [87] M. T. Martinez, M. A. Callejas, A. M. Benito, W. K. Maser, M. Cochet, J. M. Andres, J. Schreiber, O. Chauvet, and J. L. Fierro. Microwave single walled carbon nanotubes purification. *Chemical Communications*, (9):1000–1001, 2002.

- [88] E. Vazquez, V. Georgakilas, and M. Prato. Microwave-assisted purification of HiPco carbon nanotubes. *Chemical Communications*, (20):2308–2309, 2002.
- [89] A. R. Harutyunyan, B. K. Pradhan, J. Chang, G. Chen, and P. C. Eklund. Purification of single-wall carbon nanotubes by selective microwave heating of catalyst particles. *Journal of Physical Chemistry B*, 106(34):8671–8675, 2002.
- [90] M. S. Dresselhaus and R. Saito. *Physical Properties of Carbon Nanotubes*. Imperial College Press, 1998.
- [91] S. Niyogi, M. A. Hamon, H. Hu, B. Zhao, P. Bhowmik, R. Sen, M. E. Itkis, and R. C. Haddon. Chemistry of single-walled carbon nanotubes. *Accounts of Chemical Research*, 35(12):1105–1113, 2002.
- [92] M. Damnjanović, I. Milošević, T. Vuković, and R. Sredanović. Full symmetry, optical activity, and potentials of single-wall and multiwall nanotubes. *Physical Review B*, 60(4):2728–2739, 1999.
- [93] H. Dai. Carbon nanotubes: Synthesis, integration, and properties. *Accounts of Chemical Research*, 35(12):1035–1044, 2002.
- [94] B. Stojetz, C. Miko, L. Forró, and C. Strunk. Effect of Band Structure on Quantum Interference in Multiwall Carbon Nanotubes. *Physical Review Letters*, 94(18):186802, 2005.
- [95] C. Schönenberger, A. Bachtold, C. Strunk, J. P. Salvetat, and L. Forró. Interference and Interaction in multi-wall carbon nanotubes. *Applied Physics A: Materials Science & Processing*, 69(3):283–295, 1999.
- [96] P. G. Collins and P. Avouris. Nanotubes for electronics. *Scientific American*, 283(6):62–69, 2000.
- [97] F. Kreupl, A. P. Graham, G. S. Duesberg, W. Steinhögl, M. Liebau, E. Unger, and W. Hönlein. Carbon nanotubes in interconnect applications. *Microelectronic Engineering*, 64(1-4):399–408, 2002.
- [98] R. Klesse. Electron scattering in multiwall carbon nanotubes. *Physical Review B*, 66(8):85409, 2002.

- [99] S. Frank, P. Poncharal, Z. L. Wang, and W. A. de Heer. Carbon Nanotube Quantum Resistors. *Science*, 280(5370):1744–1746, 1998.
- [100] P. Poncharal, C. Berger, Y. Yi, Z. L. Wang, and W. A. de Heer. Room Temperature Ballistic Conduction in Carbon Nanotubes. *Journal of Physical Chemistry B*, 106(47):12104–12118, 2002.
- [101] J. O. Lee, C. Park, J. J. Kim, J. Kim, J. W. Park, and K. H. Yoo. Formation of low-resistance ohmic contacts between carbon nanotube and metal electrodes by a rapid thermal annealing method. *Journal of Physics D: Applied Physics*, 33(16):1953–1956, 2000.
- [102] P. G. Collins, M. S. Arnold, and P. Avouris. Engineering Carbon Nanotubes and Nanotube Circuits Using Electrical Breakdown. *Science*, 292(5517):706–709, 2001.
- [103] L. Vaisman, H. D. Wagner, and G. Marom. The role of surfactants in dispersion of carbon nanotubes. *Advances in Colloid and Interface Science*, 128:37–46, 2006.
- [104] O. Lourie, D. M. Cox, and H. D. Wagner. Buckling and Collapse of Embedded Carbon Nanotubes. *Physical Review Letters*, 81(8):1638–1641, 1998.
- [105] L. A. Girifalco and M. Hodak. Van der Waals binding energies in graphitic structures. *Physical Review B*, 65(12):125404, 2002.
- [106] K. D. Ausman, R. Piner, O. Lourie, R. S. Ruoff, and M. Korobov. Organic solvent dispersions of single-walled carbon nanotubes: toward solutions of pristine nanotubes. *Journal of Physical Chemistry B*, 104(38):8911–8915, 2000.
- [107] J. Liu, M. J. Casavant, M. Cox, D. A. Walters, P. Boul, W. Lu, A. J. Rimberg, K. A. Smith, D. T. Colbert, and R. E. Smalley. Controlled deposition of individual single-walled carbon nanotubes on chemically functionalized templates. *Chemical Physics Letters*, 303(1-2):125–129, 1999.
- [108] Y. Sun, S. R. Wilson, and D. I. Schuster. High dissolution and strong light emission of carbon nanotubes in aromatic amine solvents. *Journal of the American Chemical Society*, 123(22):5348–9, 2001.
- [109] J. L. Bahr, E. T. Mickelson, M. J. Bronikowski, R. E. Smalley, and J. M. Tour. Dissolution of small diameter single-wall carbon nanotubes in organic solvents. *Chemical Communications*, 193:194, 2001.

- [110] S. H. Wu and P. Pendleton. Adsorption of Anionic Surfactant by Activated Carbon: Effect of Surface Chemistry, Ionic Strength, and Hydrophobicity. *Journal of Colloid and Interface Science*, 243(2):306–315, 2001.
- [111] K. Esumi. Interactions between Surfactants and Particles: Dispersion, Surface Modification, and Adsolubilization. *Journal of Colloid and Interface Science*, 241:1–17, 2001.
- [112] R. D. Nelson. *Dispersing powders in liquids*. Elsevier, 1988.
- [113] J. C. Slattery. *Momentum, energy, and mass transfer in continua*. McGraw-Hill New York, 1972.
- [114] M. von Smoluchowski. Versuch einer mathematischen Theorie der Koagulationskinetik kolloider Lösungen. *Zeitschrift für Physikalische Chemie*, pages 129–168, 1918.
- [115] L. Jiang, L. Gao, and J. Sun. Production of aqueous colloidal dispersions of carbon nanotubes. *Journal of Colloid Interface Science*, 260(1):89–94, 2003.
- [116] M. J. Rosen. *Surfactants and interfacial phenomena*. New York, 1989.
- [117] K. Yurekli, C. A. Mitchell, and R. Krishnamoorti. Small-angle neutron scattering from surfactant-assisted aqueous dispersions of carbon nanotubes. *Journal of the American Chemical Society*, 126(32):9902–9903, 2004.
- [118] H. T. Ham, Y. S. Choi, and I. J. Chung. An explanation of dispersion states of single-walled carbon nanotubes in solvents and aqueous surfactant solutions using solubility parameters. *Journal of Colloid and Interface Science*, 286(1):216–223, 2005.
- [119] M. S. Strano, V. C. Moore, M. K. Miller, M. J. Allen, E. H. Haroz, C. Kittrell, R. H. Hauge, and R. E. Smalley. The role of surfactant adsorption during ultrasonication in the dispersion of single-walled carbon nanotubes. *Journal of Nanoscience and Nanotechnology*, 3(1-2):81–6, 2003.
- [120] D. W. Schaefer, J. M. Brown, D. P. Anderson, J. Zhao, K. Chokalingam, D. Tomlin, and J. Ilavsky. Structure and dispersion of carbon nanotubes. *Journal of Applied Crystallography*, 36(3):553–557, 2003.

- [121] L. Vaisman, G. Marom, and H. D. Wagner. Dispersions of Surface-Modified Carbon Nanotubes in Water-Soluble and Water-Insoluble Polymers. *Advanced Functional Materials*, 16(3):357–363, 2006.
- [122] V. C. Moore, M. S. Strano, E. H. Haroz, R. H. Hauge, R. E. Smalley, J. Schmidt, and Yeshayahu T. Individually suspended single-walled carbon nanotubes in various surfactants. *Nano Letters*, 3(10):1379–1382, 2003.
- [123] E. A. Whitsitt and A. R. Barron. Silica coated single walled carbon nanotubes. *Nano Letters*, 3(6):775–778, 2003.
- [124] O. Matarredona, H. Rhoads, Z. Li, J. H. Harwell, L. Balzano, and D. E. Resasco. Dispersion of single-walled carbon nanotubes in aqueous solutions of the anionic surfactant NaDDBS. *Journal of Physical Chemistry B*, 107(48):13357–13367, 2003.
- [125] M. F. Islam, E. Rojas, D. M. Bergey, A. T. Johnson, and A. G. Yodh. High weight fraction surfactant solubilization of single-wall carbon nanotubes in water. *Nano Letters*, 3(2):269–273, 2003.
- [126] R. Czerw, M. Terrones, J.-C. Charlier, X. Blase, B. Foley, R. Kamalakaran, N. Grobert, H. Terrones, D. Tekleab, P. M. Ajayan, W. Blau, M. Rühle, and D. L. Carroll. Identification of Electron Donor States in N-Doped Carbon Nanotubes. *Nano Letters*, 1(9):457 – 460, 2001.
- [127] M. J. O’Connell, S. M. Bachilo, C. B. Huffman, V. C. Moore, M. S. Strano, E. H. Haroz, K. L. Rialon, P. J. Boul, W. H. Noon, C. Kittrell, J. Ma, R. H. Hauge, R. B. Weisman, and R. E. Smalley. Band Gap Fluorescence from Individual Single-Walled Carbon Nanotubes. *Science*, 297(5581):593–596, 2002.
- [128] A. Hirsch. Functionalization of Single-Walled Carbon Nanotubes. *Angewandte Chemie International Edition*, 41(11):1853, 2002.
- [129] X. Gong, J. Liu, S. Baskaran, R. D. Voise, and J.S. Young. Surfactant-assisted processing of carbon nanotube/polymer composites. *Chemistry of Materials*, 12(4):1049–1052, 2000.
- [130] K. A. Watson, S. Ghose, D. M. Delozier, J. G. Smith, and J. W. Connell. Transparent, flexible, conductive carbon nanotube coatings for electrostatic charge mitigation. *Polymer*, 46(7):2076–2085, 2005.

- [131] T. Takenobu, T. Takahashi, T. Kanbara, K. Tsukagoshi, Y. Aoyagi, and Y. Iwasa. High-performance transparent flexible transistors using carbon nanotube films. *Applied Physics Letters*, 88:033511, 2006.
- [132] K. Parikh, K. Cattanach, R. Rao, D. S. Suh, A. Wu, and S. K. Manohar. Flexible vapour sensors using single walled carbon nanotubes. *Sensors and Actuators B*, 113(1):55–63, 2006.
- [133] M. Kaempgen and S. Roth. Transparent and flexible carbon nanotube/polyaniline pH sensors. *Journal of Electroanalytical Chemistry*, 586(1):72–76, 2006.
- [134] Q. H. Wang, A. A. Setlur, J. M. Lauerhaas, J. Y. Dai, E. W. Seelig, and R. P. H. Chang. A nanotube-based field-emission flat panel display. *Applied Physics Letters*, 72:2912, 1998.
- [135] A. Du Pasquier, H. E. Unalan, A. Kanwal, S. Miller, and M. Chhowalla. Conducting and transparent single-wall carbon nanotube electrodes for polymer-fullerene solar cells. *Applied Physics Letters*, 87:203511, 2005.
- [136] R. Martel, T. Schmidt, H. R. Shea, T. Hertel, and P. Avouris. Single-and multi-wall carbon nanotube field-effect transistors. *Applied Physics Letters*, 73(17):2447–2449, 1998.
- [137] A. Bachtold, P. Hadley, T. Nakanishi, and C. Dekker. Logic Circuits with Carbon Nanotube Transistors. *Science*, 294(5545):1317, 2001.
- [138] P. Avouris. Molecular electronics with carbon nanotubes. *Accounts of Chemical research*, 35(12):1026–1034, 2002.
- [139] P. Calvert. Nanotube composites- A recipe for strength. *Nature*, 399(6733):210, 1999.
- [140] P. M. Ajayan, L. S. Schadler, C. Giannaris, and A. Rubio. Single-Walled Carbon Nanotube–Polymer Composites: Strength and Weakness. *Advanced Materials*, 12(10):750–753, 2000.
- [141] B. Safadi, R. Andrews, and E. A. Grulke. Multiwalled carbon nanotube polymer composites: Synthesis and characterization of thin films. *Journal of Applied Polymer Science*, 84(14):2660–2669, 2002.

- [142] A. A. Mamedov, N. A. Kotov, M. Prato, D. M. Guldi, J. P. Wicksted, and A. Hirsch. Molecular design of strong single-wall carbon nanotube/polyelectrolyte multilayer composites. *Nature Materials*, 1(3):190–194, 2002.
- [143] W. A. de Heer, A. Châtelain, and D. Ugarte. A Carbon Nanotube Field-Emission Electron Source. *Science*, 270(5239):1179, 1995.
- [144] A. G. Rinzler, J. H. Hafner, P. Nikolaev, P. Nordlander, D. T. Colbert, R. E. Smalley, L. Lou, S. G. Kim, and D. Tomanek. Unraveling Nanotubes: Field Emission from an Atomic Wire. *Science*, 269(5230):1550, 1995.
- [145] W. B. Choi, D. S. Chung, J. H. Kang, H. Y. Kim, Y. W. Jin, I. T. Han, Y. H. Lee, J. E. Jung, N. S. Lee, G. S. Park, and J. M. Kim. Fully sealed, high-brightness carbon-nanotube field-emission display. *Applied Physics Letters*, 75:3129, 1999.
- [146] Y. Saito and S. Uemura. Field emission from carbon nanotubes and its application to electron sources. *Carbon*, 38(2):169–182, 2000.
- [147] H. Sugie, M. Tanemura, V. Filip, K. Iwata, K. Takahashi, and F. Okuyama. Carbon nanotubes as electron source in an x-ray tube. *Applied Physics Letters*, 78:2578, 2001.
- [148] N. S. Lee, D. S. Chung, I. T. Han, J. H. Kang, Y. S. Choi, H. Y. Kim, S. H. Park, Y. W. Jin, W. K. Yi, M. J. Yun, J. E. Jung, C. J. Lee, J. H. You, S. H. Joo, C. G. Lee, and J. M. Kim. Application of carbon nanotubes to field emission displays. *Diamond and Related Materials*, 10(2):265–270, 2001.
- [149] C. Liu, Y. Y. Fan, M. Liu, H. T. Cong, H. M. Cheng, and M. S. Dresselhaus. Hydrogen Storage in Single-Walled Carbon Nanotubes at Room Temperature. *Science*, 286(5442):1127–1129, 1999.
- [150] A. C. Dillon, K. M. Jones, T. A. Bekkedahl, C. H. Kiang, D. S. Bethune, and M. J. Heben. Storage of hydrogen in single-walled carbon nanotubes. *Nature*, 386(6623):377–379, 1997.
- [151] M. Hirscher, M. Becher, M. Haluska, U. Dettlaff-Weglikowska, A. Quintel, G. S. Duesberg, Y. M. Choi, P. Downes, M. Hulman, S. Roth, I. Stepanek, and P. Bernier. Hydrogen storage in sonicated carbon materials. *Applied Physics A: Materials Science & Processing*, 72(2):129–132, 2001.

- [152] L. Schlapbach and A. Züttel. Hydrogen-storage materials for mobile applications. *Nature*, 414(6861):353–8, 2001.
- [153] D. T. Colbert. Single-wall nanotubes: a new option for conductive plastics and engineering polymers. *Plastics Additives and Compounding*, 5:18–25, 2003.
- [154] B. Berkowitz and R. P. Ewing. Percolation Theory and Network Modeling Applications in Soil Physics. *Surveys in Geophysics*, 19(1):23–72, 1998.
- [155] T. Minami. Transparent conducting oxide semiconductors for transparent electrodes. *Semiconductor Science and Technology*, 20(4):S35–S44, 2005.
- [156] H. Sato, T. Minami, S. Takata, and T. Yamada. Transparent-conducting *p*-type *NiO* thin films prepared by magnetron sputtering. *Thin Solid Films*, 236(1):27–31, 1993.
- [157] H. Kawazoe, M. Yasukawa, H. Hyodo, M. Kurita, H. Yanagi, and H. Hosono. *P*-type electrical conduction in transparent thin films of *CuAlO₂*. *Nature*, 389(6654):939, 1997.
- [158] N. Duan, AW Sleight, MK Jayaraj, and J. Tate. Transparent *p*-type conducting *CuScO* films. *Applied Physics Letters*, 77:1325, 2000.
- [159] H. Yanagi, S. Inoue, K. Ueda, H. Kawazoe, H. Hosono, and N. Hamada. Electronic structure and optoelectronic properties of transparent *p*-type conducting *CuAlO*. *Journal of Applied Physics*, 88:4159, 2000.
- [160] T. Minami. Transparent and conductive multicomponent oxide films prepared by magnetron sputtering. *Journal of Vacuum Science & Technology A: Vacuum, Surfaces, and Films*, 17:1765, 1999.
- [161] T. Minami. New *n*-type transparent conducting oxides. *Materials Research Society Bulletin*, 25(8):38–44, 2000.
- [162] T. Minami, H. Nanto, S. Shooji, and S. Takata. Stability of zinc oxide transparent electrodes fabricated by R. F. magnetron sputtering. *Thin Solid Films*, 111(2):167–174, 1984.
- [163] H. Enoki, T. Nakayama, and J. Echigoya. The electrical and optical properties of the *ZnO – SnO₂* thin films prepared by RF magnetron sputtering. *physica status solidi (a)*, 129(1):181–191, 1992.

- [164] K. Yanagawa, Y. Ohki, T. Omata, H. Hosono, N. Ueda, and H. Kawazoe. Preparation of $CdYSbO$ thin film on glass substrate by radio frequency sputtering. *Applied Physics Letters*, 65:406, 1994.
- [165] A. Kurz and M.A. Aegerter. Transparent Conducting Films in the Zn–Sn–O Tie Line. *Journal of Sol-Gel Science and Technology*, 31(1):267–271, 2004.
- [166] T. Minami, H. Sonohara, T. Kakumu, and S. Takata. Highly Transparent and Conductive $Zn_2In_2O_5$ Thin Films Prepared by RF Magnetron Sputtering. *Japanese Journal of Applied Physics*, 34:L971–L974, 1995.
- [167] T. Minami, S. Takata, T. Kakumu, and H. Sonohara. New transparent conducting $MgIn_2O_4$ – $Zn_2In_2O_5$ thin films prepared by magnetron sputtering. *Thin Solid Films*, 270(1-2):22–26, 1995.
- [168] A. J. Freeman, K. R. Poeppelmeier, T. O. Mason, R. P. H. Chang, and T. J. Marks. Chemical and Thin-Film Strategies for New Transparent Conducting Oxides. *Materials Research Society Bulletin*, page 45, 2000.
- [169] R.G. Gordon. Criteria for choosing transparent conductors. *Materials Research Society Bulletin*, 25(8):52–57, 2000.
- [170] T. J. Coutts, D. L. Young, and X. Li. Characterization of Transparent Conducting Oxides. *Materials Research Society Bulletin*, 2000, 2000.
- [171] H. K. Schmidt, E. Geiter, M. Mennig, H. Krug, C. Becker, and R. P. Winkler. The Sol-Gel Process for Nano-Technologies: New Nanocomposites with Interesting Optical and Mechanical Properties. *Journal of Sol-Gel Science and Technology*, 13(1):397–404, 1998.
- [172] H. K. Schmidt. *Synthesis and Processing of Nano-Scale Materials Through Chemistry*. Science and Technology of Polymers and Advanced Materials. Emerging Technologies and Business Opportunities, 1998.
- [173] K. Daoudi, B. Canut, M. G. Blanchin, C. S. Sandu, V. S. Teodorescu, and J. A. Roger. Densification of In_2O_3 : Sn multilayered films elaborated by the dip-coating sol-gel route. *Thin Solid Films*, 445(1):20–25, 2003.
- [174] H. Tomonaga and T. Morimoto. Indium–tin oxide coatings via chemical solution deposition. *Thin Solid Films*, 392(2):243–248, 2001.

- [175] R. Ota, S. Seki, M. Ogawa, T. Nishide, A. Shida, M. Ide, and Y. Sawada. Fabrication of indium–tin-oxide films by dip coating process using ethanol solution of chlorides and surfactants. *Thin Solid Films*, 411(1):42–45, 2002.
- [176] M. J. Alam and D. C. Cameron. Investigation of annealing effects on sol–gel deposited indium tin oxide thin films in different atmospheres. *Thin Solid Films*, 420:76–82, 2002.
- [177] E. Shigeno, K. Shimizu, S. Seki, M. Ogawa, A. Shida, M. Ide, and Y. Sawada. Formation of indium-tin-oxide films by dip coating process using indium dipropionate monohydroxide. *Thin Solid Films*, 411(1):56–59, 2002.
- [178] Y. Takahashi, S. Okada, R. Bel Hadj Tahar, K. Nakano, T. Ban, and Y. Ohya. Dip-coating of ITO films. *Journal of Non-Crystalline Solids*, 218:129–134, 1997.
- [179] N. Al-Dahoudi and M. A Aegerter. Wet Coating Deposition of ITO Coatings on Plastic Substrates. *Journal of Sol-Gel Science and Technology*, 26(1):693–697, 2003.
- [180] S. C. Lee, J. H. Lee, T. S. Oh, and Y. H. Kim. Fabrication of tin oxide film by sol-gel method for photovoltaic solar cell system. *Solar Energy Materials and Solar Cells*, 75(3):481–487, 2003.
- [181] C. Terrier, J. P. Chatelon, J. A. Roger, R. Berjoan, and C. Dubois. Analysis of Antimony Doping in Tin Oxide Thin Films Obtained by the Sol-Gel Method. *Journal of Sol-Gel Science and Technology*, 10(1):75–81, 1997.
- [182] M. J. Alam and D. C. Cameron. Preparation and properties of transparent conductive aluminum-doped zinc oxide thin films by sol–gel process. *Journal of Vacuum Science & Technology A: Vacuum, Surfaces and Films*, 19:1642, 2001.
- [183] J. Puetz, G. Gasparro, and M. A. Aegerter. Liquid film spray deposition of transparent conducting oxide coatings. *Thin Solid Films*, 442(1-2):40–43, 2003.
- [184] T. R. Giralidi, M. T. Escote, M. I. B. Bernardi, V. Bouquet, E. R. Leite, E. Longo, and J. A. Varela. Effect of Thickness on the Electrical and Optical Properties of *Sb* Doped *SnO₂* (ATO) Thin Films. *Journal of Electroceramics*, 13(1):159–165, 2004.
- [185] A. N. Banerjee, S. Kundoo, P. Saha, and K. K. Chattopadhyay. Synthesis and Characterization of Nano-Crystalline Fluorine-Doped Tin Oxide Thin Films by Sol-Gel Method. *Journal of Sol-Gel Science and Technology*, 28(1):105–110, 2003.

- [186] H. Cachet, A. Gamard, G. Campet, B. Jousseume, and T. Toupance. Tin dioxide thin films prepared from a new alkoxyfluorotin complex including a covalent $Sn-F$ bond. *Thin Solid Films*, 388(1-2):41–49, 2001.
- [187] S. C. Ray, M. K. Karanjai, and D. DasGupta. Tin dioxide based transparent semiconducting films deposited by the dip-coating technique. *Surface and Coatings Technology*, 102(1):73–80, 1998.
- [188] T. Chaudhuri, A. De, and P. K. Biswas. Development of Sol-Gel Fluorine Doped Tin Oxide Film on Glass. *Transactions of the Indian Ceramic Society*, 62(4):208–212, 2003.
- [189] Y. Natsume and H. Sakata. Electrical and optical properties of zinc oxide films post-annealed in H_2 after fabrication by sol-gel process. *Materials Chemistry and Physics*, 78(1):170–176, 2003.
- [190] J. H. Lee and B. O. Park. Transparent conducting $ZnO : Al, In$ and Sn thin films deposited by the sol-gel method. *Thin Solid Films*, 426(1-2):94–99, 2003.
- [191] J. H. Lee, K. H. Ko, and B. O. Park. Electrical and optical properties of ZnO transparent conducting films by the sol-gel method. *Journal of Crystal Growth*, 247(1):119–125, 2003.
- [192] G. G. Valle, P. Hammer, S. H. Pulcinelli, and C. V. Santilli. Transparent and conductive $ZnO : Al$ thin films prepared by sol-gel dip-coating. *Journal of the European Ceramic Society*, 24(6):1009–1013, 2004.
- [193] V. Musat, B. Teixeira, E. Fortunato, R. C. C. Monteiro, and P. Vilarinho. Al-doped ZnO thin films by sol-gel method. *Surface & Coatings Technology*, 180:659–662, 2004.
- [194] V. Musat, B. Teixeira, E. Fortunato, R. C. C. Monteiro, and P. Vilarinho. Effect of thermal treatment on the properties of sol-gel derived Al-doped ZnO thin films. *Materials Science Forum*, 455:16–19, 2004.
- [195] T. Schuler and M. A. Aegerter. Optical, electrical and structural properties of sol gel $ZnO : Al$ coatings. *Thin Solid Films*, 351(1-2):125–131, 1999.
- [196] W. Tang and D. C. Cameron. Aluminum-doped zinc oxide transparent conductors deposited by the sol-gel process. *Thin Solid Films*, 238(1):83–7, 1994.

- [197] G. K. Paul and S. K. Sen. Sol-gel preparation, characterization and studies on electrical and thermoelectrical properties of gallium doped zinc oxide films. *Materials Letters*, 57(3):742–746, 2002.
- [198] G. K. Paul and S. K. Sen. Optical properties of some sol-gel-derived gallium-doped ZnO films. *Materials Letters*, 57(4):959–963, 2002.
- [199] G. K. Paul, S. Bandyopadhyay, S. K. Sen, and S. Sen. Structural, optical and electrical studies on sol-gel deposited Zr doped ZnO films. *Materials Chemistry and Physics*, 79(1):71–75, 2003.
- [200] G. Torres-Delgado, C. I. Zuniga-Romero, O. Jimenez-Sandoval, R. Castanedo-Perez, B. Chao, and S. Jimenez-Sandoval. Percolation mechanism and characterization of $(CdO)_y(ZnO)_{1-y}$ thin films. *Advanced Functional Materials*, 12(2):129–133, 2002.
- [201] R. Kaur, A. V. Singh, and R. M. Mehra. Development of highly transparent and conducting yttrium-doped ZnO films: the role of sol-gel stabilizers. *Materials Science*, 22(3):201–210, 2004.
- [202] C. H. Kim, J. H. Lee, and B. O. Park. Preparation and characterization of IZO transparent conducting films by sol-gel method. *Materials Science Forum*, 449:469–472, 2004.
- [203] C. M. Cardile, A. J. Koplick, R. McPherson, and B. O. West. ^{119}Sn Mössbauer spectroscopic study of cadmium stannate films prepared by dip-coating. *Journal of Materials Science Letters*, 8(3):370–372, 1989.
- [204] M. Jayachandran, B. Subramanian, M. J. Chockalingam, and A. S. Lakshmanan. Cd_2SnO_4 - its sol-gel preparation and materials properties. *Bulletin of Materials Science*, 17:989–998, 1994.
- [205] T. Sei, Y. Nomura, and T. Tsuchiya. Preparation of $ZnGa_2O_4$ thin film by sol-gel process and effect of reduction on its electric conductivity. *Journal of non-crystalline solids*, 218:135–138, 1997.
- [206] W. S. Dabney, N. E. Antolino, B. S. Luisi, A. P. Richard, and D. D. Edwards. Sol-gel deposition and characterization of In_6WO_{12} thin films. *Thin Solid Films*, 411(2):192–197, 2002.

- [207] I. Stambolova, K. Konstantinov, M. Khristova, and P. Peshev. NO Sensitivity of Spinel Type Zn_2SnO_4 Spray Deposited Films. *physica status solidi (a)*, 167:R11, 1998.
- [208] T. M. Lopez, D. Avnir, and M. A. Aegerter. *Emerging Fields in Sol-gel Science and Technology*. Kluwer Academic Publishers, 2003.
- [209] Q. H. Wang, T. D. Corrigan, J. Y. Dai, R. P. H. Chang, and A. R. Krauss. Field emission from nanotube bundle emitters at low fields. *Applied Physics Letters*, 70:3308, 1997.
- [210] S. S. Wong, J. D. Harper, P. T. Lansbury, and C. M. Lieber. Carbon nanotube tips: High-resolution probes for imaging biological systems. *Journal of the American Chemical Society*, 120(3):603–604, 1998.
- [211] S. J. Tans, A. R. M. Verschueren, and C. Dekker. Room-temperature transistor based on a single carbon nanotube. *Nature*, 393(6680):49–52, 1998.
- [212] Y. Long, Z. Chen, X. Zhang, J. Zhang, and Z. Liu. Synthesis and electrical properties of carbon nanotube polyaniline composites. *Applied Physics Letters*, 85:1796, 2004.
- [213] R. Sainz, A. M. Benito, M. T. Martínez, J. F. Galindo, J. Sotres, A. M. Baró, B. Corraze, O. Chauvet, A. B. Dalton, R. H. Baughman, and W. K. Maser. A soluble and highly functional polyaniline–carbon nanotube composite. *Nanotechnology*, 16(5):S150–S154, 2005.
- [214] S. A. Curran, P. M. Ajayan, W. J. Blau, D. L. Carroll, J. N. Coleman, A. B. Dalton, A. P. Davey, A. Drury, B. McCarthy, and S. Maier. A Composite from Poly (m-phenylenevinylene-co-2, 5-dioctoxy-p-phenylenevinylene) and Carbon Nanotubes: A Novel Material for Molecular Optoelectronics. *Advanced Materials*, 10(14):1091–1093, 1998.
- [215] H. Ago, K. Petritsch, M. S. P. Shaffer, A. H. Windle, and R. H. Friend. Composites of Carbon Nanotubes and Conjugated Polymers for Photovoltaic Devices. *Advanced Materials*, 11(15):1281–1285, 1999.
- [216] H. S. O. Chan and S. C. Ng. Synthesis, characterization and applications of thiophene-based functional polymers. *Progress in Polymer Science*, 23(7):1167–1231, 1998.

- [217] F. Tanaka, T. Kawai, S. Kojima, and K. Yoshino. Electrical and optical properties of poly (3-alkoxythiophene) and their application for gas sensor. *Synthetic Metals*, 102(1):1358–1359, 1999.
- [218] D. T. McQuade, A. E. Pullen, and T. M. Swager. Conjugated polymer-based chemical sensors. *Chemical Reviews*, 100(7):2537–74, 2000.
- [219] G. Viswanathan, N. Chakrapani, H. Yang, B. Wei, H. Chung, K. Cho, C.Y. Ryu, and P. M. Ajayan. Single-step in situ synthesis of polymer-grafted single-wall nanotube composites. *Journal of the American Chemical Society*, 125(31):9258–9259, 2003.
- [220] D. E. Hill, Y. Lin, A. M. Rao, L. F. Allard, and Y. P. Sun. Functionalization of carbon nanotubes with polystyrene. *Macromolecules*, 35(25):9466–9471, 2002.
- [221] Y. Lin, B. Zhou, K. A. S. Fernando, P. Liu, L. F. Allard, and Y. P. Sun. Polymeric carbon nanocomposites from carbon nanotubes functionalized with matrix polymer. *Macromolecules*, 36(19):7199–7204, 2003.
- [222] A. B. Kaiser, G. Düsberg, and S. Roth. Heterogeneous model for conduction in carbon nanotubes. *Physical Review B*, 57(3):1418–1421, 1998.
- [223] J. N. Coleman, S. Curran, A. B. Dalton, A. P. Davey, B. McCarthy, W. Blau, and R. C. Barklie. Percolation-dominated conductivity in a conjugated-polymer-carbon-nanotube composite. *Physical Review B*, 58(12):7492–7495, 1998.
- [224] M. S. P. Shaffer and A. H. Windle. Fabrication and characterization of carbon nanotube/poly (vinyl alcohol) composite. *Advanced Materials*, 11(11):937–941, 1999.
- [225] J. Sandler, M. S. P. Shaffer, T. Prasse, W. Bauhofer, K. Schulte, and A. H. Windle. Development of a dispersion process for carbon nanotubes in an epoxy matrix and the resulting electrical properties. *Polymer*, 40(21):5967–5971, 1999.
- [226] R. Haggmueller, H. H. Gommans, A. G. Rinzler, J. E. Fischer, and K. I. Winey. Aligned single-wall carbon nanotubes in composites by melt processing methods. *Chemical Physics Letters*, 330(3-4):219–225, 2000.
- [227] J. W. Connell, J. G. Smith, J. S. Harrison, C. Park, K. A. Watson, and Z. Ounaies. Electrically conductive, optically transparent polymer/carbon nanotube composites and process for preparation thereof, May 15 2003. WO Patent WO/2003/040,026.

- [228] P. J. Glatkowski. Coatings comprising carbon nanotubes and methods for forming same, March 7 2003. US Patent 20030122111.
- [229] P. Glatkowski, J. Connell, D. Landis Jr, J. Smith Jr, and J. Piché. ESD Coatings for use with spacecraft, March 27 2003. WO Patent WO/2003/024,798.
- [230] J. Grunlan, V. Cross, and K. Smith. Conductive carbon nanotube-polymer composite, November 11 2004. WO Patent WO/2004/097,853.
- [231] S.O. Friend. Conductive coatings and inks, March 24 1992. US Patent 5,098,771.
- [232] D. Shibuta. Method for disentangling hollow carbon microfibers, electrically conductive transparent carbon microfibers aggregation film and coating for forming such film, December 29 1998. US Patent 5,853,877.
- [233] P. Glatkowski, J. Piche, M. Sakai, and H. Ito. Articles with protruding conductive coatings, August 19 2004. WO Patent WO/2004/069,736.
- [234] F. Dalmas, L. Chazeau, C. Gauthier, K. Masenelli-Varlot, R. Dendievel, J. Y. Cavaille, and L. Forro. Multiwalled carbon nanotube/polymer nanocomposites: Processing and properties. *Journal of Polymer Science, Part B, Polymer Physics*, 43(10):1186–1197, 2005.
- [235] C. M. Trottier, P. Glatkowski, P. Wallis, and J. Luo. Properties and characterization of carbon-nanotube-based transparent conductive coating. *Journal of the Society for Information Display*, 13:759, 2005.
- [236] N. Saran, K. Parikh, D.S. Suh, E. Munoz, H. Kolla, and S.K. Manohar. Fabrication and characterization of thin films of single-walled carbon nanotube bundles on flexible plastic substrates. *Journal of the American Chemical Society*, 126(14):4462–4463, 2004.
- [237] M. Kaempgen, G. S. Duesberg, and S. Roth. Transparent carbon nanotube coatings. *Applied Surface Science*, 252(2):425–429, 2005.
- [238] A. Rinzler and Z. Chen. Transparent electrodes from single wall carbon nanotubes, July 10 2004. US Patent 20040197546.
- [239] Z. Wu, Z. Chen, X. Du, J. M. Logan, J. Sippel, M. Nikolou, K. Kamaras, J. R. Reynolds, D. B. Tanner, A. F. Hebard, and A. G. Rinzler. Transparent, Conductive Carbon Nanotube Films. *Science*, 305(5688), 2004.

- [240] M. Mennig, P. W. Oliveira, and H. K. Schmidt. Method for producing multilayered optical systems, September 24 2002. US Patent 6,455,103.
- [241] M. S. Dresselhaus, G. Dresselhaus, R. Saito, and A. Jorio. Raman spectroscopy of carbon nanotubes. *Physics Reports*, 409(2):47–99, 2005.
- [242] ASTM Standard. E914–83. *Practice for Evaluating Temperature Scale for Thermogravimetry (Withdrawn 1994)*, 1993.
- [243] D. Tasis, N. Tagmatarchis, V. Georgakilas, and M. Prato. Soluble carbon nanotubes. *Chemistry*, 9(17):4000–4008, 2003.
- [244] R. P. Winkler, E. Arpac, H. Schirra, S. Sepeur, I. Wegner, and H. Schmidt. Aqueous wet coatings for transparent plastic glazing. *Thin Solid Films*, 351(1-2):209–211, 1999.
- [245] Norm. DIN 58196–6. *Dünne Schichten für die Optik - Teil 6: Prüfung der Haftfestigkeit mit einem Klebeband; Optical coatings - Part 6: Testing of the adhesion with a tape (tape test)*, 1995.
- [246] ASTM Standard. D–3363–92a. *Standard Test Method for Film Hardness by Pencil Test*, pages 441–442, 1993.
- [247] J. L. Sauvajol, E. Anglaret, S. Rols, and O. Stephan. Spectroscopies on carbon nanotubes. *Lecture Notes in Physics*, 677:277–334, 2006.
- [248] K. Hernadi, E. Ljubovic, J. W. Seo, and L. Forro. Synthesis of MWNT-based composite materials with inorganic coating. *Acta Materialia*, 51(5):1447–1452, 2003.
- [249] Y. Zhu, T. Yi, B. Zheng, and L. Cao. The interaction of C fullerene and carbon nanotube with Ar ion. *Applied Surface Science*, 137:83–90, 1999.
- [250] P. Vincent, A. Brioude, C. Journet, S. Rabaste, S. T. Purcell, J. Le Brusq, and J. C. Plenet. Inclusion of carbon nanotubes in a TiO_2 sol–gel matrix. *Journal of Non-Crystalline Solids*, 311(2):130–137, 2002.
- [251] J. Y. Lee, J. S. Kim, K. H. An, K. Lee, D. Y. Kim, D. J. Bae, and Y. H. Lee. Electrophoretic and Dynamic Light Scattering in Evaluating Dispersion and Size Distribution of Single-Walled Carbon Nanotubes. *Journal of Nanoscience and Nanotechnology*, 5(7):1045–1049, 2005.

- [252] T. Miyake and S. Saito. Band-gap formation in (n, 0) single-walled carbon nanotubes (n= 9, 12, 15, 18): A first-principles study. *Physical Review B*, 72(7):73404, 2005.
- [253] E. C. Aifantis. The Physics of Plastic Deformation. *International Journal of Plasticity*, 3(3):211–247, 1987.
- [254] X. Yu, R. Rajamani, K. A. Stelson, and T. Cui. Carbon Nanotube Based Transparent Conductive Thin Films. *Journal of Nanoscience and Nanotechnology*, 6(7):1939–1944, 2006.
- [255] H.-Z Geng, K. K. Kim, K. Lee, G. Y. Kim, H. K. Choi, D. S. Lee, K. H. An, Y. H. Lee, Y. Chang, Y. S. Lee, B. Kim, and Y. J. Lee. Dependence of material quality on performance of flexible transparent conducting films with single-walled carbon nanotubes. *NANO: Brief Reports and Reviews*, 2(3):157–167, 2007.
- [256] D. Zhang, K. Ryu, X. Liu, E. Polikarpov, J. Ly, M.E. Tompson, and C. Zhou. Transparent, Conductive, and Flexible Carbon Nanotube Films and Their Application in Organic Light-Emitting Diodes. *Nano Lett*, 6(9):1880–1886, 2006.
- [257] L. Hu, D. S. Hecht, and G. Grüner. Percolation in transparent and conducting carbon nanotube networks. *Nano Letters*, 4(12):2513–2517, 2004.
- [258] R. H. Baughman, A. A. Zakhidov, and W. A. de Heer. Carbon Nanotubes-the Route Toward Applications. *Science*, 297(5582):787–792, 2002.
- [259] A. Corma, P. Atienzar, H. Garcia, and J. Y. Chane-Ching. Hierarchically mesostructured doped CeO_2 with potential for solar-cell use. *Nature Materials*, 3(6):394–397, 2004.
- [260] M. R. S. Castro and H. K. Schmidt. Transparent conducting antimony-doped tin oxide films containing functionalized multi-walled carbon nanotubes. *physica status solidi(a)*, 204(10):3380, 2007.
- [261] D. Shibuta. Electrically conductive transparent film and coating composition for forming such film, June 1 1999. US Patent 5,908,585.
- [262] M. R. S. Castro, P. W. Oliveira, and H. K. Schmidt. Enhanced mechanical and electrical properties of antimony-doped tin oxide coatings. *Semiconductor Science and Technology*, 23(3):035013 (5pp), 2008.

- [263] T. Ohsaka, E. Izumu, and Y. Fujiki. Raman spectrum of anatase, TiO_2 . *Journal of Raman Spectroscopy*, 7:321–324, 1978.
- [264] M. R. S. Castro, P. W. Oliveira, and H. K. Schmidt. Optical, structural and electrical investigations of TiO_2 /Multi-walled carbon nanotube composites. *Accepted for publication, Journal of Nanoscience and Nanotechnology*, 2007.
- [265] Z. S. Wang, C. H. Huang, Y. Y. Huang, Y. J. Hou, P. H. Xie, B. W. Zhang, and H. M. Cheng. A highly efficient solar cell made from a dye-modified ZnO-covered TiO_2 nanoporous electrode. *Chemistry of Materials*, 13(2):678–682, 2001.
- [266] K. H. Jung, S. R. Jang, R. Vittal, D. Kim, and K. J. Kim. Photocurrent Improvement by Incorporation of Single-Wall Carbon Nanotubes in TiO_2 Film of Dye-Sensitized Solar Cells. *The Bulletin of the Korean Chemical Society*, 24:1501–1504, 2003.
- [267] M. R. S. Castro, N. Al-Dahoudi, P. Oliveira, and H. K. Schmidt. Comparing the efficiency of multi-walled carbon nanotubes as transparent conductive layers on glass and polymeric substrates. *Submitted*, 2007.
- [268] M. R. S. Castro, A. F. Lasagni, H. K. Schmidt, and F. Mücklich. Direct Laser Interference Patterning of Multi-Walled Carbon Nanotube-based Transparent Conductive Coating. *Submitted*, 2007.
- [269] M. R. S. Castro, M. Veith, and P. W. Oliveira. Electro-optical characterization of carbon nanotube-based coatings under CO_2 laser irradiation. *physica status solidi (b) - Basic Research*, 244(11):3998, 2007.
- [270] M. R. S. Castro, E. D. Sam, M. Veith, and P. W. Oliveira. Structure, wettability and photocatalytic activity of CO_2 laser sintered TiO_2 /multi-walled carbon nanotube coatings. *Nanotechnology*, 19(10):105704 (5pp), 2008.